UNIVERSITY OF OKLAHOMA

GRADUATE COLLEGE

INTERPRETATION OF INTER-WELL CHEMICAL TRACER TEST

A THESIS

SUBMITTED TO THE GRADUATE FACULTY

in partial fulfillment of the requirements for the

Degree of

MASTER OF SCIENCE

By

TONG SHEN
Norman, Oklahoma
2017

INTERPRETATION OF INTER-WELL CHEMICAL TRACER TEST

A THESIS APPROVED FOR THE
MEWBOURNE SCHOOL OF PETROLEUM AND GEOLOGICAL ENGINEERING

BY

_____
Dr. Rouzbeh Ghanbarnezhad Moghanloo, Chair

_____
Dr. Deepak Devegowda

_____
Dr. Xingru Wu

I dedicate this thesis to

My handsome husband, for his unconditional love, support, patience, and help.

My perfect parents, Ming and Chen, for their unconditional love and support.

My lovely pet, Ginger, for her companion and loyalty.

Acknowledgements

I would first like to thank my thesis advisor Dr. Rouzbeh Ghanbarnezhad Moghanloo of the Mewbourne School of Petroleum & Geological Engineering at University of Oklahoma. The door to Dr. Rouzbeh's office was always open whenever I had questions about my research. His patience, immense knowledge, invaluable advice, guidance helped me all the time of research.

Besides my advisor, I would like to thank the rest of my thesis committee: Dr. Xingru Wu and Dr. Deepak Devegowda for their insightful comments and encouragement, but also for the hard question which incented me to widen my research from various perspectives.

I would also like to thank my husband, Wei Tian. Without his love, encouragement, patience, support and help, it would not be possible to conduct this research.

I thank my fellows: Dustin R. Oney, Douglas S. West, William H. Gifford and Kevin Coleman. Without their passionate participation and input, our project could not have been successfully conducted.

Finally, I must express my very profound gratitude to my parents Chen Shen and Ming Chen for providing me with unfailing support and continuous encouragement throughout my years of study and through the process of researching and writing this thesis. This accomplishment would not have been possible without them. Thank you.

To all my friends, I say a big thank you for making my stay at University of Oklahoma worthwhile and memorable. You always were heralds of light in the midst of darkness.

Table of Contents

List of Tables

List of Figures

Abstract

For the first time, this thesis presents a new approach to characterize reservoir layering and cross flow between layers using Inter-Well Chemical Tracer Test (ICTT). ICTT is a well-known reliable test for reservoir characterization. During ICTT, a slug of chemical components is injected into subsurface and monitored at producers. Analysis of tracer production history (i.e. tracer produced concentration versus time) provides the reservoir properties. Since reservoirs are usually layered with significant heterogeneity, it is crucial to understand and interpret tracer movement in a stratified system. This study is divided into three parts:

Part1- A comprehensive literature review on inter-well tracer test applications in oil reservoirs is presented. The review includes analytical/numerical methods used to evaluate the results. Limitations and advantages of various evaluation methods are reviewed in detail.

Part2- A new formulation is presented to study tracer propagation along streamlines in heterogeneous reservoirs. The streamlines in this study are modeled as analogous reservoir layers with no cross flow. The fraction of layers where tracer transport occurs faster than the solution of convection–diffusion equation(CDE) is determined; this fraction represents layers through which channeling may take place; obviously, the larger the fraction, the lower the sweep efficiency. Moreover, Ranger field is used to demonstrate how to decouple the convoluted effects of the channeling from small-scale heterogeneity.

Part3- A new formulation is developed to model the crossflow between layers through calculating the dynamic fraction of injected fluid permeating into each layer as a

function of time. Previous models fail to detect crossflow between layers. Several numerical simulation and the same field examples are employed to verify the proposed method. A ‘bridge’ is artificially created in numerical simulation to mimic the major crossflow. The simulation results indicate that tracer can be used to detect and evaluate crossflow. The distance between injector and crossflow can significantly change the tracer production history. The field example was based on the ICTT conducted in Ranger Field. We successfully match the field tracer data and our result indicates the existence of crossflow. Identification of crossflow between layers is critical step to understand reservoir complexity and could provide helpful insight for successful enhance oil recovery (EOR) projects. The proposed method can be easily performed in spreadsheet with the limited data.

Chapter 1. Introduction

1.1 Background

Tracer tests have been widely used in the oil industry for decades. With the development of technology, tracer tests became more mature and powerful (Bjornstad et al., 1990; Divine and McDonnell, 2005). Tracer applications in the petroleum industry started in the 1950s with limited capacity due to uncertainty and complexity associated with their analyses. This significantly affected the advancement of tracer's usage in our industry. In 1990s, with the development of chemical tracer, tracer tests became broadly used to enhance oil recovery. When properly deployed, tracer analysis could give information regarding how fluid flows through the reservoir, breakthrough times from injector to producers, and also give useful estimations of the inter-well oil saturation (Sanni et al., 2015). Therefore, it is imperative to understand how the tracer particles flow within the reservoir and what factors affect it to gain proper qualitative and quantitative information about the reservoir properties.

There are four types of tracer: Conservative, Radioactive, Partitioning tracers and Nanoparticle tracers. Each of these tracers have different purposes depending on the reservoir qualities. Conservative Tracers are chemical tracers which are used to evaluate the media it is being pushed through. Radioactive tracers are similar to conservative tracers, but are also radioactive. This radioactivity allows them to be measured in other ways conservative tracers cannot. Partitioning tracers which interact with the oil and it allows, with the use of a conservative tracer, the calculation of potential oil in place and remaining oil saturation. Nanoparticle tracer has been designed to be more environmentally friendly and less expensive. Nanoparticles can also be used to see how

the tracer moves through the rock layers of the reservoir unlike normal chemical tracers (Rahmani et al., 2015).

These tracers all have specific uses and reasons to use specific chemicals. These reasons can be based on natural occurrences of the chemical in the reservoir that would avoid getting a misreading when they do the analysis of the tracer test. Du and Guan (2005) and Serres-Piole (2012) provided details of tracer selection and tracer criteria. Tracer tests should be economically viable or they defeat the purpose, so if over 50% of the OOIP is already been obtained there is no point in doing a tracer test (Devegowda et al., 2009). There is also the decision to determine whether to use a water or gas tracer. This can be dependent on the size of the reservoir as well at which tracers the reservoir would have to be injected.

There are multiple ways to perform a tracer well test. Each of these methods have specific variables which allow them to be more advantageous than each other in specific scenarios. While radioactive tracers have some major benefits, they are not being widely used due to their environmental damages. This could prove to be a key point in tracer development in the future with more constraints being put on what can be injected into a well. Tracer testing is a key component to determining the subsurface using as well as finding out the residual oil in place by using the partitioning tracer tests. While which tracer we use has a range of variable, they usually depend on either economics or ethics.

1.2 Objective of the study

This study is divided into three parts. The first part presents a fundamental literature review about inter-well tracer test in oil reservoirs. The second part examines the decoupling of small-scale heterogeneity (dispersion) and permeability variation using inter-well tracer test data. The third part presents a systematic approach to evaluate

crossflow between layers of a heterogeneous reservoir using conservative tracer test results.

1.3 Thesis outline

We first discussed the tracer development history and methods to extrapolate the incomplete data. Then, we revisited the basic definition of tracer in oil reservoir and methods of estimating swept volume and oil saturation. In the following section, we discusses three numerical methods: finite-difference, streamline simulator approach and random walk modeling.

Next, we introduce a new formulation to study tracer propagation along streamline in heterogeneous reservoir. Synthetic numerical simulations and field data are both used to verify the proposed approach. Hundreds of cases with different heterogeneous permeability field are simulated in a quarter of five-spot pattern and only one mobile aqueous phase is modeled. Decoupling of permeability variation and dispersion is conducted for simulation cases using a self-developed program.

Finally, we present a systematic approach to evaluate crossflow between layers of a heterogeneous reservoir using conservative tracer test. A hypothesis is made that total number of peaks observed in tracer production history plot cannot exceed number of layers and major crossflow events. Several numerical simulation and field examples are employed to verify the proposed method.

Chapter 2. Literature Review on Inter-Well Tracer Test in Oil Reservoirs

The Chapter is organized as follows: section 2.1 reviews the tracer development history and methods to extrapolate the incomplete data. Section 2.2 introduce fundamental definition on swept volume. It states the difference between mean residence time and residence time distribution. Section 2.3 discusses methods of estimating oil saturation by tracer test. Mobile oil and Immobile oil are considered as well. Section 2.4 discusses numerical modeling methods which are the most complex methods in terms of mathematical precision and intricacy. It can also sometimes be the most accurate method used since there is less user error involved due to sampling or history matching.

2.1 Extrapolation of Incomplete Data

Tracer tests usually have long testing periods and the tracer data obtained are quite spread out and often incomplete. These 'bad' data often affect the data analysis, providing wrong information. Therefore, predicting the tracer decline trails and reducing errors become necessary.

Shook and Forsmann (2005) developed an exponential solution which was used to extrapolate tracer data for large times.

$$f(t) = be^{at} \tag{2-1}$$

Where a is exponent in exponential decline equation (day^{-1}), b is coefficient in exponential decline equation (day^{-1}). However, it was difficult to extrapolate tracer data when tracer tests were terminated early.

Maroongroge (1994) developed a one-dimensional, error functional analytical solution to the convection-dispersion equation (Crank, 1979) that was extended to include multi-phase flow and is valid for partitioning tracers in heterogeneous reservoirs consisting of non-uniform distribution of oil saturation. The solution could extrapolate tracer history data to predict peak tracer concentration time as a function of dispersivity and volume swept. In the tracer test performed at The Shallow Oil Zone in Elk Hills Naval Petroleum Reserve in California, Maroongroge noted that extrapolation of the tracer tails to complete recovery may be erroneous when the test was stopped prematurely due to small recovery of the tracers.

Dugstad et al. (2013) used a type curve function similar to Maroongroge's one-dimensional function for tracer transport. The function was used to compare field data from the Lagrave field in South West France, and the Lagrave field is a small carbonate field with relatively quick communication between injectors and producers. Dugstad obtained a good fit to the dataset using the one-dimensional equation developed by Maroongroge within a three-dimensional, heterogeneous reservoir. However, Dugstad et al. (2013) noted that the summed recovery for the conservative tracer was greater than 100% due to sampling error and the fact that extrapolation was "uncertain and may overestimate tracer mass for extrapolated times". For the partitioning tracers, it was noted that the summed recoveries did not sum to 100%. This was due to "extrapolation of the tracer curves beyond their measured values" (Dugstad et al., 2013).

Based on the work of Maroongroge, Sharma et al. (2014) developed a method that could extrapolate tracer histories before the start of exponential decline of conservative tracer concentration data to explore the possibility of early termination of tracer tests.

They described the tracer concentration vs. time by curve fitting a log-normal probability distribution function (PDF) to their simulated data set, which included the standard deviation and the mean of the distribution.

Dean et al. (2016) extended upon the work of Maroongroge (1994) and Sharma (2014) by using a modified log-normal curve fit to match both conservative and partitioing tracer data for multiple flowpaths. They used Maroongroge's method which relates the peak concentration times of a partitionting tracer and conservative tracer for given a flowpath, based on the Dykstra-Parsons coefficient of that flowpath (Sharma et al., 2014). It was also noted that their approach was only predictive of future partitioning tracer response when conservative tracer data was matched smoothly and tracer partitioning coefficients as well as remaining oil saturation estimates for each flow path were known.

However, it is important to note that tracer testing does not need to cease when the log-normal curve fit appears to be a good fit. By continuing to sample the tracer response the curve fit could be refined to reduce discrepancy of interpreted tracer data (Sharma et al. 2014).

2.2 Swept Volume

2.2.1 Mean Residence Volume and Moment Analysis

The pore volume swept was determined from the mean residence volume of a conservative tracer. Mean residence volume was determined from produced tracer concentration histories at a given production well (Shook et al., 2009). Generally, tracers were produced at multiple production wells and observed the pore volume swept between a given injector and producing well where the tracer was detected.

Tracer tests were normally terminated before tracer response falls to zero due to tracer concentrations decreasing to values below the detection limit. As mentioned above, produced tracer concentrations generally declined exponentially such that ln(C) vs. time is linear, and swept volume could be estimated from incomplete tracer recovery (Shook and Foresmann, 2005). The swept volume for an entire well pattern was the sum of the calculated swept pore volumes between each injector-producer flow path. Failure to account for the tracer concentration tails could lead to an underestimation of swept pore volume (Sharma et al., 2014). Shook and Foresmann (2005) put together instructions to set up a spreadsheet that used these equations to help make these calculations with ease.

2.2.2 Residence Time Distribution Analysis (RTDA)

The use of the distribution of residence times, or residence time distribution analysis, was first conducted by Shook and Foresmann (2003) to calculate swept volume as function of time using only produced tracer data. Using the distribution of residence times, along with the mean residence time, contributed into the description of flow geometry and estimation of swept volume.

Within moment analysis, there were no assumptions regarding non-ideal conditions or fractured medium (Asakawa, 2005; Shook et al., 2009). So, the residence time distribution of the produced tracer data could be used to determine flow geometry and extent of heterogeneity in the form of Flow Capacity – Storage Capacity diagrams, or F-C curves. F-C diagrams were first used for two-dimensional vertical cross sections that were non-communicating layered reservoirs (Lake, 1989). The layers were put into order according to decreasing fluid velocity where the flow capacity of a single layer is the volumetric flow of the layer divided by the total volumetric flow. Storage capacity of

a single layer is the pore volume of the layer divided by the total pore volume. From F-C curves, a Lorenz coefficient can be determined to identify the level of heterogeneity in a reservoir.

Achieving accurate estimations of swept pore volume using conventional moment analysis required the observation of exponential decline in tracer concentration at every producer, which could take hundreds of days or even years depending upon well pattern and processing rates (Sharma et al., 2014).

Using the residence time distribution along with mean residence time, instead of only mean residence time, has several advantages. Although they cover the same answer over longer periods of time, RTDA does not integrate the time weighted-tracer recovery, and allow decisions to be made based on volume swept and economic limit (Shook et al., 2016). Another benefit of using residence time distribution analysis along with mean residence time is that reservoir volume swept can be estimated as a function of time, in real time.

2.3 Oil Saturation

2.3.1 Chromatographic Transformation Theory (Immobile)

Chromatographic separation was the partitioning tracer in and out of the aqueous and oil phase and this separation was a function of the partition coefficient and oil saturation. Partitioning coefficients were defined as the ratio of tracer concentration in oil phase to that in the water phase (Oyerinde, 2004). If a partitioning tracer had a high partition coefficient and was traveling at a low velocity, it would spend more time in the oil phase. Likewise, if the partition coefficient was low and the tracer was traveling at a high velocity it would spend less time in the oil phase (Maroongroge, 1994). Partition

coefficients were measured in the lab, and oil saturation was estimated from produced tracer history (Shook et al., 2009)

Joseph Tang developed one of the most applied analytical methods in the industry to estimates residual oil saturation based on chromatographic transformation theory (Tang and Harker, 1991; Tang, 1995; Tang and Zhang, 2000; Tang, 1992; Tang, 2003). Tang showed that a partitioning and non-partitioning tracer's curves could be collapsed into a single curve by accounting for the difference in residence times by a delay factor related to the partition coefficient and oil saturation. Tang also extended upon the Brigham and Smith (1965) model to estimate oil saturation in individual layers from tracer response (Tang, 2003). Remaining oil saturation could be estimated, without simulation, by comparing the partitioning and conservative production times over the whole production profile at a given landmark (normalized concentration) and normalized recovery.

2.3.2 Chromatographic Transformation Theory (Mobile)

When mobile oil is present, the partitioning tracer would propagate at a faster rate as it contacts, partitions into, and moves with the flowing oil. Thus, assuming zero oil rate would lead to an error in oil saturation estimation. Tang and Zhang (2000) made oil saturation estimates in the presence of mobile oil under steady state and unsteady state conditions. In steady state conditions, water and oil were flowing together within the medium and it was noted that fractional flow and saturation were not changing with time. Apparent oil saturation was then estimated by comparing the ratio of the non-partitioning tracer velocity to the partitioning tracer velocity

In unsteady state conditions, chromatographic theory could be coupled with the Buckley-Leverett fractional flow equation was related to the characteristic oil velocity that the tracer encountered when injected with water. Conservative tracers would move with the associated water saturation and would travel at equal characteristic velocities. Tang and Zhang also mentioned that conducting a tracer test with two partitioning tracers with different partitioning coefficients and using the chromatographic transformation theory was a viable method for detecting mobile oil in the field.

2.3.3 Method of Moments (Immobile)

The method of moments could also be used to make estimates of oil saturation from partitioning tracers (Jin et al., 1995; Oyerinde, 2004; Asakawa, 2005). Two tracers were simultaneously injected with different partition coefficients and subsequently produced. Using the mean residence volumes of the two tracers, an estimation of oil saturation could be made. Given a swept volume, average oil saturation between a well pair could be estimated. This estimation was an average oil saturation using the mean residence volumes assumes that oil saturation was not changing with time. Meaning that once the mean residence volume of the first tracer was produced, no oil production could occur so that the partitioning tracer would acquire a different swept volume (Sinha et al., 2004). Shook et al. (2009) developed a method of obtaining oil saturation estimates through continuous integration of non-partitioning and partitioning tracers based on the residence time distribution of produced tracer data. Estimating oil saturation as function of time could yield saturation estimates times when only a fraction of water containing tracers was produced, or when the reservoir had not been completely swept (Dugstad et

al., 2013). Dugstad et al. (2013) made estimates of oil saturation using the method of moments as well as chromatographic theory to compare the techniques.

2.3.4 Method of Moments (Mobile)

Asakawa (2005) subtracted produced oil from the initial amount of oil calculated after an average time in order to account for the change in saturation between two mean residence times. This correction in oil volume did not yield an accurate estimate of oil volume when large amounts of oil were being produced, large changes in saturation occurred, or a water-flood was active. In cases where this occurred, conventional moment analysis was not sufficient. However, the RTDA method could estimate the volume of oil remaining behind the water-flood by accounting for the fractional flow of each phase as water oil was being produced simultaneously (Shook et al., 2009; Dean et al. 2016). These equations were validated via simulation and lab experimentation even for high, unfavorable mobility ratio tracer tests (Shook et al. 2009). Asakawa (2005) used the method of moments within a simulation to make oil saturation estimates when mobile oil was present. He noted that the majority of the mobile oil was produced before the tracers were produced, which resulted in a small difference between the residual oil saturation and the saturation estimated from the simulated PITT.

2.4 Numerical Modeling

Numerical modeling is an alternate method which provides the complex analysis. Due to the large upside potential of investing in numerical modeling of tracer flow, the accuracy and prediction of such projects become highly advanced and allow the industry to make more informed decisions that ultimately stretch their dollars.

The numerical modeling technique specifically uses three methods: finite-difference method, streamline simulator approach and random walk modeling method.

The finite-difference technique can be considered the lengthier process of the three methods since it handles flow propagation along with changing parameters throughout a gridlocked system which is often large. A reservoir is usually very massive with many changing elements and both vertical and lateral heterogeneity that must be accounted for. Converging algorithms must account and compute block by block in order to simulate the flow. Streamline approach on the other hand allows the user to simulate the flow of the fluid along a streamline with adjusted parameters as it propagates, much like a wave. It allows for the model to run a full length, quick streamline and sum the individual streamline results to obtain the larger picture. A method called random walk modeled how fluid flowed as a large number of molecules with each molecule having a certain probability of randomness (Stalgorova 2011). The random walk approach was developed to show and explain how the tracer flow move with advection and dispersion. It considered how the tracer underwent molecular diffusion, longitudinal and transverse dispersion, as well as adsorption onto the surface of the reservoir. This was required because analytical methods could usually only be used to help compute a homogenous reservoir, or very specific flow patterns (Yi et al., 1994). In comparison, the random walk method could be used to solve for micro heterogeneities caused by the diffusion and fingering processes tracers undergo. This allowed the tracer to be modeled considering an actual scenario instead of continuum modeling which required much more computational time involved (Stalgorova and Babadagli 2010). However, these numerical methods all have their pros and cons which are discussed in detail. The following paragraphs contained fuller descriptions of each method along with their respective pro's and con's.

2.4.1 Finite-Difference Method

As previously stated, the finite difference method is generally the slower technique and has been used a great deal to obtain accurate models of tracer flow. The model can be imagined as numerically computing and converging results within a large grid block with many sub blocks of changing parameters and conditions. This method allows for fairly accurate results when large quantities of data are known. Thus, the reservoir parameters can be entered accounting for the changing grid blocks and thus the converging algorithm will be Taylor made to the reservoir conditions. As this may provide more accuracy, it also can cause the computing device to encounter issues with time sensitivity for a project and the projects that can set guiding parameters to speed processes by avoiding diverging algorithms become extremely important. With if a study utilizing the finite difference modeling approach may not be able to accurately account for these changes in grid block dispersity, and in such cases the method may not be entirely accurate and as such a decent but quick streamline method could be just as effective. One downside made apparent by Ali (2000) was that the results of the tracer simulation would rely heavily on the input of the actual results in the field. This process took time and could also add error. In the end, most the tracer peaks and final data turn out to be successfully helpful to build their improved reservoir model. Finite-difference model in combination with grid refinement, large data storage and history matching has the necessary means to provide solutions to complex issues. These solutions come at the expense of time and some slight possibilities for error, but certainly provide a better solution than streamline approach.

2.4.2 Streamline Simulator Approach

The second method, the streamline approach to numerical modeling provides a much quicker and more efficient method of tracer flow modeling. As previously mentioned it models tracer flow along a streamline and takes the sum in order to provide the total results. The primary advantage of a streamline based approach is the speed at which the study may be conducted. A large portion of the streamline method included the ability to handle sensitivity (Datta-Gupta, 2002). In exploiting an analogy between seismic ray tracings, Datta-Gupta's streamline approach allowed to calculate these sensitivities by evaluating one-dimensional integrals along a streamline. This allowed for very quick and efficient mathematical computations. Another advantage of streamline method is that it can handle very complex heterogeneous reservoirs. However, the result may not be accurate without the proper refinements of data and would in turn slow the process down. This streamline model does deal with small incremental change by assessing penalties on certain results in order to maintain the speed of calculation. One such penalty used included the model norm in which the new model could not be significantly different than the previous model and the roughness penalty in which the small fluctuations were taken care of and this way they were more associated with the large-scale trends according to Datta-Gupta (2002).

2.4.3 Random Walk Modeling Method

Random walk modeling method is a numerical method instead of an analytical method. In which we can diminish the significant numerical error induced by finite difference modeling. We can reduce the dispersion factor as well as ensure mass conservation of the small volume of injected tracer (Yi et al., 1994). In addition, it handles

the problem with transverse dispersion which is neglected in streamline modeling. This method works because we can assign a tracking algorithm to map out how the tracer should move through the reservoir. To solve for this, we need certain variables including the Jacobian units in cube space, velocities on the cell face, the well component which is given by cylindrical flow, and particle reflection. These equations and proofs can be found in the literature (Liu et al., 1999). The random walk method has been modified time and time again to allow for different characteristics to be changed in the algorithm. One example is when we can change the random walk method to take into account miscible flow. The required parameters only include knowing the oil and water diffusivity compared to the six unknowns in the classical modeling being the, Solvent and oil diffusivity, fracture, matrix, and longitudinal and transverse dispersivities (Stalgorova and Babadagli 2010). Another advancement in the random walk model was to account for what are known as walkers. These walkers are particles that move randomly but has a probability of certain movements based off physics. The method of random walk particle tracking (RWPT) could be used to simulate miscible flooding of light and heavy oils in naturally fractured reservoirs (Stalgorova and Babadagli 2010).

2.4.4 Discussion

Tracers are extremely important for industries dealing with the flow of fluids through a porous medium. At a minimum, they lace the flowing fluid with a chemical signal which can be detected later at another location, thus letting the person know where the fluid went. For this very reason, modeling tracer flow is extremely important for the petroleum industry because it yields predicted results and can also provide intricate details regarding the reservoir and its properties. Tracers can be used practically for

secondary and tertiary recovery, but with the onset of the numerical modeling techniques of finite-difference and streamline method, properties such as reservoir flow performance, gas and water displacement, well to well communication, permeability distribution, flow patterns and residual oil saturation all can become evident to the company or entity needing the information. The method can be quick or slow, accurate or lofty-at-best, and therefore it is extremely important to have a good idea of what type of reservoir is under study and assess what type of time and resources are available to the scholars in order to yield the best and most efficient results for that specific project.

Chapter 3. Decoupling of Channeling and Dispersion Effects using Multi-Well Tracer Test

The chapter is organized as follows: following from G. Moghanloo (2012), an analytic solution is derived to determine growth of the average tracer concentration in a heterogeneous stratified reservoir in the absence of cross-flow (a simple example of shear flow); in other words, the analytic solution is obtained under the assumption that all streamlines are parallel to the formation bedding. Furthermore, we evaluate the impact of heterogeneity and dispersivity on the growth of the mixing zone within each layer. In addition, the fraction of layers in which the mixing zone grows faster than that of the dispersive flow regime (G. Moghanloo, R. and Lake 2011), is determined as a function of the Koval factor (H_k) and input dispersivity. Next, a formulation is presented to determine the distribution of tracer concentration along streamlines between the injector and the producer in heterogeneous quarter five-spot pattern; the streamlines could be considered as layers with no communication as there is no cross-flow between them (based on the definition). Finally, the proposed approach is used to evaluate inter-well heterogeneity in a field example. The approach presented in this paper is restricted to tracer flow with unit mobility ratio and no gravity effect; i.e. we only focus on channeling among other 2D phenomena (viscous fingering and gravity override/underride).

3.1 Literature Review

Transport of tracer components through heterogeneous permeable media has been studied quite extensively in the past (Gelhar et al. 1979; Matheron and de Marsily, 1980; Sposito and Dagan, 1994). Tracer transport is governed by mixing and spreading. Even though mixing and spreading are strongly coupled (Thierrin and Kitanidis 1994), a fundamental

difference exists between them. Spreading is the change of plume shape (deformation) due to permeability heterogeneity; i.e. a tracer that is transported through a high permeable layer breaks through considerably faster than the one that travels through a less permeable layer. Mixing, on the other hand, is associated with an increase in the size (volume) of the plume. Plume is considered as the fluid volume that contains tracer particles.

The mixing and spreading in a homogeneous permeable medium (Gaussian plume) with constant velocity are related in a simple fashion, and both are characterized by the dispersion coefficient. Dispersion is caused by local velocity gradients, locally heterogeneous streamline lengths, mechanical dispersion, and diffusion in permeable media (Lake 1989). Dispersivity, as the measure of dispersion, represents how far tracer particles stray from the path of the fluid carrying them. Dispersivity in the field is measured through tracer tests involving injection of an inert (conservative), non-reactive and non-adsorbing solute followed by monitoring of concentration data and analysis of the breakthrough curve at the same or another well. Depending on the method of measurement and flow direction, two different types of dispersion coefficients are obtained (Mahadevan et al., 2003): (1) echo dispersion coefficient defined as the reservoir mixing that is observed when the flow injected from a well is produced from the same well after flow reversal; (2) transmission dispersion coefficient obtained from analysis of concentration data when more than one well is involved (inter-well tracer test). The depth-averaged concentration of tracer is measured at the production well. Similarly, Dentz and Carrera (2007) and Zavala-Sanchez et al. (2009) identified two different dispersion

coefficients: apparent and effective. The former represents spreading of the plume based on the second centered moment whereas the latter measures the actual mixing.

However, the concentration gradients in all directions diminish with time. Therefore, Dagan (2012) discussed three different transport regimes based on the travel time: (1) when $t << L^2/DT$ (where L is the length and DT is the transverse dispersion), the transverse dispersion can be neglected; (2) when $L^2/DT << t << H^2/DT$ (where H is the thickness of the reservoir), complete mixing occurs between layers but no boundary effect yet has been realized; (3) $H^2/DT << t$ for which the transverse dispersion effectively has created a complete mixing (negligible concentration gradient) over the entire thickness; this is called Taylor-Aris regime. Hence, the Taylor-Aris approach to quantify mixing is strictly valid only at late times.

Tracer transport in heterogeneous permeable media during pre-asymptotic times (non-Fickian/non-Gaussian) has not yet been thoroughly understood (Bloster et al., 2010). Neuman et al. (2009) compared the modern theories of non-Fickian transport in heterogeneous permeable media in the velocity fields that are uniform/non-uniform in the mean. As long as the asymptotic behavior has not reached in a heterogeneous permeable medium, a constant dispersivity in the convection-diffusion (CD) equation cannot properly predict the concentration distribution. This occurs because of the convoluted impacts of dispersion and permeability heterogeneity. The contribution of spreading yields large superficial values for dispersivity in the field-scale (Dagan 1982; Gelhar and Axness 1983; John 2008; Fiori et al., 2002). Several review papers present measured dispersivities over a wide range of length scales (Schulze-Makuch 2005; Vandeborght and Vereecken 2007; Zhou et al., 2007). In these datasets, the longitudinal dispersivity

increases with distance traveled. Furthermore, Su et al. (2005) used a dispersivity coefficient that varies with time to match concentration history plots. Greenkorn et al. (1983) discussed the scaling of mixing during miscible displacement in heterogeneous permeable media.

Gelhar and Axness (1981) chose a different approach and studied the interplay between dispersion and the permeability variability in stratified permeable media. Rather than just focusing on dispersivities to match the concentration data, they considered the role of permeability variation. They found that dispersive transport exhibits non-Fickian behavior for a stratified medium in early timeb and asymptomatically approaches Fickian dispersive transport at late time if there is cross-flow between layers. Matheron and DeMarsily (1980) show that cross-flow between layers restores Fickian transport, asymptomatically, at large times. Lake and Hirasaki (1981) also studied dispersion in stratified formations and concluded that transverse dispersion between layers yields an average longitudinal dispersion coefficient asymptotically.

In addition, Coats et al. (2009) used a constant physical scale-independent dispersivity to account for pore-scale heterogeneity and additional scale-dependent dispersivity reflecting permeability heterogeneity. The latter is used as a fitting parameter to match concentration history plots. However, our approach is different from their method because we use a permeability heterogeneity as an indicator instead of a random fitting parameter. In terms of application, tracers are categorized into conservative and partitioning tracers. This classification is based on the relative interaction of the tracers with aqueous and oleic phases present in the reservoir.

3.2 Methodology

Figure 3-1 indicates a stratified permeable medium consisting of an ensemble of n layers with different properties: permeability, thickness, and porosity separated by very thin barriers with no vertical permeability. This configuration is a simple case of shear flow, which has been also investigated in the physics literature (Castiglione et al., 1999).

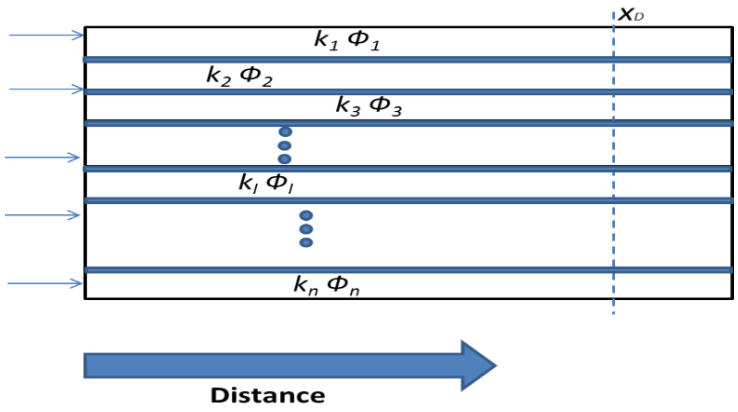

Figure 3-1: Schematic of a 2D heterogeneous reservoir with no convective cross-flow between layers. The reservoir layers are separated by thin impermeable layers (blue strata).

In this study, we re-visit the shear flow using cumulative flow and storage capacities. The cumulative flow capacity F and cumulative storage capacity C at a given vertical cross-section is defined as (Lake, 1989):

$$F = \sum_{l=1}^{n} \frac{k_l h_l}{H_t \bar{k}} \qquad \text{i=1, 2… n (number of layers)} \qquad (3\text{-}1)$$

Where $\bar{k}$ and H_t are the arithmetic average of horizontal permeability and total thickness of the given cross-section, respectively. Therefore,

$$C = \sum_{l=1}^{n} \frac{\phi_l h_l}{H_t \bar{\phi}} \qquad (3\text{-}2)$$

Where $\bar{\phi}$ is the arithmetic porosity average for that cross section. From Darcy's law, the interstitial velocity of a passive tracer through each layer is represented by the

ratio of permeability to porosity of the same layer $r_l = \frac{k_l}{\phi_l}$. If we rearrange the interstitial velocity of flow in all layers in decreasing order of r_l , F_l represents the fraction of flow at a velocity greater or equal to r_l. Similarly, C_l indicates the associated pore volume with the fraction of flow that travels at the velocity of r_l or faster. From the definition, the derivative of a continuous F with respect to C at any given C_l is the interstitial velocity within the corresponding layer divided by the arithmetic average of interstitial velocity of the whole ensemble.

The approximate solution of the dimensionless convection-dispersion equation in one-dimensional (1D) flow that describes the conservation of the injected component (tracer) through an isothermal miscible displacement has the form of (Lake, 1989)

$$c_D = \frac{1}{2}\left[1 - erf\left(\frac{x_D - t_D}{2\sqrt{\alpha_D t_D}}\right)\right], \tag{3-3}$$

Where α_D is the dimensionless dispersivity normalized by the length of the permeable medium; equivalently, we can use the reciprocal of the Peclet number (N_{pe}^{-1}) instead of α_D. Also, c_D is the dimensionless concentration and t_D and x_D are the dimensionless time and distance, respectively. The above solution is derived considering the following premises: incompressible fluid and pore space, ideal mixing, single-phase flow, the same dispersivity (α) for all layers, and semi-infinite medium assumptions.

The arithmetic average of the tracer concentration over a vertical cross-section at the distance of x_D from the injector and at the given time t_D is determined as

$$c_D = \frac{\sum_{l=1}^{n} c_{D,l} h_l}{H_t}, \tag{3-4}$$

Where$C_{D,l}$, the dimensionless concentration at each layer, is defined as

$$\begin{cases} c_{D,1} = \frac{1}{2}\left[1 - erf\left(\frac{x_D - \beta_1 t_D}{2\sqrt{\alpha_{D,1} t_D}}\right)\right] \\ c_{D,2} = \frac{1}{2}\left[1 - erf\left(\frac{x_D - \beta_2 t_D}{2\sqrt{\alpha_{D,2} t_D}}\right)\right] \\ c_{D,3} = \frac{1}{2}\left[1 - erf\left(\frac{x_D - \beta_3 t_D}{2\sqrt{\alpha_{D,3} t_D}}\right)\right] \\ , \\ \ldots \\ c_{D,n} = \frac{1}{2}\left[1 - erf\left(\frac{x_D - \beta_n t_D}{2\sqrt{\alpha_{D,n} t_D}}\right)\right] \end{cases},$$

Where β_l is the fraction of injected volume that enters layer *l*. Furthermore, $\alpha_{D,l}$ is the reciprocal of Peclet number of layer *l*. However, we assume that the Peclet number is the same for all layers in the remainder of this paper. There is no viscous cross-flow between layers and, thus, the fluid injected in any layer stays within the same layer until it breaks through. Traditionally, the above system of equations should be solved numerically to obtain the c_D for a given t_D and x_D. However, we incorporate the notion of cumulative flow and storage capacities into Eq. (3-4) to find an analytic solution for c_D.

Considering the tracer flow assumptions (mobility ratio of unity and matched density), in addition to no inter-layer flow communication, β_l can be interpreted as the fraction of injected volume entering layer l at the inlet face. The volume injected in each layer remains in the same layer throughout flow, as there is no convective cross-flow between layers. Therefore, F can be translated as the cumulative distribution function of β when F is a continuous function of C. Hence, the derivative of a continuous F with respect to C calculated at C_l will be equal to β_l (Jennings et al., 2000).

The following analytic solution was proposed (G. Moghanloo, R. 2012) for the tracer concentration at a layer with cumulative storage capacity of C (Appendix A):

$$c_D\,|_C = \frac{1}{2}\left[1 - erf\left(\frac{x_D - \frac{dF}{dC}|_C\; t_D}{2\sqrt{\alpha_D \frac{dF}{dC}|_C\; t_D}}\right)\right]. \tag{3-5}$$

Eq. (3-5) is obtained from substitution of (β, t_D) by $(\frac{dF}{dC}\Big|_C\; t_D)$ in the 1D solution of the convection-diffusion equation.

The dimensionless mixing zone within each layer is defined as the distance between locations where the dimensionless concentrations of 0.1 and 0.9 occur. Following Lake (1989),

$$\Delta x_D\,|_C = \left(x_D\,|_C\right)_{c_D=0.1} - \left(x_D\,|_C\right)_{c_D=0.9}\ , \tag{3-6}$$

Where $x_D|_C$ is distance in the layer with the cumulative storage capacity of *C*. Also, $\Delta x_D|_C$ represents length of the mixing zone normalized by the length of permeable medium.

To calculate the mixing zone, we invert Eq. (3-3) for $(x_D|_C)_{c_D=0.1}$ to yield

$$\left(x_D\,|_C\right)_{c_D=0.1} = 2erfc^{-1}(0.2)\sqrt{\alpha_D \frac{\partial F}{\partial C}|_C\; t_D} + \frac{\partial F}{\partial C}|_C\; t_D\,. \tag{3-7}$$

Similarly, we determine $(x_D|_C)_{c_D=0.9}$ and substitute into Eq. (3-6); hence,

$$\Delta x_D\,|_C = 3.625\sqrt{\alpha_D \frac{\partial F}{\partial C}|_C\; t_D}\,. \tag{3-8}$$

3.3 Mixing Zone Analysis

We evaluate the growth of mixing zone within layers of a heterogeneous reservoir with no cross-flow between layers. The length of the mixing zone is obtained from Eq. (3-8).

Figure 3-2 compares the lengths of the mixing zone depicted at t_D=0.5 for two cases: H_k = 1 and H_k = 10 when α_D is equal to 0.01, where H_k is the Koval factor. The mixing zone grows differently within layers when H_k = 10. The mixing zone grows faster within layers represented by cumulative storage capacity smaller than 0.25 than the vertical blue line representing H_k = 1 in **Figure 3-2**. Larger flow velocity in those layers indicates the channeling flow regime as discussed in the remainder. Smaller fraction of the injected volume moves into the layers represented by larger cumulative storage capacity; consequently, the dispersive transport will dominate over the convective flow in those layers.

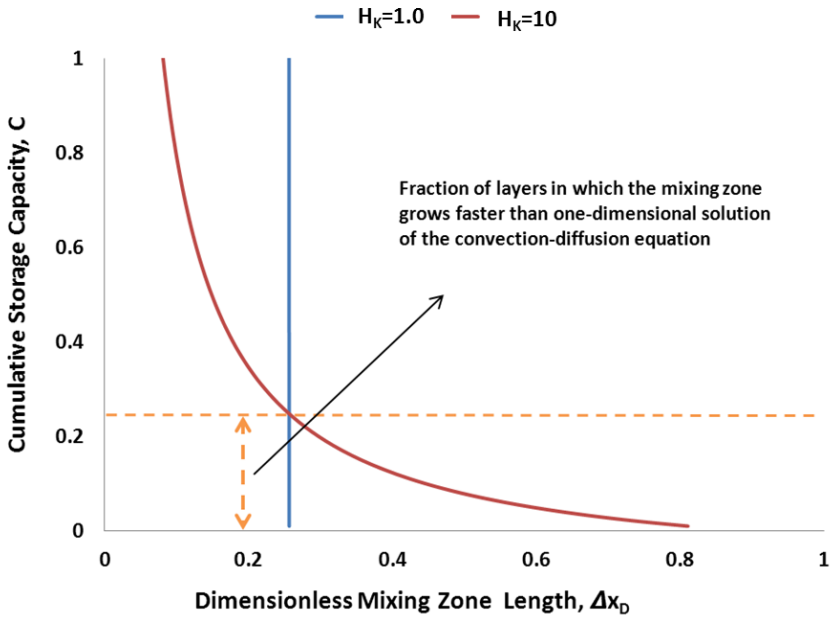

Figure 3-2: A comparison between length of the mixing zone (normalized by the length of the reservoir) for two cases: H_k=1.0 and H_k=10 at t_D=0.5 when α_D is equal to 0.01. Two examples are considered: H_k =1 and H_k =10. The length of the mixing zone is obtained from Eq. (3-8). The larger the H_k, the more convection-dominated the flow is and, consequently, the mixing zone grows faster (with time) rather than the square root of time.

Figure 3-3 indicates the ratio of the sweep efficiency of a heterogeneous reservoir to homogenous counterpart as a function of H_k. This graph has been obtained similar to **Figure 3-2** but for different H_k values. Since there is no cross flow between layers (the amount of injected volume gets into each layer, stays in the same layer until it breaks through), it turns out the graph remains the same for various α_D and times. The Y-axis in **Figure 3-3** represents the intersection points of H_k = 1 and H_K. The concentration equal to 0.5 always will travel at the bulk velocity; in other words, when tracer breaks through at X_D equals to 1.0, the produced C_D (dimensionless tracer concentration) will have the value of 0.5. Eq. (3-9) shows how Eq. (3-5) can be adapted to consider for heterogeneous layered system with no cross flow:

$$C_D|_c(x_D, t_D) = \frac{1}{2}\left[1 - erf\left(\frac{x_D - \left(\frac{H_k}{[1+(H_k-1)C]^2}\right)t_D}{2\sqrt{\frac{\left(\frac{H_k}{[1+(H_k-1)C]^2}\right)t_D}{N_{Pe}}}}\right)\right] \quad (3\text{-}9)$$

The same graph (**Figure 3-3**) result is obtained for different t_D and N_{pe}^{-1}. As H_k increases, the cumulative storage capacity of the layers with faster growing mixing length than that of convection-diffusion equation decreases. In other words, channeling flow regime is more pronounced and a large amount of fluid will be getting into a smaller fraction of layers; equivalently, sweep efficiency decreases as heterogeneity increases. This is consistent with field observations.

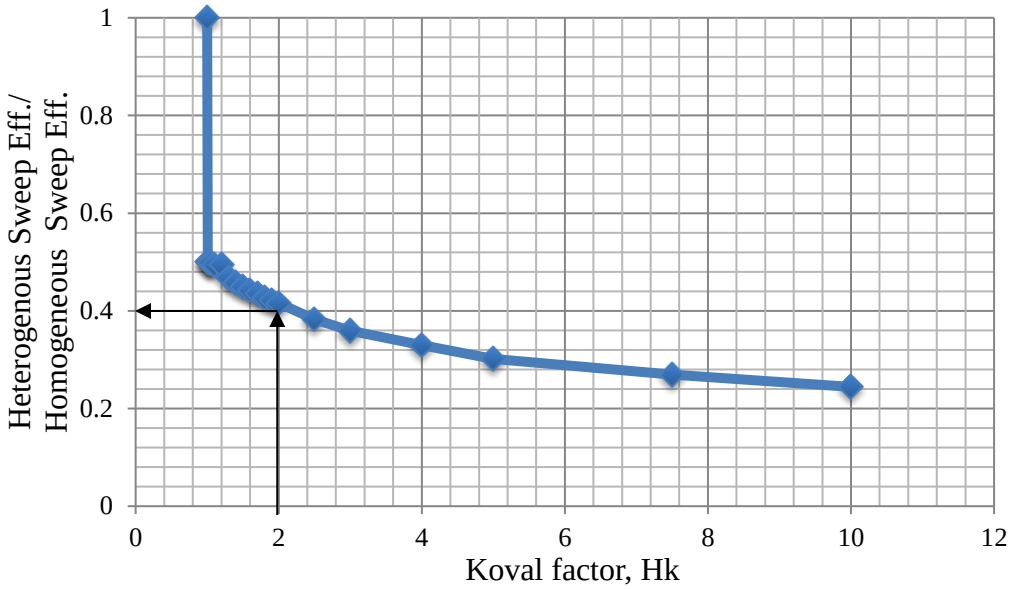

Figure 3-3: The Y- axis represents the ratio of heterogeneous sweep efficiency to homogenous sweep efficiency. The same plot is obtained for different t_D and N_{pe}^{-1} as there is no cross flow between layers. For example, when $H_k = 2$ for a heterogeneous reservoir, its sweep efficiency will be only 0.4 of the homogenous counterpart. Overall, sweep efficiency decreases as heterogeneity increases.

3.4 Converting into Streamlines

As streamlines are independent from each other and there is no cross-flow between them, they could be considered as layers with no communication; furthermore, the solution is semi-analytic as the trajectories of streamlines are known at any time from simulation. Therefore, above analytical solution we proposed to determine the average tracer concentration in a heterogeneous stratified reservoir is also applicable for a 2D, one layered reservoir.

3.5 Simulation

In this section, a 2D simulation model is built to verify the semi-analytical solution presented earlier. **Figure 3-4** indicates the flowchart used in this section. The reservoir model is 100 ×100 grid prescribed with a quarter five-spot pattern and saturated with

single phase. More than 100 heterogeneous permeability fields (realization) with input H_k ranges from 5.3 to 12.7, λ_{xD} (represents dimensionless range distance in the x-direction) values of 0.01, 0.1, 1, and 10, and λ_{yD} (represents dimensionless range distance in the y-direction.) values of 0.01, 0.1 and 1 were generated using sequential Gaussian simulation with an exponential variogram model and imported into reservoir simulator (Appendix C). Two tracer components are introduced into the reservoir model at a constant rate: an inert tracer followed by an active tracer that follows the Langmuir isotherm adsorption described by Eq. (B.2) in Appendix B; the same mole fraction of 0.5% is used for both tracer components A finite amount of tracer slug (for half of a day) is injected into the reservoir model and followed by chase water. The tracers' concentrations are monitored at the producer. The details of simulation parameters are given in

Table 3-1.

Table 3-1: Reservoir properties

Depth, ft	6415
Pressure, psi	4925
Thickness, ft	5
Porosity, %	10
Water Saturation, %	100
Injection/Production Rate, STB/D	300
Length, ft	100
Width, ft	100
Temperature, ^{o}F	219
Slug Size, day	0.5
Tracers Injected Mole Fraction, %	0.5
Langmuir Isotherm tad1, lbmol/ft3	0.68
Langmuir Isotherm tad3, dimensionless	1

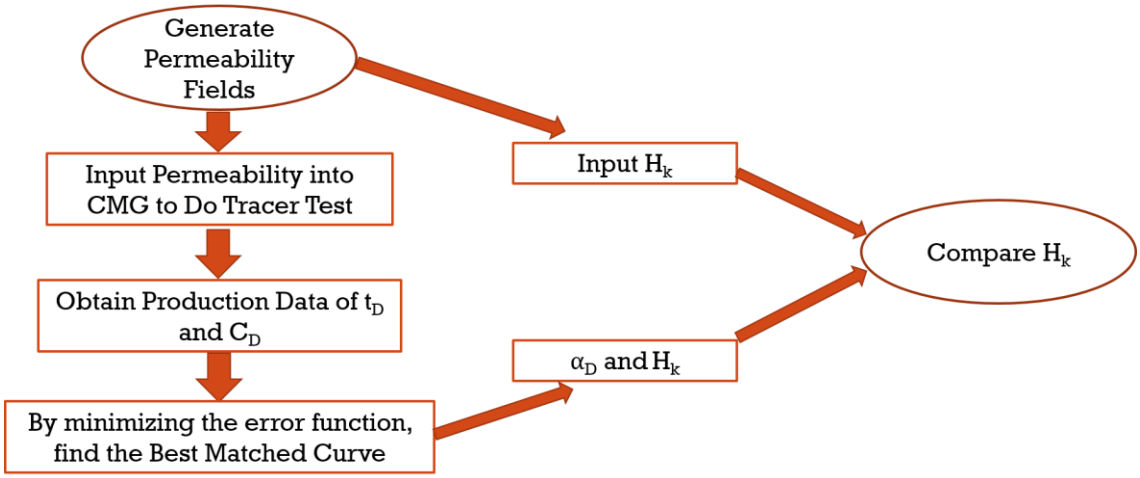

Figure 3-4: Flowchart

We modified Eq. (3-9) to consider slug injection impact and adsorption impact (Appendix B). MATLAB code is used to find the best matching curves (Appendix D). The retardation factor for active tracer is 1.195 obtained using Eq. (B.6). **Figure 3-5** shows the concentration profile of $H_k = 1.4$ (right) and $H_k = 1$ (left) after 1 day. From the graph, we can observe that left graph represents almost an even distribution as opposed to the right graph. This is due to heterogeneity: the tracer preferentially propagates through high permeability grid blocks.

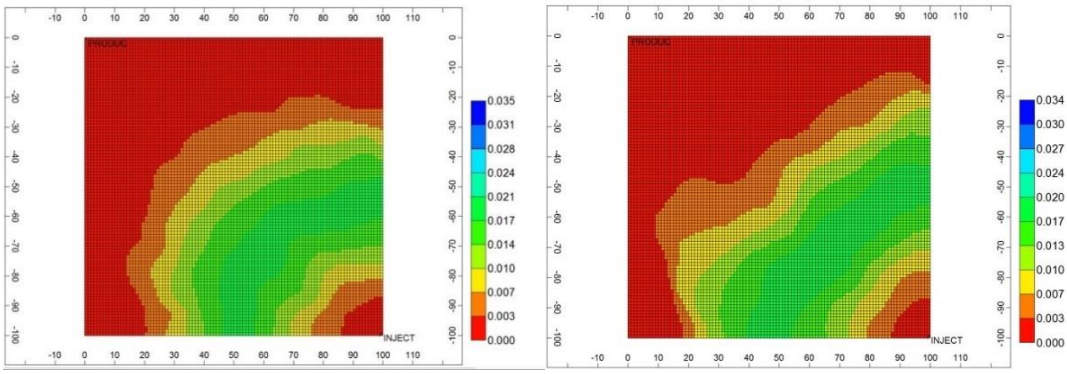

Figure 3-5: the concentration profile for H_k=1.4 (right) and H_k=1 (left) after 1day

To illustrate data interpretation procedure, the case with permeability of $\lambda_{xD} = 0.1$, $\lambda_{yD} = 0.1$, $V_{DP} = 0.6$ is presented as **Figure 3-6**. Two tracers' production concentrations (in mole fraction) are recorded and their dimensionless values are calculated following Eq. (B.10) and (B.11). The solid lines represent the dimensionless simulation results of active tracer and inert tracer respectively.

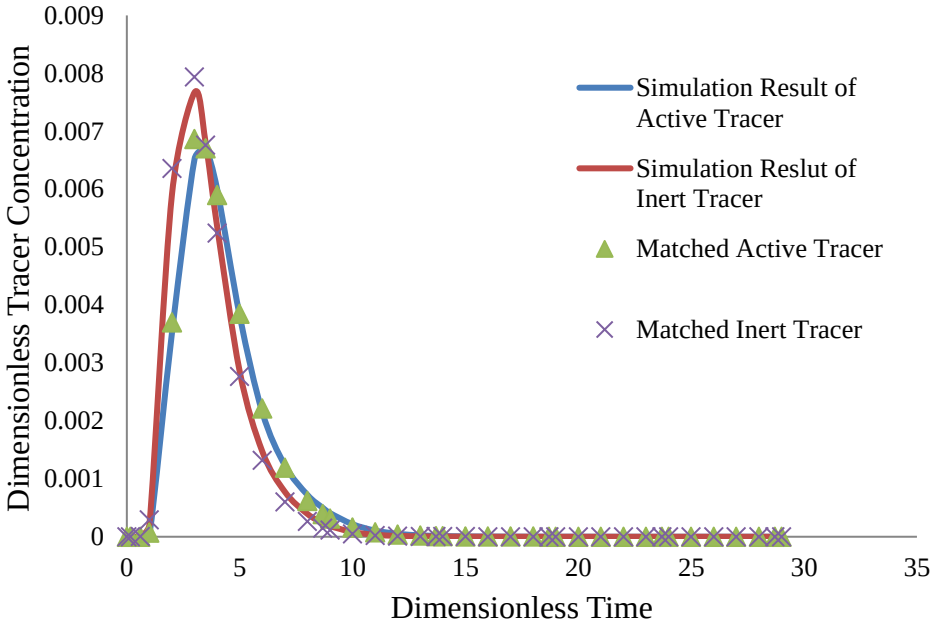

Figure 3-6 Comparison of simulations and matched result.

3.6 Practical Aspects

In this section, we evaluate the practical aspects of the proposed equation; three scenarios with different conditions are studied.

3.6.1 Scenario 1

A set of 100 simulation models without considering physical dispersion (dispersion only limited to numerical dispersion) with grid block size of 1 sq. ft (1ft x 1 ft).

Figure 3-7 and **Figure 3-8** show the histogram plots of Koval factors H_k and α_D. It turns out that 63 % of calculated Koval factors H_k (using Eq. (3-4)) are close to 1 indicating pseudo 1D flow with no concentration gradient in the transverse direction (vertical equilibrium); in other words, dispersion number (Johns and Garmeh 2012) becomes zero for 63% of the cases. Dispersion number is a dimensionless group representing the ratio of time scales required for a tracer particle to travel along cross section because of transverse dispersion to that of longitudinal path owing to longitudinal dispersion. The calculated longitudinal α_D has the range of 0.06 to 0.2; in other words, the effective longitudinal Peclect number is in the range of 5-13.

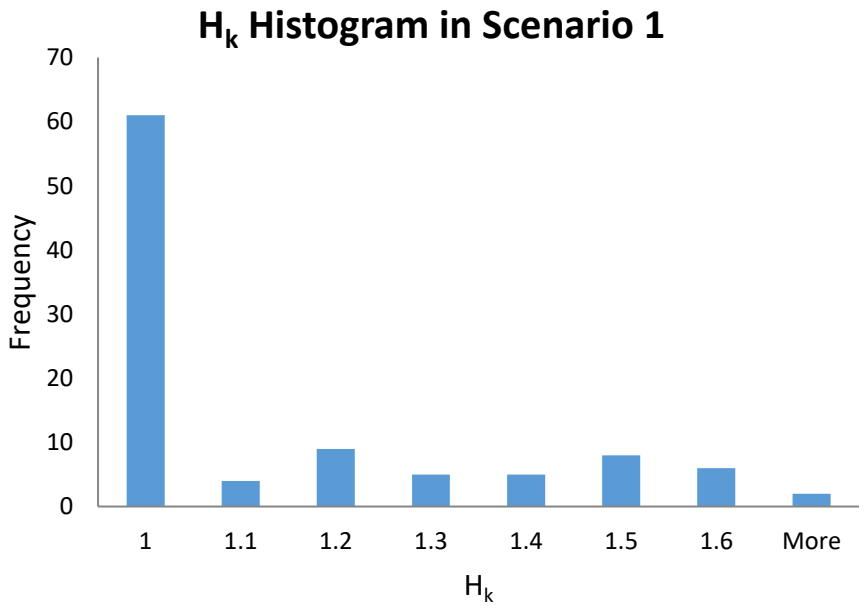

Figure 3-7: H_k calculated for 100 cases in scenario 1.

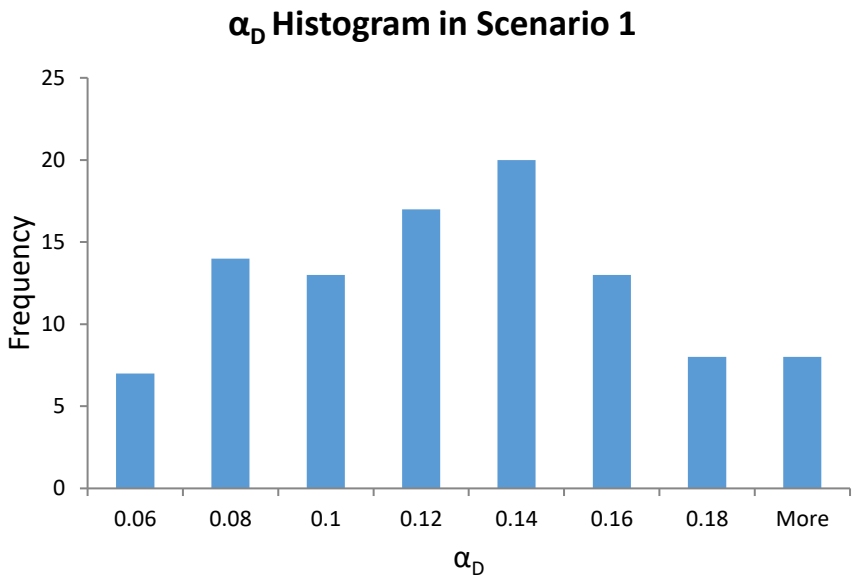

Figure 3-8: α_D calculated for 100 cases in scenario 1. The range of α_D is from 0.06 to 0.2.

3.6.2 Scenario 2

100 simulation models with larger grid blocks are compared to Scenario 1, but still no physical dispersion is considered. The purpose of Scenario 2 is to examine the scale impact on the effective Koval factor and dimensionless dispersion.

The results (**Figure 3-9**, **Figure 3-10**) suggest that larger grid block size, almost do not change the representative α_D or mixing in the longitudinal direction. This is expected from Eq. (3-5). However, 87 % of calculated Koval factors (using Eq. (3-4)) are close to 1 representing pseudo 1D flow; this is almost 30% more than Scenario 1 indicating large grid blocks greatly changes the governing flow regime, something that has not been addressed before. Pseudo 1D flow is the manifestation of diminishing the concentration gradient across the transverse direction (vertical equilibrium); the dispersion number remains the same for both Scenario 1 and 2, using large grid blocks has been translated into establishing vertical equilibrium. This is consistent with Coats et

al. (2009) and and Mahadevan et al. (2003); i.e. field dispersivities should be local dispersivities (scale- independent) in the same order as the echo dispersitivies.

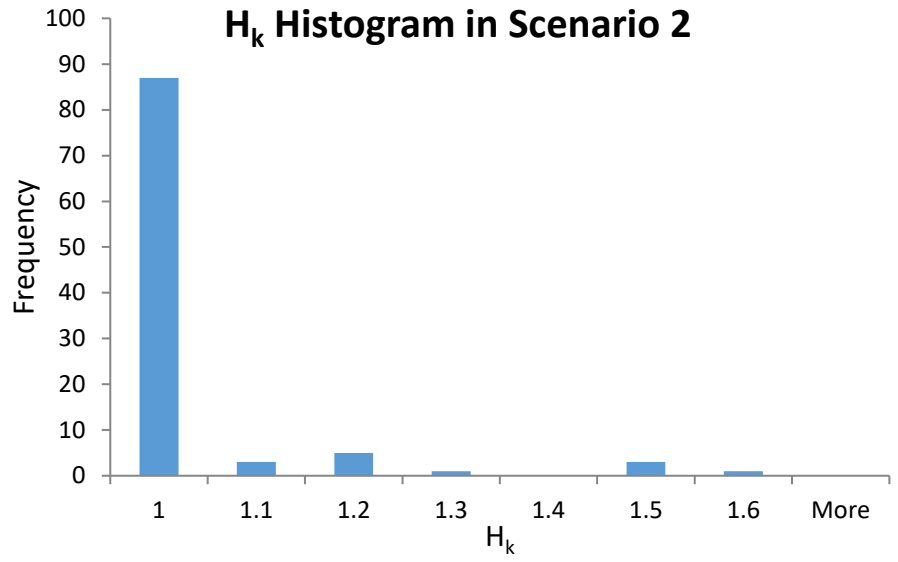

Figure 3-9: H_k calculated for 100 cases in scenario 2.

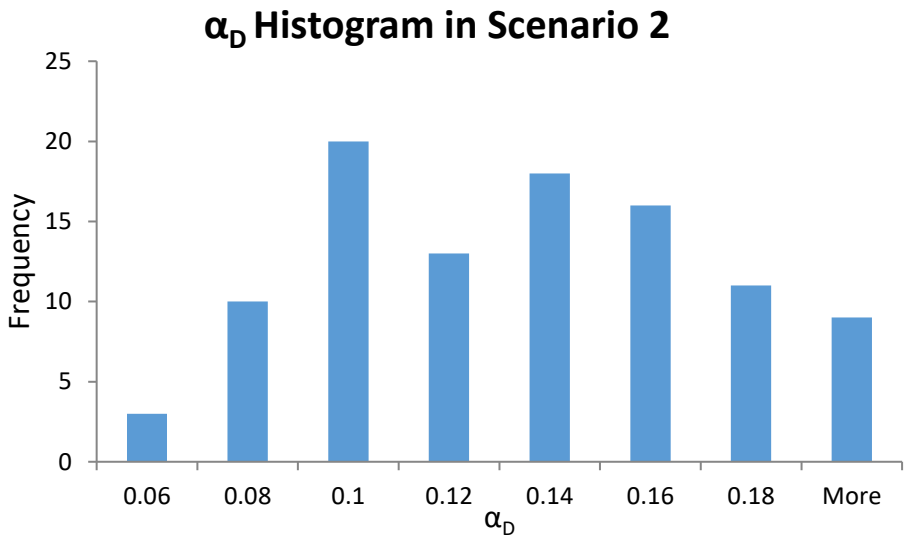

Figure 3-10: α_D calculated for 100 cases in scenario 2.

3.6.3 Scenario 3

A set of 100 cases with physical dispersion and grid block size of 1ft × 1ft are studied despite previous cases where we assumed there is no physical dispersion.

We observed that with physical dispersivity of 10ft (purposely chosen to be extremely large value to yield the same input dispersivity as Scenario 2); it appears that pseudo 1D flow occurs in almost 60% of the cases, same as the Scenario 1. In other words, changing longitudinal physical dispersion does not affect cross flow/transverse flux, as expected. However, α_D shifts to the right (**Figure 3-11**) compared to **Figure 3-7** indicating much stronger mixing. The other important observation is that the distributions (**Figure 3-7**, **Figure 3-9** and **Figure 3-11**) are not alike.

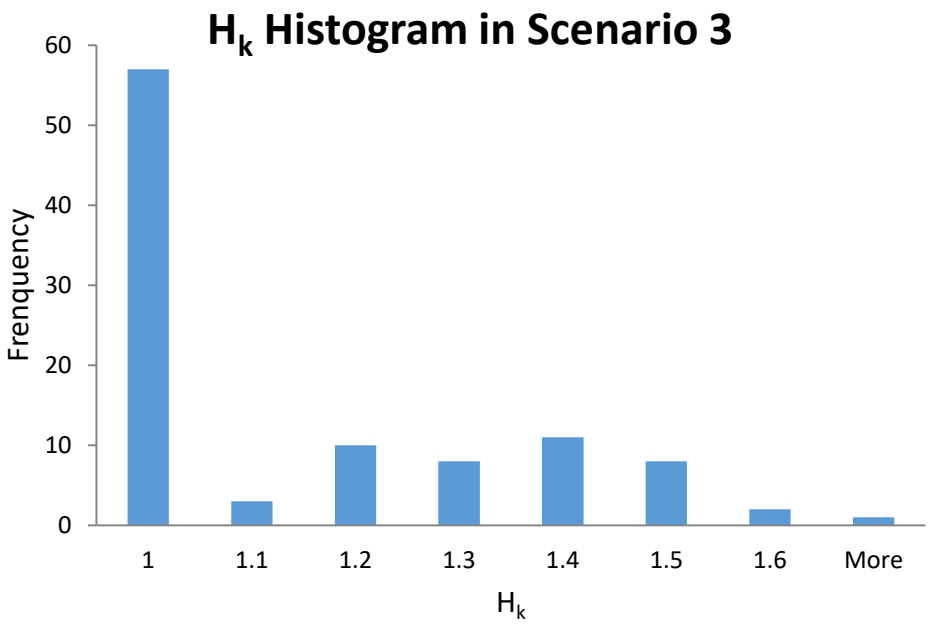

Figure 3-11: H_k calculated for 100 cases in scenario 3.

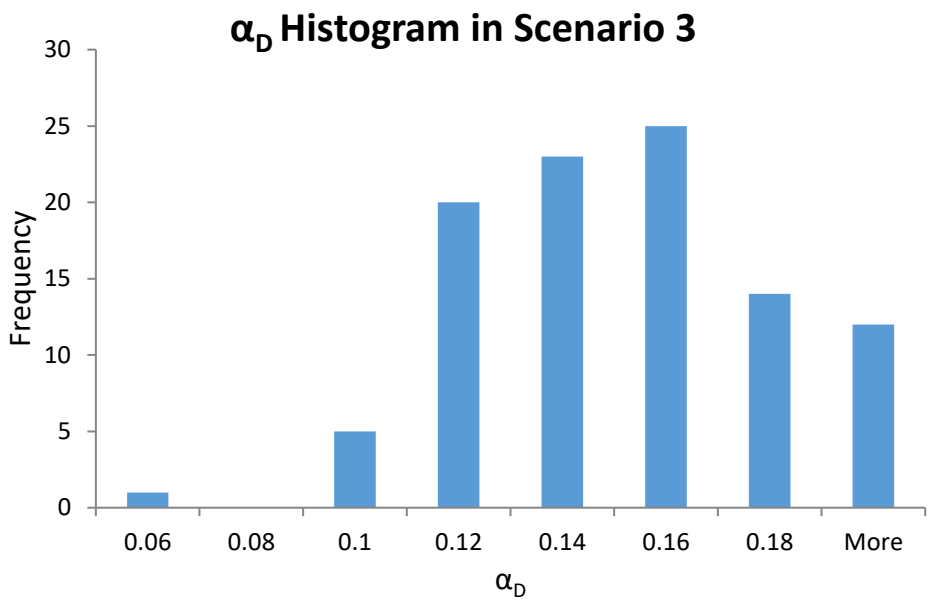

Figure 3-12: α_D calculated for 100 cases in scenario 3. The range of α_D is from 0.1 to 0.2.

The general perception is that Peclet number is around 50-100 in the large-scale system. However, according to our simulation results, the Peclet number should be around 10. This result indicates that the front will be smeared out faster than earlier expectations; consequently, there would be more residual oil saturation left behind of multi-contact miscible displacement and thus less chance of miscibility development in the field scale. This could significantly decrease the displacement efficiency. Of course, the impact of numerical dispersion should be further investigated. The following equation was obtained for the oil sample used in an study by G.Moghanloo and Lake (2012) and G.Moghanloo (2012):

$$S_{orm} = -0.046 \ln\left(N_{pe}\right) + 0.4 \qquad (3\text{-}10)$$

Where S_{orm} is the miscible residual oil saturation. The outcome of this paper suggests that there will be more than 25% increase in the miscible residual oil saturation (for that particular oil sample) when Peclet number is around 10 instead of 50.

We also noticed in all three scenarios that when input H_k is larger than 8, the best fit is obtained with H_k equals to 1; i.e. channeling flow regime is dominant (G. Moghanloo, R. and Lake 2011); in other words, there will be a very poor sweep efficiency. When the input H_k is smaller than 8, the best match is obtained for early stage with H_k equal to 1 followed by larger H_k representing a transition to dispersive flow regime (G. Moghanloo and Lake 2011).

3.7 Description of Field

One field example is presented from McClesky sandstone of the Ranger field. It has been focused on the multi-well, multi-tracer injection study over years (Lichtenberger, 1991 and Oyerinde, 2004). We have used these data as our input data, and compared the results from the analytical solution. Ranger field is a heterogeneous reservoir with Dyksrea-Parson coefficient of 0.74 (H_k is 9.3) (Illiasov et al. 2000). There are seven tracers injected, including 5 conservation tracers, one chemical tracer, and two partitioning tracers. In this paper, we only focused on conservation tracer or inert tracer (NaSCN) and partitioning tracer or active tracer (TBA).

NaSCN and TBA were injected through Well 38 along with water phase and produced from Well 39, 37, 19 and 40 (**Figure 3-13**). There is 0.41 of tracer producer from well 37, 0.18 of tracer producer from well 39 and 0.04 of tracer producer from well 40. Net Swept volume for well 37, well 39 and well 40 are 109700bbls, 55909bbls and 7258bbls respectively (**Table 3-2**). The slug size and injection rate are 20 days and 840

bbl /day, respectively. The injection concentration of NaSCN and TBA is 960 ppm. The partitioning coefficient for TBA is 0.2. Oil saturation is in the range of 0.45 to 0.6, residual oil saturation after water flooding is 0.45 (**Table 3-3**). Allison et al. (1991) indicated oil cuts at wells 37 and 39 were around 30% at the start of tracer test and decreased to 10% at the end of sampling time. No oil production is reported for well 40. Since there was nearly no oil cut at well 40, we consider well 40 is in single phase flow, and well 37 is multi-phase flow. We calculate dimensionless time using Eq. (B.10).

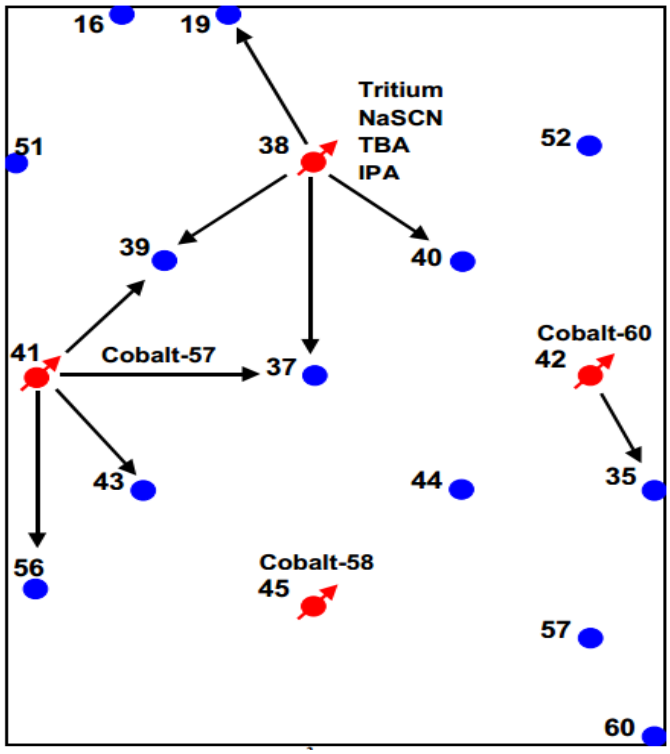

Figure 3-13: Tracer injection pattern in Ranger field. (Oyerinde, 2004)

Table 3-2: Result of MOM calculated from Oyerinde (2004)

tritium	**Well 19**	**Well 37**	**Well 39**	**Well 40**
f (Fraction of tracer produced	0.0009	0.08	0.43	0.007
Net Swept Volume (bbls)	424	22800	120322	1130
Break Through* (days)	380	100	100	85
sodium thiocyanate(NaSCN)	**Well 19**	**Well 37**	**Well 39**	**Well 40**
f(Fraction of tracer produced)	0.006	0.41	0.18	0.04
Net Swept Volume (bbls)	3058	109700	55903	7258
Break Through* (days)	420	95	150	65
TBA and tritium				
Average Oil Saturation	-	0.436	0.541	-
TBA and NaSCN				
Average Oil Saturation	-	0.491	0.388	-

* Extrapolated estimates.

Table 3-3: Summary of tracer properties (Oyerinde, 2004 and Illiasov et al. 2000)

Parameter	Tritium	NaSCN	TBA
Slug Size	20 days		
Slug Size	10 Ci	5655 lbs	880 glas
Injection rate	840 bbl/day		
Normalization Concentration	3744 pC/mL	960 ppm	960 ppm
Initial oil saturation	0.45 and 0.6		
Residual to water oil saturation	0.45		

3.8 Field Data Analysis

MATLAB code is used to find the best matching curves. **Figure 3-14** shows the tracer concentration monitored at well 40 in dimensionless domain. The solid line represents the dimensionless field data and the dots represent the semi-analytical solution. It takes very long time for breakthrough to happen; hence, it is expected that only fraction of the injected fluid has travelled toward the targeted producer. Therefore, observed tracer tail may not be accurate to match. We divide this figure into two segments: before peak breakthrough and after peak breakthrough. Before peak breakthrough the fluid flow

occurs mainly through high perm channels as one-dimensional model and our result matches the tracer field data when H_k equals to 1 and α_D equals to 0.02. After peak breakthrough, our results match the tracer data with H_k of 1.6 representing a transition toward dispersive flow regime and α_D equals to 0.02. This result can be explained using **Figure 3-3**: when H_k equals to 1, all injected fluid flow through high perm zone, which results in 100% of cumulative storage capacity; whereas, cumulative storage capacity of 44% is realized when H_k equals to 1.8. As H_k increases, dispersive flow regime begins. As dispersive flow regime occurs, larger sweep efficiency is observed, and lower displacement efficiency is realized (G.Moghanloo and Lake 2011).

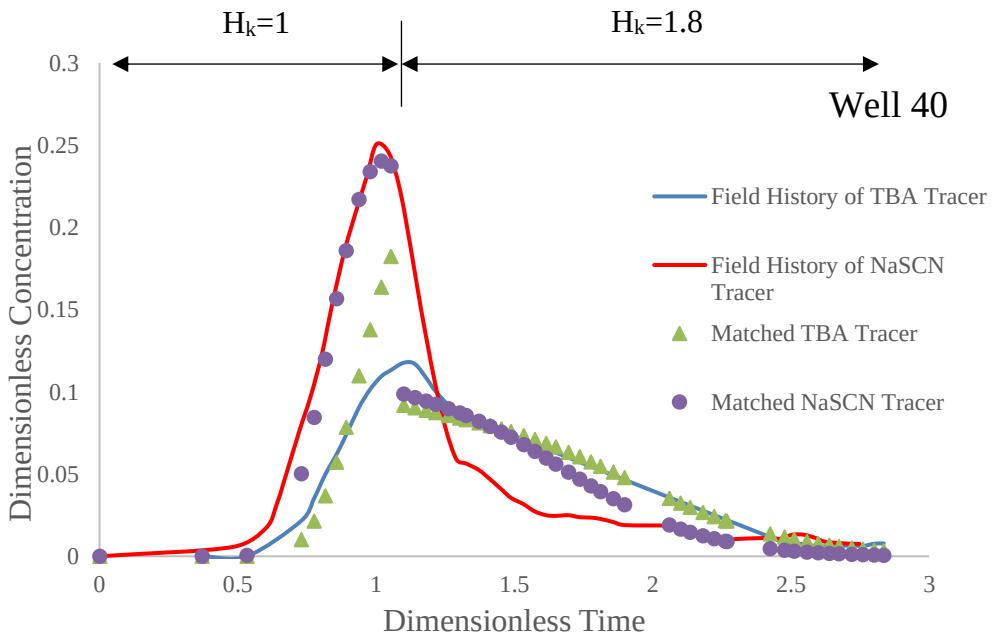

Figure 3-14: the comparison of field data with semi-analytical solution for well 40. The solid line represents the dimensionless field data and the dots represent the semi-analytical solution. Tracer breakthrough from well 38. H_k=1.6 at later stage indicates that only 40% of the swept volume in this case.

As mentioned before, well 37 is multi-phase flow, the original method previously discussed in this paper is limited to single phase. Therefore, we need to adjust the

proposed method so that it can be applicable to two phase systems. According to the fractional flow theory (Buckley and Leveret 1942, Lake 1989, Orr 2007, Ghanbarnezhad and Lake 2012, and Ghanbarnezhad, 2012), the lower initial water saturation (higher oil saturation) results in a faster water displacing velocity. We also know conservative tracer travels with its carrier fluid (Deans 1978, Tian 2017), which was the water phase in the Ranger field case. Therefore, when the oil phase is mobile, the tracer breaks through faster than the in the immobile oil phase (the slope of tangent line in fractional flow plot is larger than unity). Therefore, we introduce the approximate equation to adjust the tracer arrival time:

$$\frac{t_{adjusted}}{t_{actual}} = \frac{1-S_{or}}{1-S_{o_{ave}}} \tag{3-11}$$

Where, S_{or} is the residual oil saturation, $S_{o_{ave}}$ is the average oil saturation behind the water front. This adjustment of tracer production data is applicable when residual water saturation is 0 or close to 0. We should keep in mind that if the residual water saturation is significant, Eq. (3-11) will only provide a rough approximation. Residual oil saturation is 0.45, average oil saturation is get from Allison's paper (1989). In that paper, finite difference model was used to simulate the oil saturation profile for three layers (he assumed the reservoir contains three layers) at the end of sampling. To calculate average oil saturation, we locate well 37 and find the corresponding oil saturation for each layer, then calculate the average oil saturation to be around 0.69. Using Eq. (3-11) we can calculate the adjusting coefficient, which is approximately 0.6.

Figure 3-15 demonstrates that the matching curve has been shifted to the right after implementing the correction based on Eq. (3-11). Blue dots represent field inert tracer data, red dots represent field active tracer data, yellow solid line represents the

adjusted field inert tracer data, and gray solid line represents the adjusted field active data. At the end of water flooding, oil cut has dropped from 30% to 10%. However, the change in oil cut can only affect tracer breakthrough time and curves can be still matched using the adjusting coefficient (Eq. (3-11)). Thus, Koval factor remains the same in all of this since it measures the reservoir heterogeneity.

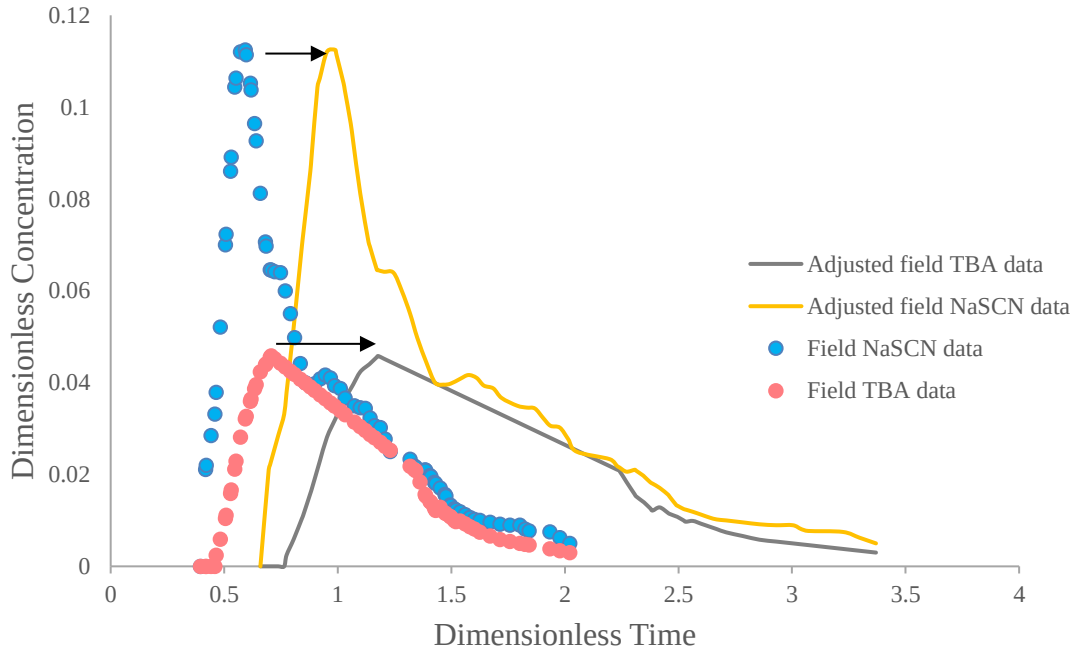

Figure 3-15: Field data before and after adjustment (Well 37). Blue dots represent field inert tracer data (NaSCN), red dots represent active tracer data in field (TBA), yellow solid line represents the adjusted inert tracer data, and gray solid line represents the adjusted active tracer data.

Figure 3-16 shows the tracer concentration of the field data and calculated curves for well 37. The result is similar to well 40. Before peak breakthrough, our solution matches the tracer field data using H_K equals 1 and H_k is 2.1 after peak breakthrough; α_D before and after peak breakthrough is close to 0.025. Using **Figure 3-3**, it turns out that only 39% of cumulative storage capacity will be ultimately swept.

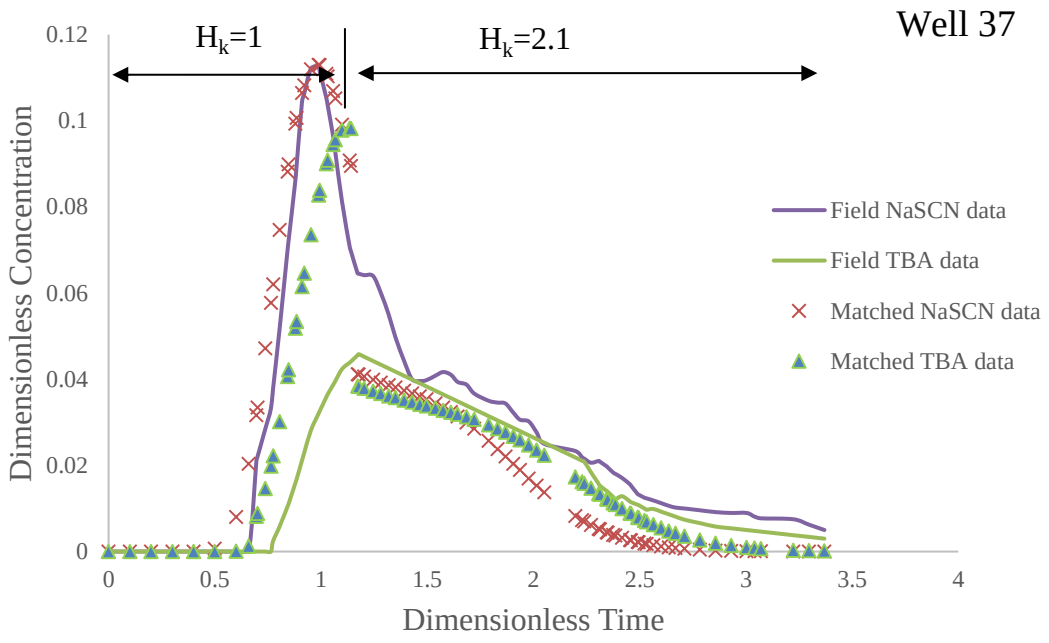

Figure 3-16: the comparison between field data and semi-analytical solution for well 37

3.9 Discussion

There is a major difference between the approach taken in this study and the practical approach of matching the concentration history plots obtained from production data with 1D solution of the convection-diffusion equation. Here, there is no need to use an inverse calculation to find an apparent dispersivity to predict the concentration profile at different times; instead, we can use true dispersivity (Mahadevan et al., 2003) and the permeability variation coefficient to predict the average concentration propagation. In this paper, transverse dispersivity has been ignored; however, transverse dispersion in layered systems may play an important role as described by Lake and Hirasaki (1981).

In this study, the convective spreading because of channeling is decoupled from small-scale heterogeneity for two different types of flow patterns with parallel and non-parallel streamlines. The need for an apparent scale-dependent dispersivity is replaced by

the Koval factor to match the tracer concentration at pre-asymptotic times. The results are consistent with Coats et al., (2009) as they used scale-independent dispersivity and a fitting parameter to match concentration history plots using a 1D solution of the C_D equation. However, the Koval factor (large-scale heterogeneity measure) is incorporated into the commonly used solution of the C_D equation instead of a fitting parameter.

This study expands Dysktra- Parson method (1950) used for water flooding in layered system and sweep efficiency discussion in Lake (1989) to tracer flow in layered system with no cross flow. The former methods do not include dispersion effects and thus the mixing zone only grows linearly with time. However, the mixing zone may develop either linearly or with square root of time (depending upon Peclet number). In this study, the fraction of layers through which mixing zone will grow faster than what predicted by the convection diffusion equation is determined. This provide an interesting insight to the sweep efficiency in heterogeneous reservoirs (**Figure 3-3**).

Incorporation of the semi-analytic solution presented in this study (originally derived in G. Moghanloo 2011 and 2012) and the streamline simulation (SLS) may alleviate one of the major drawbacks of SLS when it comes into the dispersion (Thiele et. al 2010). To resolve this issue, an operator-splitting approach has been implemented that solves the convective part along the streamlines and the diffusive part on the Eulerian grid; however, that approach might not be always appropriate.

3.10 Conclusions

In this study, we used a modified version convection-diffusion equation solution to account for channeling in 2D flow. In addition, using the proposed formulation, the fraction of layers in which the channeling may occurs is determined. Details that disappeared when 1D solution of the convection-diffusion equation manifest themselves

as an apparent scale-dependent dispersivity at pre-asymptotic times; however, this study separates the convoluted effects of large- and small-scale heterogeneity. The major contributions of this paper are:

- The ratio of sweep efficiency for heterogeneous reservoir to that of homogenous reservoir (channeling effect) can be estimated using Koval factor (H_k).
- Dispersion coefficient obtained in this study is larger than previously considered in other studies and almost remains irrespective to the problem size scale.

Chapter 4. Interpretation of Inter-Well Chemical Tracer Tests in Layered Heterogeneous Reservoirs with Crossflow

In this chapter, we propose a formulation to interpret ICTT when crossflow occurs. Simulation models are created to verify our method. A transition period is identified during which crossflow has significantly changed the dynamic fraction of injected fluid flowing through each layer. The technique has been implemented to analyze the Ranger field and its results are compared with other published work.

4.1 Introduction

An Inter-Well Chemical Tracer Test (ICTT) is a reliable method for reservoir characterization. During ICTT, a slug of chemical component(s) is injected into the subsurface and the tracer concentration is monitored at the designated producer (s). The chemical components often used as tracer are classified as conservative tracers, which are soluble in one phase only, and partitioning tracers, which partition between phases (Tian et al. 2016). Through analysis of the tracer production history (i.e. produced tracer concentration versus time), the effective dispersivity and number of producing layers are evaluated. Since reservoirs are usually layered with significant heterogeneity, it is imperative to understand and interpret tracer transport in stratified systems (Du and Guan 2005).

Tracer production history in a layered reservoir usually contains more than one peak. It is well documented that layers with different permeability will often result in distinguished tracer breakthrough time showing multiple peaks. **Figure 4-1** shows three schematics indicating multi-peak production history. **Figure 4-1(a)** shows the layered system with no crossflow; in other words, there is no communication between layers

throughout entire reservoir. Several analytic solutions previously published about ICTT address no crossflow case. Brigham and Smith (1965) proposed a model to interpret production history of a conservative tracer in a typical five-spot flow pattern, which is useful in evaluation of permeability heterogeneity. Abbaszadeh-Dehghani and Brigham (1984) derived an analytic solution to describe the tracer breakthrough curves from layered systems with unit mobility ratio. This solution is suitable for five-spot patterns as well as other flow patterns with no crossflow between layers.

Figure 4-1(b) shows the solution of layered system under vertical equilibrium. The vertical equilibrium is achieved with three mechanisms: capillary forces, gravity and viscous flow (Coats et al, 1997; Yokoyama and Lake, 1981; Zapata and Lake, 1981; Lake et al, 1990). Continuous communication or vertical equilibrium (Yortsos, 1995) is the state at which no driving force exists in the transverse direction and, consequently, system attain equilibrium, instantaneously. Zapata and Lake (1981) showed that viscous crossflow is a potential source of mixing in all unstable flows. The mixing zone causes the vertical sweep efficiency to be greater than the corresponding purely segregated flow case (no crossflow). Lake and Hirasaki (1981) indicated that transvers dispersion mitigates heterogeneity effects toward much uniform two-dimensional flow. Gravity effects and capillary forces are the other two driving mechanisms that trigger crossflow. However, vertical equilibrium are no crossflow cases are the extreme ends of a spectrum where fluid flow can experience in multi-layer systems. In many cases, significant portion of the cross flow is limited through specific abnormal features in the system (such as sand injectites). Sand injectites is unconsolidated sand body that can be remobilized and overlying the impermeable bedding as shown in **Figure 4-2** (Slatt, 2013). **Figure 4-1(c)**

shows the focus of our study as cases where crossflow is limited to those features. We call those features “bridge” and assume that there are finite numbers of them laid over the border of adjacent layers. Unlike cases under vertical equilibrium, layers here only communicate through the bridge(s).

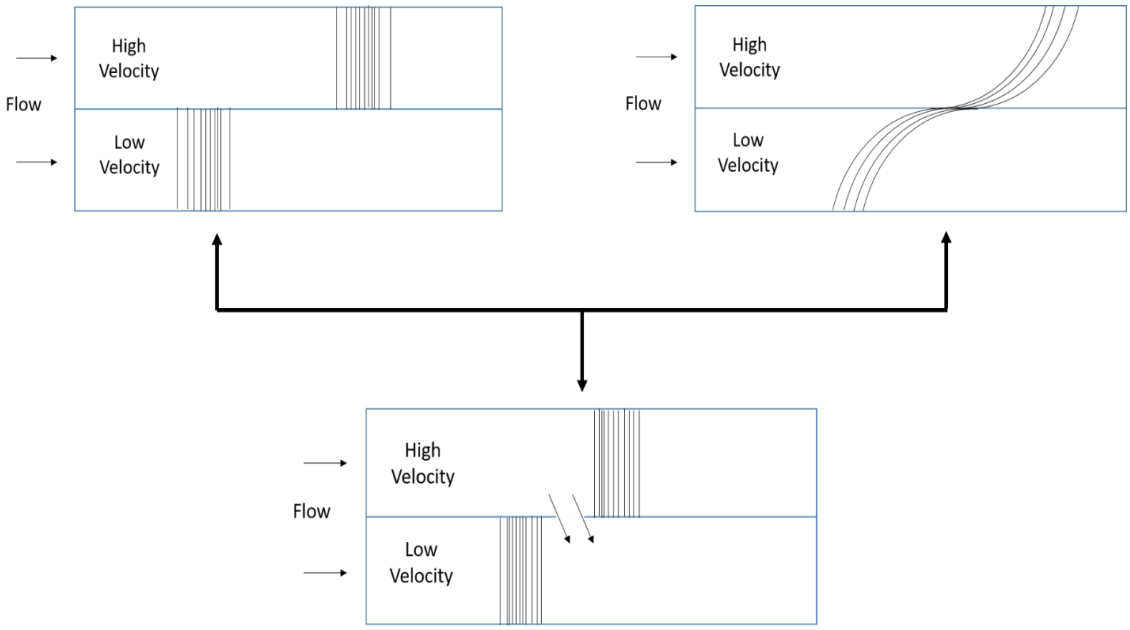

Figure 4-1 shows three schematic diagrams that address multi-peak tracer production history plots. (a) shows the layered system without any crossflow; (b) shows the layered system under vertical equilibrium. In other words, they are considered as continuous communication or vertical equilibrium; (c) shows ‘bridge’ crossflow can only be happened through the location of injectites, no vertical communication elsewhere.

Figure 4-2 Geology structure of Sand Injectites (Slatt, 2013)

In this paper, we propose a systematic approach to interpret ICTT and identify the bridge(s); simulation models and field examples are used to verify our method. The paper is structured as follows: Methodology; validation with numerical simulation; and field example.

4.2 Methodology

Tracer production history of a layered reservoir usually indicates more than one peak. It is well documented that flowing at various speeds through layers with different permeability is often result in different breakthrough time. The different breakthrough time can be detected as distinct peaks on the tracer history plots. We hypothesize in this work that the presence of cross flow through bridge(s) can affect the number of peaks in the history plot, depending upon the location of the bridge. For example, let's consider an ensample of two layers where permeability of the top layer is larger than that of the bottom layer. During tracer injection, tracer in the top layer will flow faster than tracer in the bottom layer. When tracer components arrive bridge in the high perm layer, the tracer crossflow will occur from the top layer toward the bottom layer. There are two possibilities: (1) the injected tracer component flowing through low permeable layer catch up the components transferred over from the top layer before they reach to the producer; in that case, the history plot will include one peak related to the high perm layer and a second peak with a prolong tail representing convoluted cross flow and the fluid flow through the low perm layer. This case is likely to take place when the bridge is located close to the injection well; (2) the injected tracer components flowing through low permeable layer do not catch up the components transferred over from the top layer before they reach to the producer; in that case, the history plot will include one peak related to

the high perm layer, the second peak attributed to the cross flow, and the third pick representing fluid flow through the low perm layer. This case is likely to take place when the bridge is located close to the production well.

Therefore, we hypothesize that total number of tracer peaks observed at the production history plot $\leqslant$ number of layers + number of bridge crossflow (Shen et al. 2017). For multi-layer reservoir system (**Figure 4-3**); we can divide the system into two pseudo-layers: the layer with the greatest permeability along the horizontal direction as pseudo-layer 1, and the remaining layers as pseudo-layer 2. Pseudo-layer 2, itself, can be an ensemble of several sub-layers and the methodology discussed here can be repeated internally.

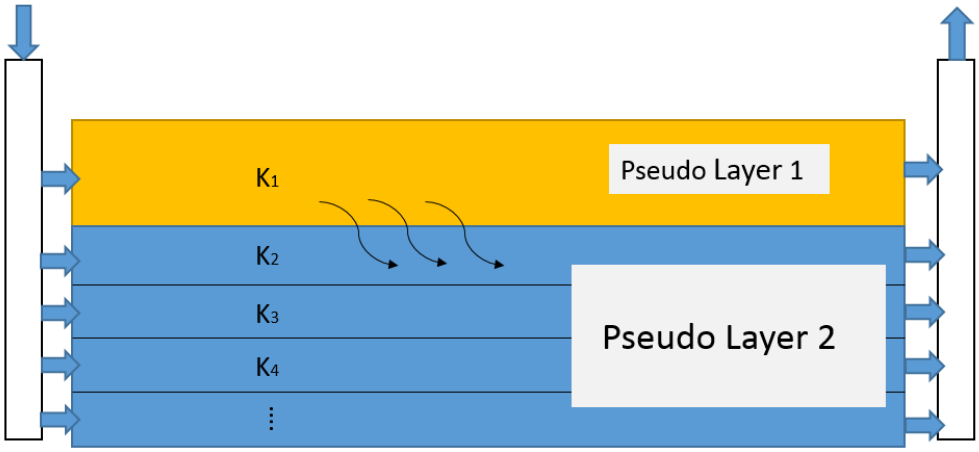

Figure 4-3: Schematic diagram of a layered reservoir. We divided the system into two pseudo-layers. Permeability in Pseudo Layer 1 (k_1) is the highest. The rest layers are regarded as Pseudo Layer 2. Tracer is injected from the left and produced from the right. Due to the crossflow, fluids from pseudo layer 1 flows into pseudo layer 2.

The following two equations explain the mass balance (in the absence of any chemical reaction) for conservative tracer flow (with unit mobility ratio and density ratio between injected fluid and the resident fluid) through a system of two layers (with

different permeability in the longitudinal direction but the same porosity) under isothermal, incompressible (both fluids and rock), and local equilibrium conditions:

Layer 1 $$\frac{\partial C_1}{\partial t_{D1}} + \frac{\partial C_1}{\partial x_D} - \alpha_{D1}\frac{\partial C_1^2}{\partial x_D^2} - f_{crossflow} = 0\,, \tag{4-1}$$

Layer 2 $$\frac{\partial C_2}{\partial t_{D2}} + \frac{\partial C_2}{\partial x_D} - \alpha_{D2}\frac{\partial C_2^2}{\partial x_D^2} + f_{crossflow} = 0\,, \tag{4-2}$$

Adding Eq. (4-1) and Eq. (4-2) yields:

$$\frac{\partial C_1}{\partial t_{D1}} + \frac{\partial C_2}{\partial t_{D2}} + (\frac{\partial C_1}{\partial x_D} + \frac{\partial C_2}{\partial x_D}) - \alpha_{D1}\frac{\partial C_1^2}{\partial x_D^2} - \alpha_{D2}\frac{\partial C_2^2}{\partial x_D^2} = 0, \tag{4-3}$$

where $C_{Di(i=1,2)}$ is the dimensionless racer concentration in each pseudo-layer;x_D is the dimensionless distance ($x_D = \frac{x}{L}$, where x is any distance, L is interwell spacing between injector and producer); $t_{Di(i=1,2)}$ is the dimensionless time (the porosity of both layers assumed to be the same); α_D represents dimensionless dispersivity and is equal to the inverse of Peclet number; $f_{crossflow}$ is the amount of crossflow through bridge and is cancelled out in Eq. (4-3) owing to the flow continuity between two layers. we define dimensionless time for each pseudo-layer as:

$$t_{D1} = F_1 * t_D, \tag{4-4}$$

$$t_{D2} = F_2 * t_D, \tag{4-5}$$

$$t_D = \frac{u_x t}{L} = \frac{qt}{A\phi L} = \frac{qt}{net\ swept\ volume}\,. \tag{4-6}$$

For calculation of t_{D1} and t_{D2}, we need to use the net sweep volume for low perm layer as it may vary based on the location of the bridge relative to the injector and the permeability ratios between two pseudo layers.

Since the fluid are incompressible, continuity equation implies that the velocity is constant spatially; moreover, we consider:

$$F_1 + F_2 = 1, \tag{4-7}$$

where F_1 and F_2 represent the dynamic fraction of injected fluid reaching at the producer through Pseudo-Layer 1 and Pseudo-Layer 2, respectively. F_1 and F_2 are functions of time and their variations with time represent cross flow between layers. Substituting Eq. (4-4) and (4-5) into Eq. (4-3) yields:

$$\left(\frac{1}{F_1}\right)\frac{\partial C_1}{\partial t_D} + \left(\frac{1}{F_2}\right)\frac{\partial C_2}{\partial t_{D2}} + \left(\frac{\partial C_1}{\partial x_{D1}} + \frac{\partial C_2}{\partial x_{D2}}\right) - \alpha_{D1}\frac{\partial C_1^2}{\partial x_D^2} - \alpha_{D2}\frac{\partial C_2^2}{\partial x_D^2} = 0. \tag{4-8}$$

Eq. (4-8) is impossible to solve because f_1 and f_2 are both functions of time. To solve this situation, we introduce the equation below. This equation provides approximate solutions. According to the mass balance theory,

$$C_{D_{produce}} * q_{prod.} = C_{D_1}F_1 * q_{prod.} + C_{D_2}F_2 * q_{prod.}, \tag{4-9}$$

Where, $C_{D_{produce}}$ is total dimensionless tracer concentration observed at the producer. Eq. (4-9) simply describes that total tracer concentration observed at the producer is the sum of contributions of each layer. Eq. (9) can be simplified as:

$$C_{D_{produce}} = C_{D_1}F_1 + C_{D_2}F_2, \tag{4-10}$$

Tracer component(s) is usually injected as a slug. We have boundary condition as listed below:

$$\begin{cases} C_D = 0 \ \ @\ t_D = 0\ ;\ \forall x_D \\ C_D = 1 \ \ @\ \ 0 < t_D \le t_{DS}\ ;\ x_D = 0 \\ C_D = 0 \ \ @\ \ t_{Ds} < t_D;\ x_D = 0 \end{cases}, \tag{4-11}$$

Where t_{DS} is the dimensionless slug injection time. Tracer concentration produced from the high perm pseudo-layer can be calculated using the solution of one-dimensional advection-dispersion equation (Lake 1989):

$$C_{D1} = -\frac{1}{2} erf\left(\frac{x_D - t_{D1}}{2\sqrt{\frac{t_{D1}}{N_{Pe}}}}\right) + \frac{1}{2} erf\left(\frac{x_D - (t_{D1} - t_{Ds1})}{2\sqrt{\frac{t_{D1} - t_{Ds1}}{N_{Pe}}}}\right), t_D > t_{Ds} \quad (4\text{-}12)$$

Where,

$$N_{Pe} = \frac{u_x L}{D_L} = \frac{qL}{A\phi D_L} = \frac{1}{\alpha_D}, \quad (4\text{-}13)$$

where N_{Pe} is the Peclet number, a dimensionless number which is the ratio of convection to diffusion transport mechanisms; α_D is the reciprocal of Peclet number. For the convenience of discussion, we use α_D instead of N_{Pe}. The amount of tracer slug size flowing through each layer will vary with time as crossflow occurs. We define t_{Ds1} and t_{Ds2} as the slug injection size for pseudo-layer 1 and pseudo-layer 2, accordingly.

The dimensionless concentration through low permeable pseudo-layer arrives later than the high permeable flow. Therefore, Eq. (12) is not applicable to describe tracer concentration in low permeable pseudo-layer. we need to subtract t_{D2} from t_{D1} in Eq. (12) to write dimensionless concentration for pseudo-layer 2:

$$C_{D2} = -\frac{1}{2}\mathrm{erf}\left(\frac{x_D - (t_{D1} - t_{D2})}{2\sqrt{\frac{t_{D1} - t_{D2}}{N_{Pe}}}}\right) + \frac{1}{2}\mathrm{erf}\left(\frac{x_D - (t_{D1} - t_{D2} - t_{Ds2})}{2\sqrt{\frac{t_{D1} - t_{D2} - t_{Ds2}}{N_{Pe}}}}\right), t_D > t_{Ds} \quad (4\text{-}14)$$

Eq. (4-12) and (4-14) provide the tracer concentration for each pseudo-layer. Total tracer concentration can be obtained from measured data at the designated producer (i.e; x_D=1.0). Therefore, F_1 or F_2 will be the only unknowns on RHS of Eq. (4-10), in case we

know the location of bridge(s) . However, F_1 and F_2 are related through Eq. (4-7) and add up to unity; thus, one can find the best match through trial and error through adjusting F_1 (and consequently F_2). The number of times F_1 changes as a functiuon of time reveals number of cross flows that take place. The remainder of paper examines the method.

4.3 Simulation Verification

4.3.1 Model Description

Numerical simulation in 2D (Figure 4-4) is used to verify the proposed approach using GEM software from Computer Modeling Group (CMG) reservoir simulator package. To clearly understand the methodology, we consider a simple schematic diagram shown in Figure 4-5
Figure **4-5**. **Figure 4-4** is the simulation model created in CMG according to

Figure 4-5. Our 2D model is 200 ft in length and 10 ft in thickness. Layer 1 has the thickness of 6 ft and Layer 2 has the thickness of 4 ft. The porosity of the system is uniformly 0.1. The horizontal permeability is 100 md for both layers (Instead of directly considering the effect of permeability heterogeneity on the fluid intake at the injection point, we set various injection rate through each layer). There is no vertical permeability which means there is no vertical equilibrium between two layers. We set the flow rate to be 0.9 bbl/day for Layer 1 and 0.1 bbl/day for Layer 2. Total production rate is 1 bbl/day, equal to total injection rate owing to incompressible assumption.

To create crossflow at specific location x_D as the bridge, we vertically refine the corresponding grid block in pseudo-layer 1 into 2 sub-grid blocks. Defining a fictitious producer in the lower sub-grid block (to represent fluid leaving the high perm layer) would allow the upper sub-grid block to maintain the fluid flow through pseudo-layer 1. Similarly, for pseudo-layer 2, we refine the corresponding grid block at the same x_D into 2 sub-grid blocks; this time, though, one fictitious injector is defined in the upper sub-grid block (representing fluid flow entering into low perm layer) while maintaining the

flow continuity from injector to producer through pseudo-layer 2 (**Figure 4-5**). We inject the same amount fluid produced from the fictitious producer defined in pseudo-layer 1 into pseudo-layer 2 through the fictitious injector; i.e. the production rate and injection rate are both 0.1 bbl/day.

With the above settings, we ensure that crossflow only occurs through a bridge as there is no vertical communication elsewhere. We study 3 cases with different bridge positions, x_D=0.1, x_D=0.5 and x_D=0.9. Tracer is injected as slug and followed by with water as chasing fluid. The injected concentration of tracer is 0.05% in mole fraction. The slug injection time is 2.5 days. Water saturation is 100%.

Table 4-1 details the other properties of simulations.

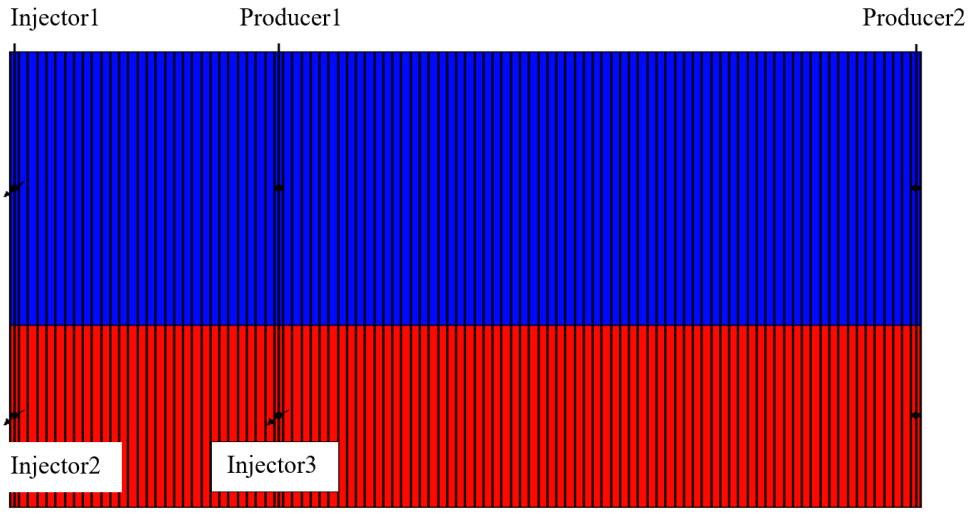

Figure 4-4: simulation model created by CMG.

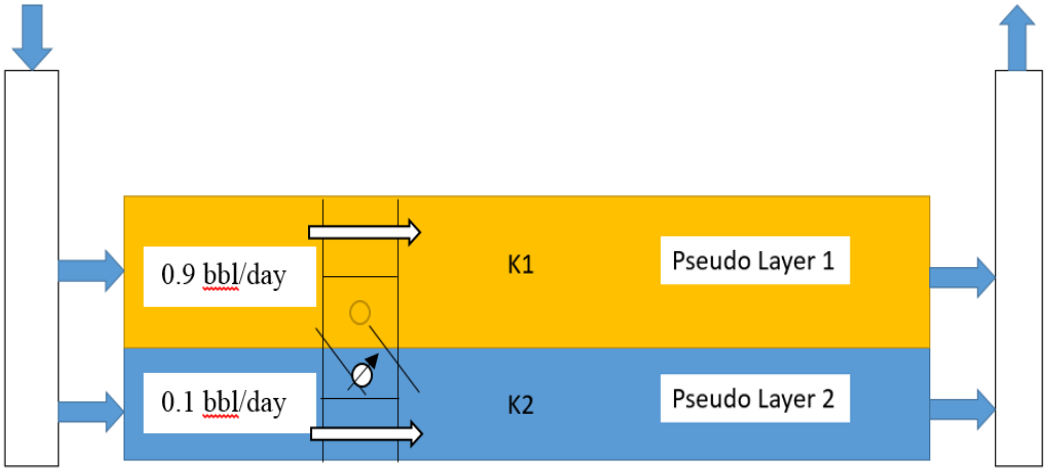

Figure 4-5: Schematic diagram of a layered reservoir. To mimic crossflow, we artificially create a 'bridge'. We choose location X_D=0.3 as the crossflow position. Refine the block in Layer 1 at X_D=0.3 into 2 blocks. Set one producer in the lower block, the upper block still allows the fluid flow through. For Layer 2, again refine the block into 2 blocks at same vertical position, set one injector on the upper block, fluid can flow through the lower block. We inject same amount fluid into Layer 2 as produced from Layer 1. The production rate is 0.1bbl/day and injection rate is 0.1bbl/day.

Table 4-1: Simulation model properties.

	Layer 1	Layer 2
Permeabiliy	100md	100md
Water Saturation	100%	
Flow rate,	0.9bbl/day	0.1
Thickness,	6 ft	4 ft
Length	200	
Width	2 ft	
Pressure	4925 psi	
Total production rate	1bbl/day	
Porosity	0.1	
Slug size	2.5 days	
Tracer Concentration	0.05%	

4.3.2 Simulation Result

Pseudo- layer 1 (Layer 1) is the high perm pseudo-layer. The ratio of injection rates through each layer (F_1 = 0.9 and F_2 = 0.1) can be considered as the initial guess for

dynamic fraction of injected volume produced from Pseudo- layer 1 and Pseudo- layer 2, respectively.

Figure 4-6 shows the comparison of our result and simulation data with bridge crossflow at x_D=0.1 (Case 1). The solid line represents our results and the dots represents the simulation results. Our method matches the simulation data very well. As we mentioned in the methodology part, our hypothesis is that number of tracer peaks $\leqslant$ number of layer + number of 'bridge' crossflow. There are only two peaks (equivalently, one step change is observed in **Figure 4-7**) observed in Case 1. The first peak is attributed to the tracer production from the high perm layer, while the second peak is the contribution of the both crossflow occurred at x_D=0.1 and the tracer flowing in low perm layer. The tracer components flowing through low perm layer in Case 1 catch up the transferred components via bridge. In this case $\alpha_D = 0.004$, t_{Ds1}=0.0468, t_{Ds2}=0.01.

Figure 4-7 shows how dynamic fraction of injected volume changes with time in Case 1. As mentioned above, the initial dynamic fraction of injected water into each layer are 0.9 and 0.1. However, since the bridge is located very close to the injector, fraction of the fluid injected into high perm layer quickly enters low perm layer through the bridge. Therefore, we need to adjust dynamic fractions of Layer 1 and Layer 2 to obtain the matched results. By trial and error, we found that the best match for dynamic fractions are F_1=0.8 and F_2=0.2. The reduction of dynamic fraction from original values (could be because of permeability difference in practice) explains the presence of bridge close to the injection well.

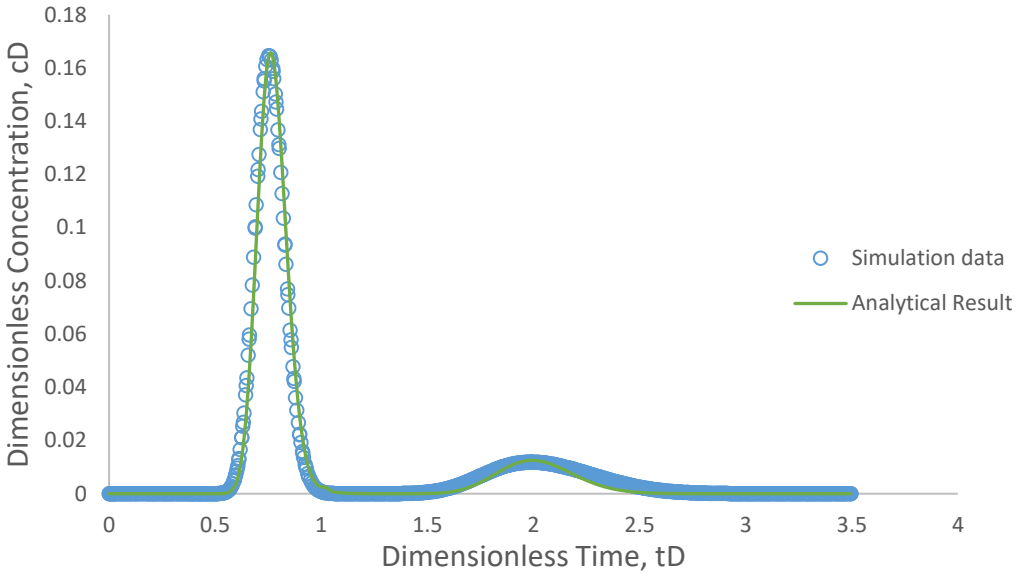

Figure 4-6: the comparison of our analytical result and simulation data with crossflow at location X_D=0.1. In this case α_D=0.004, t_{DS1}=0.0468, t_{DS2} =0.01.

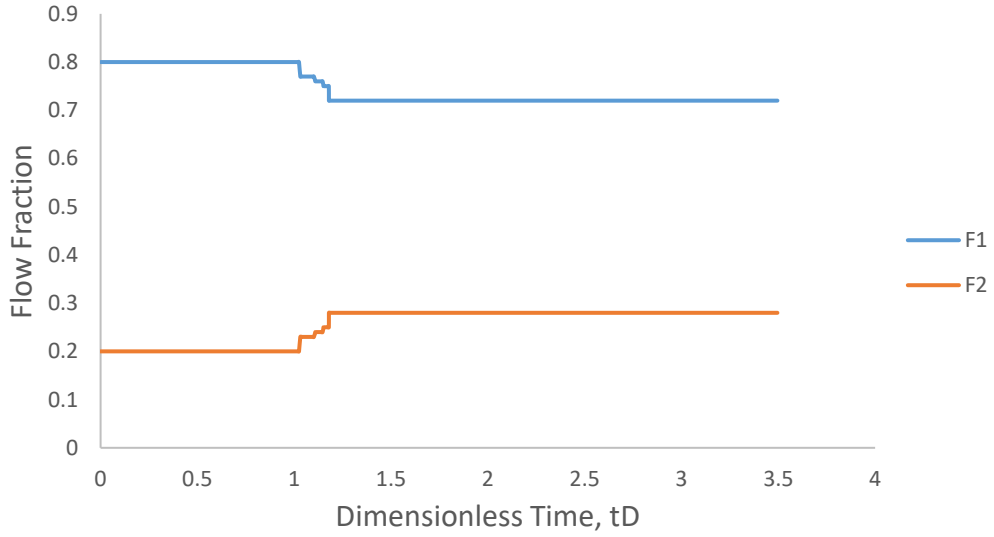

Figure 4-7 represents dynamic fraction of injected volume that is produced along with the producing time at location X_D=0.1. Dynamic fraction for Layer 1 changes from 0.8 to 0.72 and for Layer 2 changes from 0.2 to 0.28.

Figure 4-8 and **Figure 4-9** shows the results of Case 2 with bridge located at x_D = 0.5. Our method matches the simulation results quite well. Three peaks are observed in **Figure 4-8Error! Reference source not found.** (equivalently, two step changes are observed in **Figure 4-9**). First peak indicates contribution of Layer 1. Second peak is

caused by crossflow. Third peak is owing to tracer transport through Layer 2. **Figure 4-9** shows the changes in F_1 and F_2. Since bridge is in the middle of system, after adjusting dynamic fraction, the best match is obtained by F_1=0.85 and F_2=0.15.

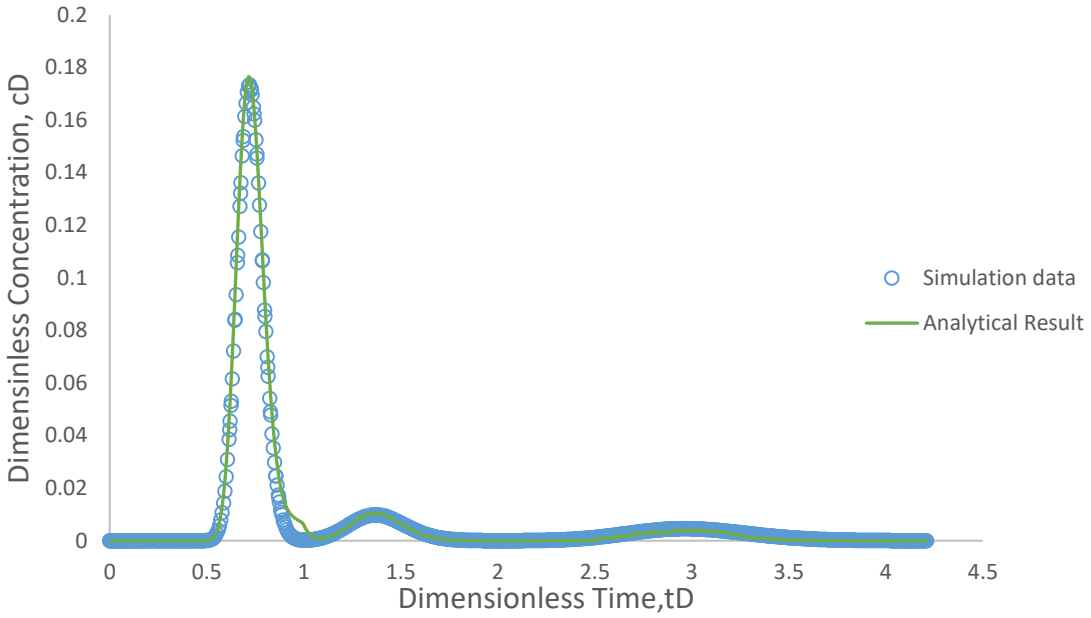

Figure 4-8: the comparison of our analytical result and simulation data with crossflow at location X_D=0.5. In this case α_D =0.0045, t_{DS1} = 0.0497, t_{DS2}=0.011.

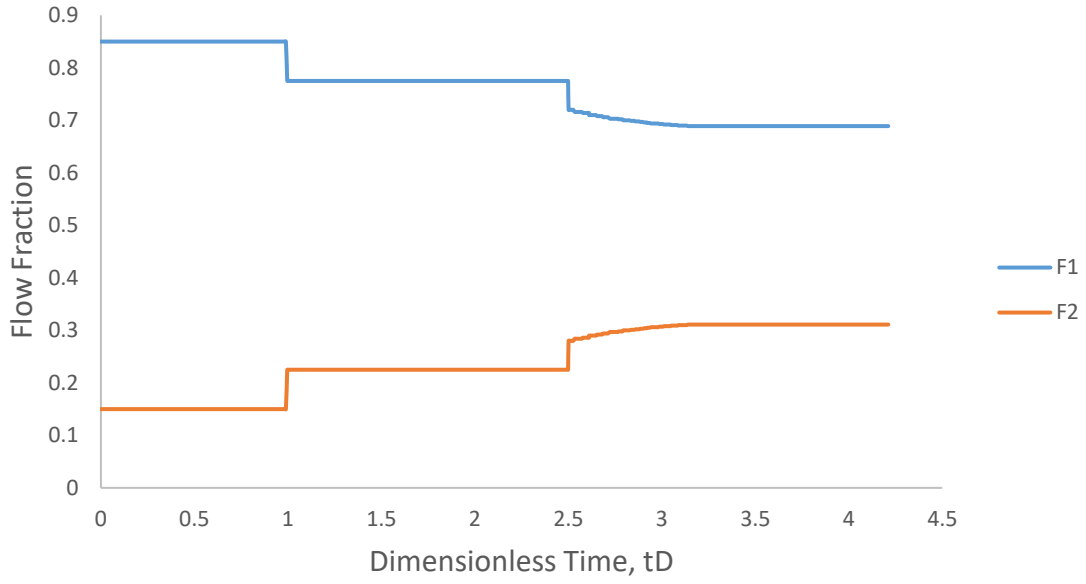

Figure 4-9 represents dynamic fraction of injected volume that is produced along with the producing time at location X_D=0.5. Dynamic fraction for Layer 1 changes from 0.85 to 0.689 and for Layer 2 changes from 0.15 to 0.311.

Figure 4-10 and **Figure 4-11** shows the interpretation of simulation model with limited crossflow located at x_D = 0.9. First peak is the outcome of tracer transport through high perm layer. The second peak is the representation of crossflow. Due to the low flow rate in low perm layer, dispersion mechanism is predominant and the third peak has a small amplitude. In Case 3, we found the best match with dynamic fractions of F_1=0.9, F_2=0.1 same as the injection ratio.

Through our proposed method, tracer test data were successfully used to detect crossflow. According to three cases discussed above, number of layers and number of bridges affects the number of peaks observed in the tracer history plot. Moreover, bridge location is an important factor which affects efficiency of the displacement. If the bridge is close to the injector, then the amount of injected fluid flowing through high perm layer will be less than initial estimation (owing to permeability difference between layers) since

part of injected fluid partitions through the bridge. When the bridge is close to the producer, impact of the crossflow is barely observed and the sweep efficiency will not be changed.

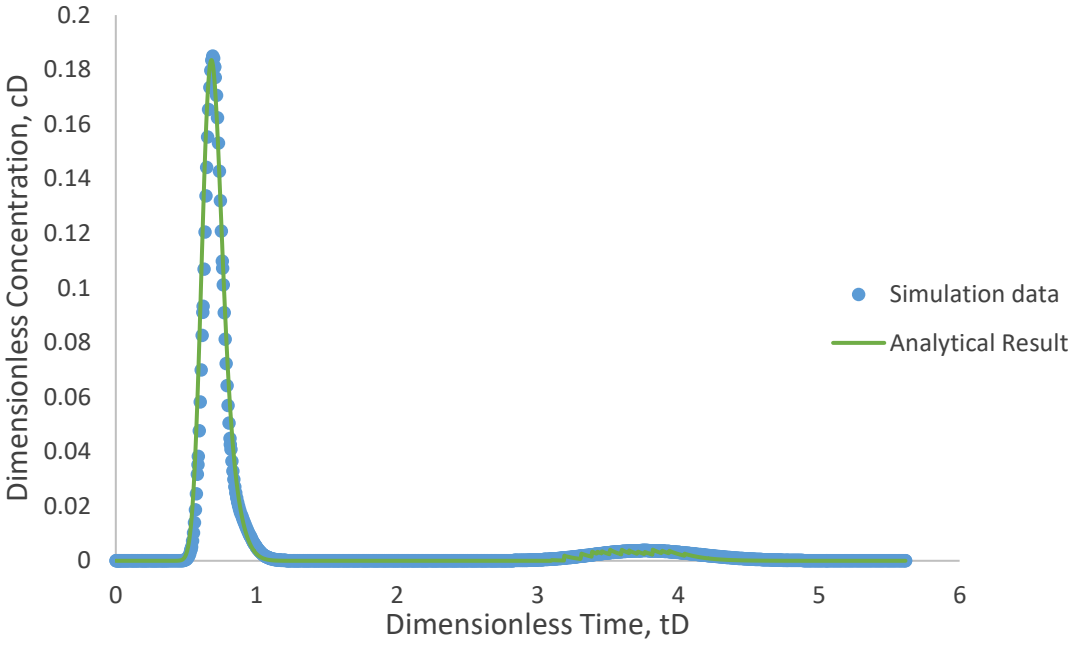

Figure 4-10 : the comparison of our analytical result and simulation data with crossflow at location X_D=0.9. In this case α_D =0.0055, t_{DS1}=0.0526, t_{DS2} =0.05.

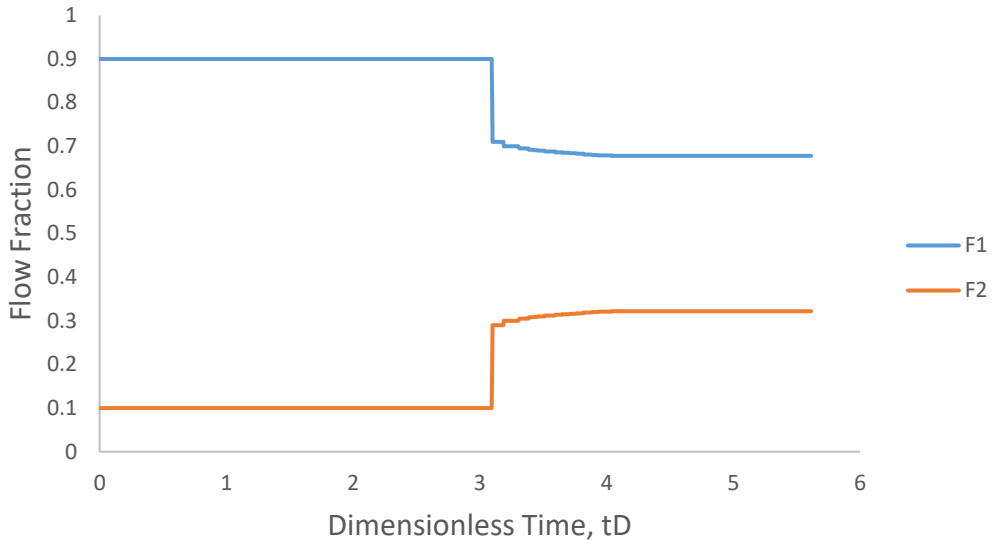

Figure 4-11 represents dynamic fraction of injected volume that is produced along with the producing time at location X_D=0.9. Dynamic fraction for Layer 1 changes from 0.9 to 0.678 and for Layer 2 changes from 0.1 to 0.322.

4.4 Field Application

The same field data (Ranger field) is used to verify our proposed method. As discussed in Chapter 3.8, well 37 and well 39 are multi-phase flow. Therefore, we need to adjust tracer arrival time.

With knowing time, dimensionless concentration, tracer injection rate (840 bbl/day), slug size (20 days), net sweep volume of well 37 (109700 bbls) and well 39 (55903 bbls), fraction of tracer producer from well 37 (0.41) and well 39 (0.18), t_{D1} and t_{D2} can be calculated by Eq. (4-4) and Eq. (4-5). However, only net swept volume for all layers is given, by trial and error, we found the ratio that layer 1 took from the total net sweep volume is 0.99 and layer 2 is 0.01.

4.4.1 Well 37

Two peaks were observed in Well 37. Thus, we divide the reservoir into two pseudo-layers and used our proposed method to analyze the test results. We adopt α_D of 0.025

following Shen et al. (2016); **Figure 4-12** compares the actual dimensionless conservative tracer concentration and the model prediction for well 37. Dots represent field data and solid lines represent the model prediction. The model clearly matches the field data, including the second peak.

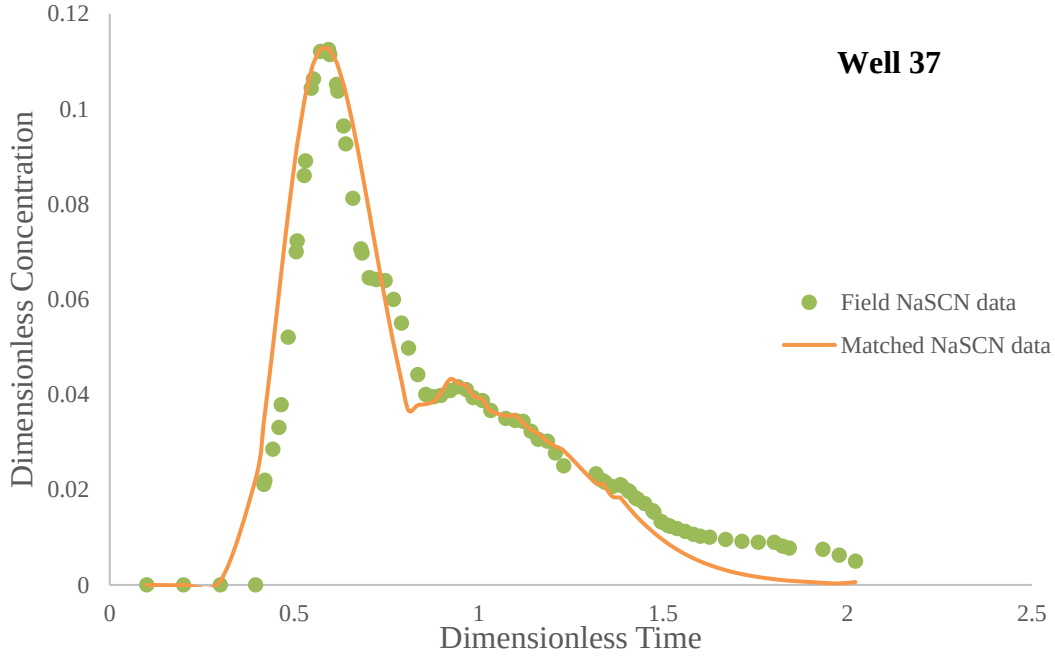

Figure 4-12: The comparison of field data with analytical solution for well 37.

Figure 4-13 illustrates the predicted dynamic fraction changes during the ICTT. Since this reservoir was a multi-layer system, tracer breaks through the high perm pseudo-layer very quickly and form the first peak. The initial dynamic flow fraction was 1 for pseudo-layer 1 (high permeable pseudo-layer). Later, due to crossflow between pseudo-layers, the tracer components start breaking through low permeable pseudo-layer. We call this time a transition period, from t_D = 0.7 to 1.45. In the transition period, the dynamic flow fraction of pseudo-layer 1 decreased. In other words, part of injected fluid originally

flowing through pseudo-layer 1 is diverted into pseudo-layer 2. After t_D =1.45, the dynamic flow fraction of both pseudo-layers stabilized again.

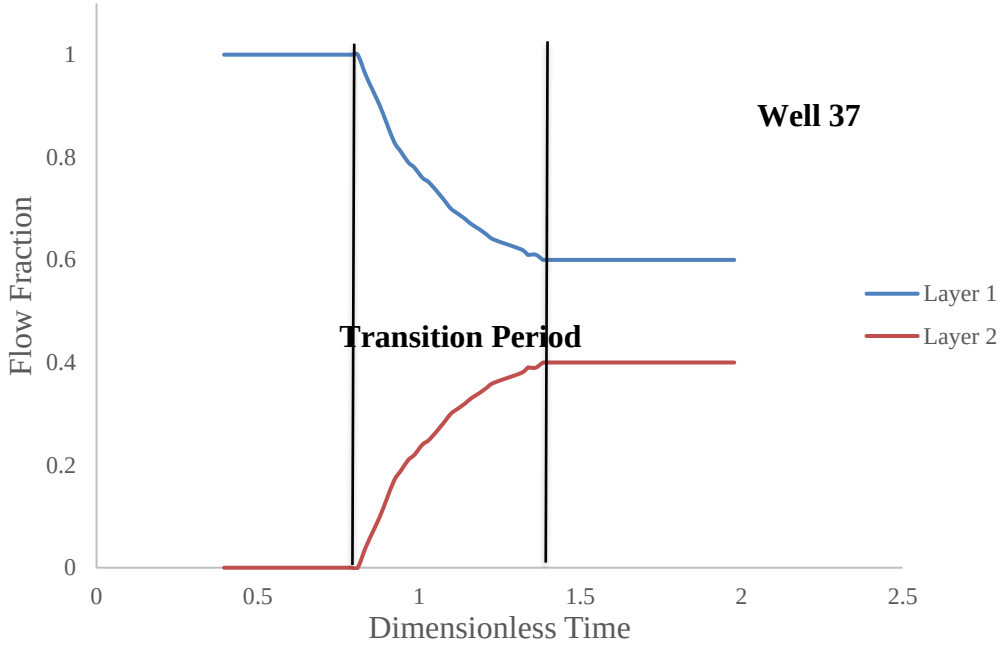

Figure 4-13: The dynamic fraction change for well 37.

4.4.2 Well 39

Figure 4-14 compares the actual data and the predicted values for Well 39. Dots represent field data and solid line represents the predicted values. Similar to Well 37, we adjust the tracer arriving time using Eq. (3-11), and then use $\alpha_D$value of 0.04 that yields the best match for the first peak (Shen et al. 2016). **Figure 4-14** shows the model fairly predicts the field data.

Figure 4-15 indicates that no crossflow was observed before 460 days. The transition period occurs during t_D=0.85 to 1. After t_D=1, both pseudo-layers became stable. Comparing **Figure 4-13** and **Figure 4-15**, we observe that it takes less time for well 39 to pass the transition period and establish a stable intake from the injector. This might be

due to multi-phase flow that occurs in the field during the test while the prediction model is based on single-phase.

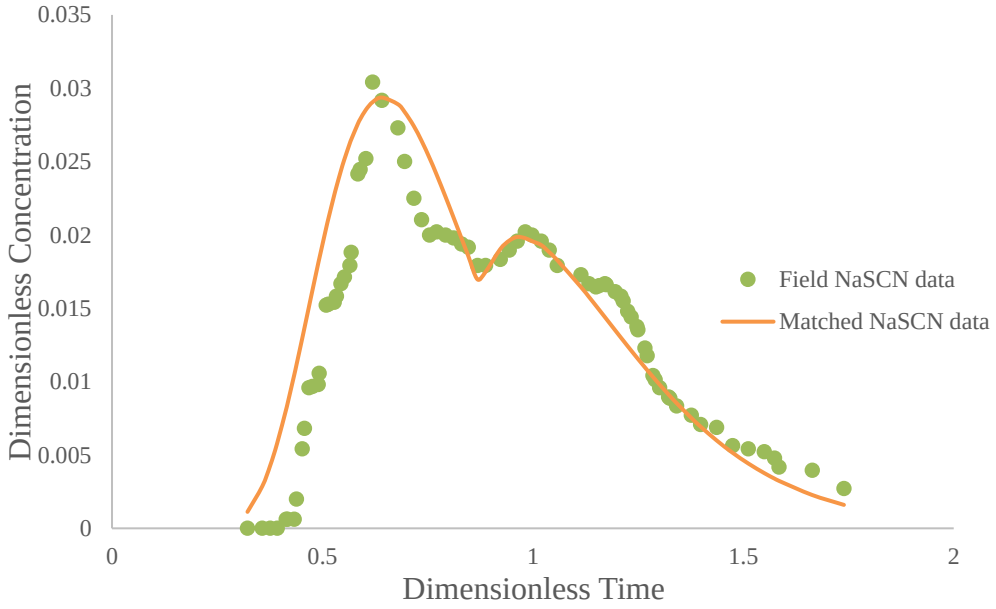

Figure 4-14: The comparison of field data with analytical solution for well 39.

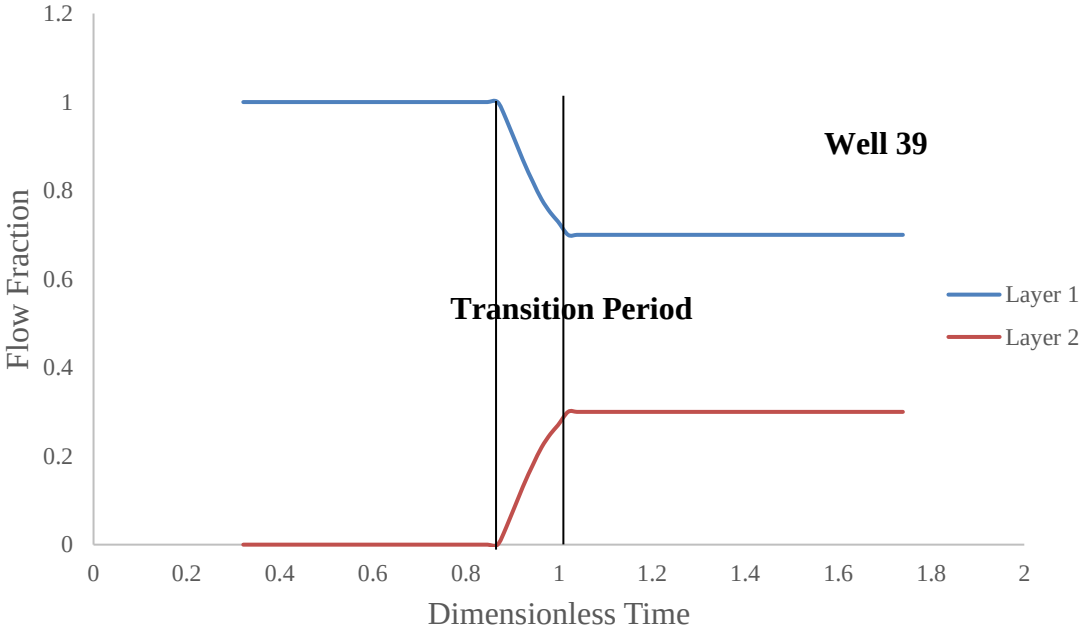

Figure 4-15: the tracer portion change in different layers for well 39.

4.5 Comparison with Published Work

Several investigators have previously interpreted the ICTT data in Ranger field through numerical simulation. Allison et al. (1991) used finite-difference compositional reservoir simulator to analyze the ICTT data (**Figure 4-16** (a) and (b)). In their simulation, they assumed three layers where each layer has constant thickness and permeability. Detailed properties are listed in **Table 4-2**. They achieved good match with field observations. Oyerinde (2004) adopted Allison's finite-difference method and combined with streamline simulation. He determined, for each well, an optimal shifting time to minimize the misfit between the simulated data and observed data. By defining a generalized travel-time, a match of tracer magnitude is easily achieved. **Figure 4-16** (c) and (d) represent Oyerinde's results after 11 iterations of inversion. Both numerical simulations included vertical dispersion and permeability and considered vertical equilibrium. However, they could not sufficiently capture the entire tracer production history, especially for the second peak. It is noted that Oyerinde's matching results are better than Allison's results.

Nevertheless, **Figure 4-16** (e) and (f) suggest that our model over-perform the previous predictions and result in better matching of the field data. The better match obtained for the second peak indicates that vertical equilibrium is not representing the actual crossflow in this field and limited crossflow seems more appropriate.

Table 4-2: Assumed properties.

	Thickness, ft	Permeability in x direction, md	Permeability in y direction, md	Permeability in z direction, md
Layer 1	11	75	150	7.5
Layer 2	7	500	1000	50
Layer 3	6	1250	2500	125

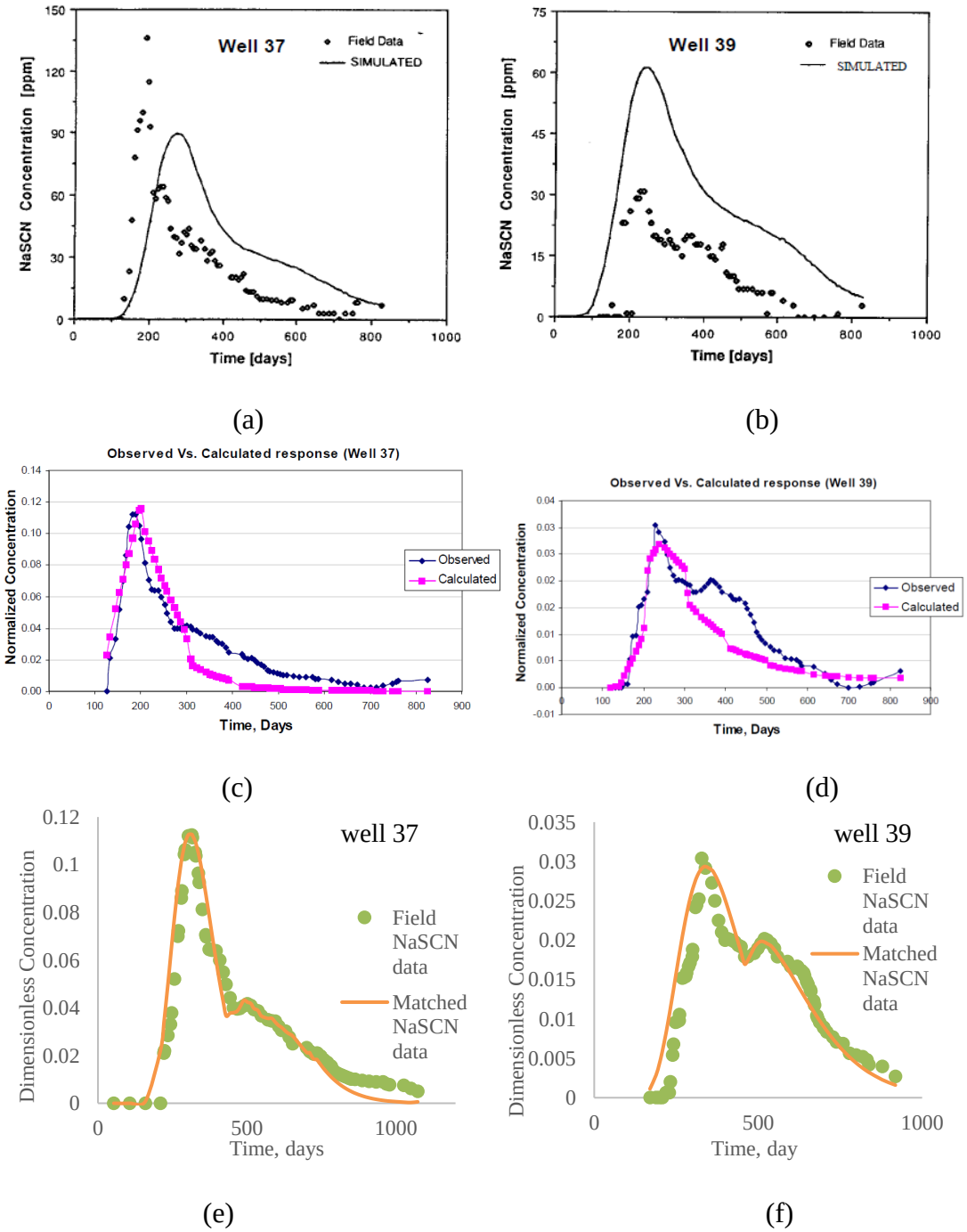

Figure 4-16: Simulation comparison for well 37 and 39. (a) and (b) represent the simulation results from Allison et al. (1991). (c) and (d) represents Oyerinde's results (2004). (c) and (d) represents our results.

4.6 Conclusions

In this study, we derived a new formulation to interpret ICTT considering limited crossflow through bridge(s). We employed both numerical simulation and field examples

to verify the proposed method. A transition period is identified during which bridge crossflow significantly changes the dynamic fraction of injected fluid flowing through each layer. The distance between injector and the bridge location can significantly change the interwell tracer results. Identification of crossflow between layers and evaluation of transition zone significantly the main conclusions are as follows:

1. For the first time, we evaluated and identified limited crossflow through a bridge using ICTT data. We identified and a transition period/specific feature through our proposed approach. Within the transition zone, dynamic layer fractions changes due to the presence of crossflow between layers.
2. Number of peaks observed in the tracer production history plot is representing the sum of number of layers and crossflow bridge (s). Traditionally, it was being thought that number of peaks is simply equal to the number of pseudo-layers. Moreover, it was shown here that the location of bridge significantly affect the production history data.

Chapter 5. Conclusions and Future Work

5.1 Conclusions

The following list entails a summary of key conclusions:

1. A modified version of convection-diffusion equation solution is examined to account for channeling in 2D flow. Using the proposed formulation, the fraction of layers in which the channeling may occurs is determined. Moreover, the ratio of sweep efficiency for heterogeneous reservoir to that of homogenous reservoir (channeling effect) was estimated using Koval factor.
2. Dispersion coefficient obtained in this study is overall larger than previously considered for miscible displacements in other studies; in addition, it almost remains constant irrespective to the problem size scale as inclusion of Koval factor into modified convection-diffusion solution takes care of spreading effects.
3. For the first time, a formulation is developed to interpret ICTT results while considering for crossflow impact. This formulation can detect and evaluate crossflow between heterogeneous layered systems using ICTT. It appears that number of peaks in concentration history plots is less than sum of numbers of layers and total numbers of crossflow bridges.
4. Location of crossflow channel is an important factor: if the crossflow bridge happens between the first tracer peak and the second peak, this crossflow will create a new peak. If the crossflow position happens during the first peak or second peak, the tracer concentration from the crossflow will add up either into the first peak tracer concentration or second peak tracer concentration, and as a result, only two peaks will be observed in the concentration effluent history. The

proposed method can be easily performed in spreadsheet with the limited data requirement.

5. For the first time, we identified a transition period/specific feature in the tracer production history indicating the existence of the crossflow. Within the transition zone, dynamic fraction of each layer changes because crossflow occurs.

5.2 Future Work

1. Our proposed method can detect and evaluate crossflow between heterogeneous layered systems using ICTT. However, how to find the accurate crossflow position will be our future work.
2. With knowing the total net sweep volume, finding the accurate ratio of net sweep volume for each layer is also important to be determined in the future.

References

Allison, S.B., Pope, G.A. and Sepehrnoori, K., 1991. Analysis of field tracers for reservoir description. *Journal of Petroleum Science and Engineering*, **5**(2), pp.173-186.

Asakawa. K 2005, *A generalized Analysis of Partitioning Interwell Tracer Tests*, PhD dissertation, The University of Texas Austin, Austin, Texas (December 2005)

Barnes, E.W., 1908. A new development of the theory of the hypergeometric functions. *Proceedings of the London Mathematical Society*, **2**(1), pp.141-177.

Brigham, W.E. and Smith Jr, D.H., 1965. Prediction of tracer behavior in five-spot flow. Presented at SPE symposium on Production Research and Engineering, Tulsa, Oklahoma, 3-4 May. SPE-1130-MS.

Buckley, S.E. and Leverett, M., 1942. Mechanism of fluid displacement in sands. *Transactions of the AIME*, **146**(01), pp.107-116.

Castiglione, P., Mazzino, A., Muratore-Ginanneschi, P. and Vulpiani, A., 1999. On strong anomalous diffusion. *Physica D: Nonlinear Phenomena*, **134**(1), pp.75-93.

Crank, J., 1979. *The mathematics of diffusion*, second edition. Oxford university press.

Coats, K.H., Whitson, C.H. and Thomas, K., 2009. Modeling conformance as dispersion. *SPE Res Eval & Eng*, **12**(01), pp.33-47.

Dagan, G., 2012. *Flow and transport in porous formations*. Springer Science & Business Media.

Dagan, G., 1982. Stochastic modeling of groundwater flow by unconditional and conditional probabilities: 1. Conditional simulation and the direct problem. *Water Resources Research*, **18**(4), pp.813-833.

Datta-Gupta, A., Yoon, S., Vasco, D.W. and Pope, G.A., 2002. Inverse modeling of partitioning interwell tracer tests: A streamline approach. *Water Resources Research*, **38**(6).

Dean, R.M., Walker, D.L., Dwarakanath, V., Malik, T. and Spilker, K., 2016. Use of Partitioning Tracers to Estimate Oil Saturation Distribution in Heterogeneous Reservoirs. Presented at SPE symposium on Improved Oil Recovery, Tulsa, Oklahoma, 11-13 April. SPE-179655-MS.

Deans, H.A., 1978. Using chemical tracers to measure fractional flow and saturation in-situ. Presented at SPE symposium on Improved methods of Oil Recovery, Tulsa, Oklahoma, 16-17 April. SPE-7076-MS.

Dentz, M. and Carrera, J., 2007. Mixing and spreading in stratified flow. *Physics of Fluids*, **19**(1), p.017107.

Devegowda, D., Akella, S., Datta-Gupta, A. and Efendiev, Y., 2009. Interpretation of Partitioning Interwell Tracer Tests Using EnKF with Coarse Scale Constraints. Presented in SPE symposium on Reservoir Simulation. The Woodlands, Texas, 2-4 February. SPE-119125-MS.

Divine, C.E. and McDonnell, J.J., 2005. The future of applied tracers in hydrogeology. *Hydrogeology journal*, **13**(1), pp.255-258.

Du, Y. and Guan, L., 2005. Interwell tracer tests: lessons learnted from past field studies. Presented in SPE symposium on Asia Pacific Oil and Gas Conference and Exhibition, Jakarta, Indonesia, 5-7 April. SPE-93140-MS. https://doi-org.ezproxy.lib.ou.edu/10.2118/93140-MS

Dugstad, O., Krognes, B., Juilla, H., Kleven, R., Renouf, P., Viig, S.O. and Huseby, O.K., 2013. Application of a new class of chemical tracers to measure oil saturation in partitioning interwell tracer tests. Presented in SPE symposium on Oilfield Chemistry, The Woodlands, Texas, 8-10 April. SPE-164059-MS. https://doi-org.ezproxy.lib.ou.edu/10.2118/164059-MS

Dykstra, H. and Parsons, R.L., 1950. The prediction of oil recovery by waterflood. *Secondary recovery of oil in the United States*, **2**, pp.160-174.

Fiori, A. and Dagan, G., 2002. Transport of a passive scalar in a stratified porous medium. *Transport in porous media*, **47**(1), pp.81-98.

Gelhar, L.W. and Axness, C.L., 1983. Three-dimensional stochastic analysis of macrodispersion in aquifers. *Water Resources Research*, **19**(1), pp.161-180.

Gelhar, L.J., Gutjahr, A.L. and Naff, R.L. 1979. Stochastic Analysis of Macrodispersion in a Stratified Aquifer. *Water Resources Research* **15**: 1387–1397.

Ghanbarnezhad, R. and Lake, L.W., 2012. Applying Fractional-Flow Theory Under the Loss of Miscibility. *SPE J.*, **17**(03), pp.661-670.

Ghanbarnezhad Moghanloo, R. 2012. *Modeling the Fluid Flow of Carbon Dioxide through Permeable Media*. PhD dissertation, University of Texas, Austin, Texas.

Ghanbarnezhad Moghanloo, R., 2012. A New Formulation for Decoupling of Large and Small Scale Heterogeneities in Multi Layered Reservoirs. Presented in SPE symposium on Improved Oil Recovery, Tulsa, Oklahoma, 14-18 April. SPE-154113-MS. https://doi-org.ezproxy.lib.ou.edu/10.2118/154113-MS

Greenkorn, R.A., 1983. *Flow phenomena in porous media: fundamentals and applications in petroleum, water and food production.* New York: Marcel Dekker

Iliassov, P.A., 2000. *Inversion of field-scale partitioning tracer response for characterizing oil saturation distribution: a streamline approach*. PhD dissertation, Texas A&M University, College Station, Texas.

Jennings Jr, J.W. and Ward, W.B., 2000. Geostatistical analysis of permeability data and modeling of fluid-flow effects in carbonate outcrops. *SPE Res Eval & Eng*, **3**(04), pp.292-303.

Jin, M., Delshad, M., Dwarakanath, V., McKinney, D.C., Pope, G.A., Sepehrnoori, K., Tilburg, C.E. and Jackson, R.E., 1995. Partitioning tracer test for detection, estimation, and remediation performance assessment of subsurface nonaqueous phase liquids. *Water Resources Research*, **31**(5), pp.1201-1211.

Johns, R.T. and Garmeh, G., 2010. Upscaling of miscible floods in heterogeneous reservoirs considering reservoir mixing. *SPE Reservoir Evaluation & Engineering*, **13**(05), pp.747-763.

John, A.K. 2008. *Dispersion in Large Scale Permeable Media*. PhD dissertation, University of Texas, Austin, Texas.

Lichtenberger, G.J., 1991. Field applications of interwell tracers for reservoir characterization of enhanced oil recovery pilot areas. Presented in SPE symposium on *Production Operations*, Oklahoma City, Oklahoma, 7-9 April. SPE-21652-MS. https://doi-org.ezproxy.lib.ou.edu/10.2118/21652-MS

Lake, L.W. 1989. *Enhanced Oil Recovery*. Englewood Cliffs, New Jersey: Prentice Hall.

Lake, L.W. and Hirasaki, G.J., 1981. Taylor's dispersion in stratified porous media. *Society of Petroleum Engineers Journal*, **21**(04), pp.459-468.

Liu, J., Parker, E.D. and Camilleri, D., 1999. A new particle tracking algorithm for tracer flow simulation. Presented in SPE symposium on reservoir simulation, Houston, Texas, 14-17 February. SPE-51905-MS.

Mahadevan, J., Lake, L.W. and Johns, R.T., 2003. Estimation of true dispersivity in field-scale permeable media. *SPE J.*, **8**(03), pp.272-279.

Maroongroge, V., 1994. *Modeling and Application of Tracers for Reservoir Characterization*, PhD Dissertation, University of Texas Austin, Austin, Texas.

Matheron, G. and De Marsily, G., 1980. Is transport in porous media always diffusive? A counterexample. *Water Resources Research*, **16**(5), pp.901-917.

Moghanloo, R.G., 2011. Numerical Dispersion Impact on Local Mixing in Heterogeneous Reservoirs. Presented in SPE symposium on *Eastern Regional Meeting*, Columbus, Ohio, 17-19 August. SPE-149420-MS. https://doi-org.ezproxy.lib.ou.edu/10.2118/149420-MS

Moghanloo, R.G. and Lake, L.W., 2011. A Regime Indicator for Flow Through Heterogeneous Permeable Media. Presented in SPE Annual Technical Conference and Exhibition, Denver, Colorado, 30 October- 2 November. SPE-146370-MS. https://doi-org.ezproxy.lib.ou.edu/10.2118/146370-MS

Neuman, S.P. and Tartakovsky, D.M., 2009. Perspective on theories of non-Fickian transport in heterogeneous media. *Advances in Water Resources*, **32**(5), pp.670-680.

Orr, F.M.J. 2007. *The Theory of Gas Injection Processes*. Copenhagen, Denmark: Tie-Line Publications.

Oyerinde, A. S. 2004. *A composite tracer analysis approach to reservoir characterization*. M.S. Thesis, Texas A&M University, College Station, Texas.

Rahmani, A.R., Bryant, S.L., Huh, C., Ahmadian, M., Zhang, W. and Liu, Q.H., 2015. Characterizing reservoir heterogeneities using magnetic nanoparticles. Presented in SPE symposium on Reservoir Simulation, Houston, Texas, 23-25 February. SPE-173195-MS. https://doi-org.ezproxy.lib.ou.edu/10.2118/173195-MS

Sanni, M.L., Al-Abbad, M.A., Kokal, S.L., Hartvig, S., Olaf, H. and Jevanord, K., 2015, April. A Field Case Study of Inter-well Chemical Tracer Test. Presented in SPE

International Symposium on Oilfield Chemistry, The Woodlands, Texas, 13-15 April. SPE-173760-MS. https://doi-org.ezproxy.lib.ou.edu/10.2118/173760-MS

Serres-Piole, C., Preud'Homme, H., Moradi-Tehrani, N., Allanic, C., Jullia, H. and Lobinski, R., 2012. Water tracers in oilfield applications: guidelines. *Journal of Petroleum Science and Engineering*, **98**, pp.22-39.

Sharma, A., Shook, G.M. and Pope, G.A., 2014. Rapid analysis of tracers for use in EOR flood optimization. Presented in SPE symposium on Improved Oil Recovery, Tulsa, Oklahoma, 12-16 April. SPE-169109-MS. https://doi-org.ezproxy.lib.ou.edu/10.2118/169109-MS

Shen, T., Rouzbeh, G. M., and Tian, W. 2016. Contribution of Dispersion and Permeability Variation on Propagation of Tracer Concentration in Permeable Media . IPTC-18954-MS. Presented at the International Petroleum Technology Conference, 13-16 November, Bangkok, Thailand. IPTC-18954-MS. https://doi-org.ezproxy.lib.ou.edu/10.2523/IPTC-18954-MS

Shen, T., Tian, W., and Rouzbeh, G. M. 2017. Interpretation of Inter-Well Chemical Tracer Tests in Layered Heterogeneous Reservoirs with Crossflow. Presented at SPE Annual Technical Conference and Exhibition, 09-11 October, San Antonio, TX. USA. SPE-187400-MS.

Shook, G.M., Pope, G.A. and Asakawa, K., 2009, January. Determining reservoir properties and flood performance from tracer test analysis. Presented in SPE Annual Technical Conference and Exhibition, New Orleans, Louisiana, 4-7 October. SPE-124614-MS. https://doi-org.ezproxy.lib.ou.edu/10.2118/124614-MS

Shook, G.M., 2003. A simple, fast method of estimating fractured reservoir geometry from tracer tests. *Geothermal Resources Council Transactions*, **27**, pp.407-411.

Shook, G.M. and Forsmann, J.H., 2005. *Tracer interpretation using temporal moments on a spreadsheet*. Idaho National Laboratory.

Shook, G.M., Sharma, A. and Pope, G., 2016. Early-Time Analysis of Tracers for Use in Enhanced-Oil-Recovery Flood Optimization. *SPE Res Eval & Eng*.

Sinha, R., Asakawa, K., Pope, G.A. and Sepehrnoori, K., 2004. Simulation of natural and partitioning interwell tracers to calculate saturation and swept volumes in oil

reservoirs. Presented in SPE symposium on Improved Oil Recovery, Tulsa, Oklahoma, 17-21 April. SPE-89458-MS.

Sposito, G. and Dagan, G., 1994. Predicting solute plume evolution in heterogeneous porous formations. *Water resources research*, **30**(2), pp.585-589.

Stalgorova, E., 2011. *Core and field scale modeling of miscible injection processes in fractured porous media using Random Walk and Particle Tracking methods*. MS thesis, University of Alberta, Edmonton, Canada (November 2011)

Stalgorova, E. and Babadagli, T., 2010. Modeling miscible injection in fractured porous media using non-classical simulation approaches. Presented in SPE Russian Oil and Gas Conference and Exhibition, Moscow, Russia, 26-28 October. SPE-135903-MS. https://doi-org.ezproxy.lib.ou.edu/10.2118/135903-MS

Su, N., Sander, G.C., Liu, F., Anh, V. and Barry, D.A., 2005. Similarity solutions for solute transport in fractal porous media using a time-and scale-dependent dispersivity. *Applied mathematical modelling*, **29**(9), pp.852-870.

Tang, J.S., 1992. Interwell Tracer Tests to Determine Residual Oil Saturation to Waterflood at Judy Creek Bhl'a'pool. *Journal of Canadian Petroleum Technology*, **31**(08).

Tang, J.S., 1995. Partitioning tracers and in-situ fluid saturation measurements. *SPE Formation Evaluation*, **10**(01), pp.33-39.

Tang, J.S. and Zhang, P.X., 2000. Effect of mobile oil on residual oil saturation measurement by interwell tracing method. Presented in International Oil and Gas Conference and Exhibition, Beijing China, 7-19 November. SPE-64627-MS. https://doi-org.ezproxy.lib.ou.edu/10.2118/64627-MS

Tang, J.S. and Harker, B., 1991. Interwell tracer test to determine residual oil saturation in a gas-saturated reservoir. Part II: Field applications. *Journal of Canadian Petroleum Technology*, **30**(04).

Tang, J.S., 2003, January. Extended Brigham model for residual oil saturation measurement by partitioning tracer tests. Presented in SPE International Improved Oil Recovery Conference in Asia Pacific, Kuala Lumpur, Malaysia, 20-21 October. SPE-84874-MS. https://doi-org.ezproxy.lib.ou.edu/10.2118/84874-MS

Tian, W., Wu, X., Shen, T., et al. 2016. Estimation of hydraulic fracture volume utilizing partitioning chemical tracer in shale gas formation. *Journal of Natural Gas Science and Engineering*, **33**: 1069-1077.

Tian, W. 2017. Improved Method of Moments to Determine Mobile Phase Saturations with Single Well Chemical Tracer Test. Presented at SPE Annual Technical Conference and Exhibition, San Antonio, Texas, 9-11 October.

Thierrin, J. and Kitanidis, P.K., 1994. Solute dilution at the Borden and Cape Cod groundwater tracer tests. *Water resources research*, **30**(11), pp.2883-2890.

Thiele, M.R., Batycky, R.P. and Fenwick, D.H., 2010. Streamline simulation for modern reservoir-engineering workflows. *J Pet Technol*, **62**(01), pp.64-70.

Yi, T., Daltaban, T.S. and Archer, J.S., 1994. Analysis of Interwell Tracer Flow Behaviour in Transient Two-phase Heterogeneous Reservoirs Using Mixed Finite Element Methods and the Random Walk Approach. Presented in European Petroleum Conference, London, United Kingdom, 25-27 October. SPE-28901-MS. https://doi-org.ezproxy.lib.ou.edu/10.2118/28901-MS

Zavala-Sanchez, V., Dentz, M. and Sanchez-Vila, X., 2009. Characterization of mixing and spreading in a bounded stratified medium. *Advances in water resources*, **32**(5), pp.635-648.

Zhou, Q., Liu, H.H., Molz, F.J., Zhang, Y. and Bodvarsson, G.S., 2007. Field-scale effective matrix diffusion coefficient for fractured rock: Results from literature survey. *Journal of Contaminant Hydrology*, **93**(1), pp.161-187.

Appendix A: Analytic Solution Derivative

In this appendix, an analytic solution is derived to determine the vertically averaged dimensionless concentration as a function of X_D, t_D, H_K, and α_D. The integration of $c_D|_C$ over an interval $[C_1, C_2]$ yields the vertically averaged concentration (according to the integral mean value theorem):

$$c_D = \frac{\int_{C_1}^{C_2} c_D|_C \, dC}{C_2 - C_1} \quad . \tag{A.1}$$

Thus, the first step to solve Eq. (A.1) is to determine the derivative of F with respect to C, $\frac{dF}{dC}$. Using the Koval (1963) heterogeneity factor, the following relationship between F and C holds true:

$$\frac{F}{1-F} = \frac{C}{1-C} H_K \, . \tag{A.2}$$

Where H_k is the Koval heterogeneity factor. Inverting Eq. (A.2) gives:

$$\frac{1-F}{F} == \frac{1-C}{C} H_K \, . \tag{A.3}$$

Hence, F can be expressed as:

$$F = \frac{C}{1-C+CH_K} H_K \tag{A.4}$$

Differentiation of F with respect to C yields an expression for $\frac{dF}{dC}$ as:

$$\frac{dF}{dC} = \frac{H_K}{\left[1+(H_K-1)C\right]^2} \quad . \tag{A.5}$$

All terms on the right side of Eq. (A.5) are positive; hence, the square root of $\frac{dF}{dC}$ can be expressed as:

$$\sqrt{\frac{dF}{dC}} = \frac{\sqrt{H_K}}{\left[1+(H_K-1)C\right]} \quad . \tag{A.6}$$

The next step is to insert Eq. (A.6) into Eq. (5) to determine the integration of the numerator of Eq. (A.1). However, there is no analytic solution for Eq. (A.1) in the standard integral tables. Therefore, we use the method of variable transformation (the substitution rule) and consider the argument of the error function as interim variable z:

$$z = \frac{x_D}{2\sqrt{\alpha_D \frac{dF}{dC} t_D}} - \frac{\sqrt{\frac{dF}{dC} t_D}}{2\sqrt{\alpha_D}} \quad . \tag{A.7}$$

Rearranging Eq. (A.7) gives:

$$t_D\left(\sqrt{\frac{dF}{dC}}\right)^2 + 2\sqrt{\alpha_D t_D}\, z\sqrt{\frac{dF}{dC}} - x_D = 0 \quad . \tag{A.8}$$

However, there are two roots (described below) and the non-negative solution of the quadratic equation (because $\sqrt{\frac{dF}{dC}}$ is always positive) that represents a proper relation between the newly defined variable z and $\frac{dF}{dC}$. The general form of the solution of Eq. (A.8) is defined as:

$$\sqrt{\frac{dF}{dC}} = \frac{-b \pm \sqrt{b^2 - 4ac}}{2a} \quad , \tag{A.9}$$

Where

$$a = t_D$$

$$b = 2\sqrt{\alpha_D t_D}\, z$$

$$c = -x_D \quad .$$

Further investigation shows that the root with a positive square root of the discriminant always leads to the non-negative solution. Therefore:

$$\sqrt{\frac{dF}{dC}} = \frac{-\sqrt{\alpha_D t_D}\, z + \sqrt{\left(\sqrt{\alpha_D t_D}\, z\right)^2 + t_D x_D}}{t_D} \quad . \tag{A.10}$$

Next, we insert Eq. (A.10) into Eq. (A.6) to determine the relation between cumulative storage capacity C and z:

$$\frac{\sqrt{H_K}}{\left[1+(H_K-1)C\right]} = \frac{-\sqrt{\alpha_D t_D}\, z + \sqrt{\left(\sqrt{\alpha_D t_D}\, z\right)^2 + t_D x_D}}{t_D}. \tag{A.11}$$

Rearranging Eq. (A.11) yields an expression for the cumulative storage capacity as a function of X_D and t_D:

$$C = \frac{1}{(H_K-1)}\left(\frac{t_D\sqrt{H_K}}{\left(-\sqrt{\alpha_D t_D}\, z + \sqrt{\left(\sqrt{\alpha_D t_D}\, z\right)^2 + t_D x_D}\right)} - 1 \right). \tag{A.12}$$

Also, we recast the integral in the numerator of Eq. (A.1) using the variable transformation. To determine the derivative with respect to the newly defined variable, we use the chain rule as

$$\boldsymbol{c}_D = \frac{\int_{C_1}^{C_2} c_D\,|_C\, dC}{C_2 - C_1} = \frac{\int_{z_1}^{z_2} c_D\,|_z\, dz \dfrac{dC}{dz}}{z_2 - z_1} \tag{A.13}$$

To evaluate the above equation, we must determine the derivative of C with respect to z, $\left(\frac{dC}{dz}\right)$, which can be expressed as:

$$\frac{dC}{dz}=\frac{t_D\sqrt{H_K}}{(H_K-1)}\left(\frac{\sqrt{\alpha_D t_D}-\frac{z\alpha_D t_D}{\sqrt{\left(\sqrt{\alpha_D t_D}\,z\right)^2+t_D x_D}}}{\left(-\sqrt{\alpha_D t_D}\,z+\sqrt{\left(\sqrt{\alpha_D t_D}\,z\right)^2+t_D x_D}\right)^2}\right) \quad . \qquad \text{(A.14)}$$

Still, there is no general equation for the integral in the numerator of Eq.(A.13):

$$\int_{z_1}^{z_2} c_D\,|_z\,\frac{dC}{dz}dz=0.5\int_{z_1}^{z2}\left(1-Erf\,(z)\right)\frac{t_D\sqrt{H_K}}{(H_K-1)}\left(\frac{\sqrt{\alpha_D t_D}-\frac{z\alpha_D t_D}{\sqrt{\left(\sqrt{\alpha_D t_D}\,z\right)^2+t_D x_D}}}{\left(-\sqrt{\alpha_D t_D}\,z+\sqrt{\left(\sqrt{\alpha_D t_D}\,z\right)^2+t_D x_D}\right)^2}\right)dz. \quad \text{(A.15)}$$

Using integration by parts, which is based upon the product rule for differentiation, we rearrange the right side of Eq. (A.15) as:

$$\int \mathrm{Erfc(z)}\,\frac{t_D\sqrt{H_K}}{(H_K-1)}\left(\frac{\sqrt{\alpha_D t_D}-\frac{z\alpha_D t_D}{\sqrt{\left(\sqrt{\alpha_D t_D}\,z\right)^2+t_D x_D}}}{\left(-\sqrt{\alpha_D t_D}\,z+\sqrt{\left(\sqrt{\alpha_D t_D}\,z\right)^2+t_D x_D}\right)^2}\right)dz$$

$$=$$

$$\mathrm{Erfc(z)}\overbrace{\left[\int\frac{\sqrt{\alpha_D t_D}-\frac{z\alpha_D t_D}{\sqrt{\left(\sqrt{\alpha_D t_D}\,z\right)^2+t_D x_D}}}{\left(-\sqrt{\alpha_D t_D}\,z+\sqrt{\left(\sqrt{\alpha_D t_D}\,z\right)^2+t_D x_D}\right)^2}dz\right]}^{A}$$

$$-$$

$$\int \mathrm{d(Erfc(z))}\overbrace{\left[\int\frac{\sqrt{\alpha_D t_D}-\frac{z\alpha_D t_D}{\sqrt{\left(\sqrt{\alpha_D t_D}\,z\right)^2+t_D x_D}}}{\left(-\sqrt{\alpha_D t_D}\,z+\sqrt{\left(\sqrt{\alpha_D t_D}\,z\right)^2+t_D x_D}\right)^2}dz\right]}^{A}dz \quad .$$

$$\text{(A.16)}$$

Furthermore, the solution for the integral A on the right side of Eq. (A.16) can be expressed as:

$$\int \left(\frac{\sqrt{\alpha_D t_D} - \frac{z\alpha_D t_D}{\sqrt{\left(\sqrt{\alpha_D t_D}\, z\right)^2 + t_D x_D}}}{\left(-\sqrt{\alpha_D t_D}\, z + \sqrt{\left(\sqrt{\alpha_D t_D}\, z\right)^2 + t_D x_D}\right)^2} \right) dz = \frac{\sqrt{\alpha_D t_D z^2 + t_D x_D} + \sqrt{\alpha_D t_D} z}{t_D x_D}.$$

. (A.17)

Also, the derivative of the complementary error function is determined as:

$$\frac{d(Erfc(z))}{dz} = -\frac{2}{\sqrt{\pi}} e^{-z^2} \tag{A.18}$$

Therefore, Eq. (A.18) is written as:

$$\int Erfc(z) \frac{t_D \sqrt{H_K}}{(H_K - 1)} \left(\frac{\sqrt{\alpha_D t_D} - \frac{z\alpha_D t_D}{\sqrt{\left(\sqrt{\alpha_D t_D}\, z\right)^2 + t_D x_D}}}{\left(-\sqrt{\alpha_D t_D}\, z + \sqrt{\left(\sqrt{\alpha_D t_D}\, z\right)^2 + t_D x_D}\right)^2} \right) dz$$

$$= \frac{\sqrt{H_K}}{(H_K - 1) x_D} \left(\begin{array}{l} Erfc(z)\left(\sqrt{\alpha_D t_D z^2 + t_D x_D} + \sqrt{\alpha_D t_D} z\right) \\ + \frac{1}{\sqrt{\pi}} \sum_{n=1}^{\infty} \frac{(-1)^{n+1}}{(n-1)!} z^{2n} \left(\frac{\sqrt{\alpha_D t_D}}{n} - \frac{2 t_D x_D \sqrt{\frac{\alpha_D}{x_D} z^2 + 1}\; {}_2F_1\left[-\frac{1}{2}, n - \frac{1}{2}; n + \frac{1}{2}; -\frac{\alpha_D}{x_D} z^2\right]}{(z - 2nz)\sqrt{\alpha_D t_D z^2 + t_D x_D}} \right) \end{array} \right)$$

.

(A.19)

Finally, we insert Eq. (A.19) back into Eq.(A.13):

$$c_D = \frac{0.5}{z_2 - z_1} \left(\frac{\sqrt{H_K}}{(H_K - 1) x_D} \left(\begin{array}{l} Erfc(z)\left(\sqrt{\alpha_D t_D z^2 + t_D x_D} + \sqrt{\alpha_D t_D} z\right) \\ - \frac{1}{\sqrt{\pi}} \sum_{n=1}^{\infty} \frac{(-1)^{n+1}}{(n-1)!} z^{2n} \left(\frac{\sqrt{\alpha_D t_D}}{n} - \frac{2 t_D x_D \sqrt{\frac{\alpha_D}{x_D} z^2 + 1}\; {}_2F_1\left[-\frac{1}{2}, n - \frac{1}{2}; n + \frac{1}{2}; -\frac{\alpha_D}{x_D} z^2\right]}{(z - 2nz)\sqrt{\alpha_D t_D z^2 + t_D x_D}} \right) \end{array} \right) \right)_{z_1}^{z_2}$$

,

(A.20)

Where, $_2F_1$ is the first hypergeometric function (Gauss's hypergeometric function) that arises in physical problems (Barnes, 1908). In general form, the first hypergeometric function for arbitrary parameters a, b, and c and variable z is expressed as:

$$ {}_2F_1(a,b;c;z) = 1 + \frac{ab}{1!c}z + \frac{a(a+1)b(b+1)}{2!c(c+1)}z^2 + \ldots = \sum_{n=0}^{\infty} \frac{(a)_n (b)_n}{(c)_n} \frac{z^n}{n!}. \tag{A.21} $$

Furthermore, z_1 and z_2 (interim variables) are determined through Eq. (A.6) and Eq. (A.7) as:

$$ \begin{cases} \text{If } C_1 = 0 \xrightarrow{\text{Eq.A.6}} \sqrt{\dfrac{dF}{dC}} = \sqrt{H_K} \xrightarrow{\text{Eq.A.7}} z_1 = \dfrac{x_D - \dfrac{dF}{dC}t_D}{2\sqrt{\alpha_D \dfrac{dF}{dC} t_D}} = \dfrac{x_D - H_K t_D}{2\sqrt{\alpha_D H_K t_D}} \\ \text{If } C_2 = 1 \xrightarrow{\text{Eq.A.6}} \sqrt{\dfrac{dF}{dC}} = \dfrac{1}{\sqrt{H_K}} \xrightarrow{\text{Eq.A.7}} z_2 = \dfrac{x_D - \dfrac{dF}{dC}t_D}{2\sqrt{\alpha_D \dfrac{dF}{dC} t_D}} = \dfrac{x_D - \dfrac{1}{H_K}t_D}{2\sqrt{\alpha_D \dfrac{1}{H_K} t_D}} \end{cases}. \tag{A.22} $$

Basically, the flow becomes 1D when the Koval heterogeneity factor tends to unity; hence, we compare concentrations obtained from Eq. (A.20) with those obtained from the 1D solution of CD equation for H_K=1.001. We compare the concentrations as a function of dimensionless distance at the fixed t_D=0.5 for two values of α_D: 0.01 and 1E-10. Figure A.1 compares the concentration history plots (at X_D=0.5) obtained from Eq. (A.20) and the 1D solution of CD equation when H_K=1.001 and α_D =1E-2. Both curves coincide illustrating that Eq. (A.20) produces the same result as the 1D solution of CD equation when H_K tends toward unity.

Figure A.2 compares the concentration history plots (at X_D=0.5) obtained from Eq. (A.20) and the 1D solution of CD equation when H_K=1.001 and α_D =1E-10. Both curves coincide showing that Eq. (A.20) produces the same result as the 1D solution of CD equation when H_K tends toward unity.

Similarly, we can show analytically that the proposed analytic solution reduces to 1D solution of CD equation when the Koval factor becomes unity. Inserting H_K=1.0 into Eq. (A.6) yields:

$$\sqrt{\frac{dF}{dC}} = \frac{\sqrt{H_K}}{[1+(H_K-1)C]} \xrightarrow{H_K=1} \sqrt{\frac{dF}{dC}} = 1.0 \qquad \text{(A.23)}$$

Inserting Eq. (A.23) into Eq. (3-5) yields Eq. (3-3), which is 1D solution of CD equation. Furthermore, the length of the mixing zone becomes zero as α_D tends to zero in Eq. (3-8) and the displacement within each layer turns into piston-like displacement.

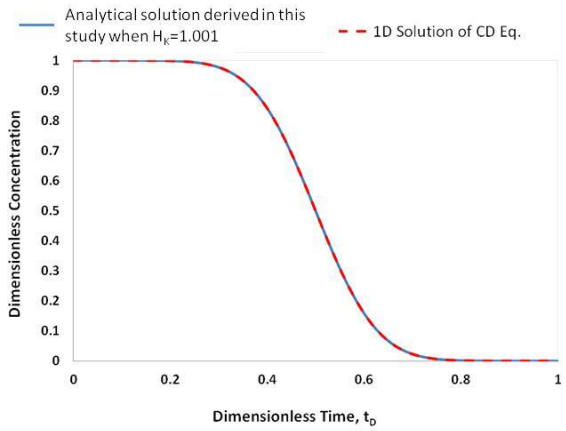

Figure A.1: A comparison between the concentrations obtained from Eq. (A.20) and the 1D solution of CD equation when H_K=1.001, X_D=0.5, and α_D =1E-2.

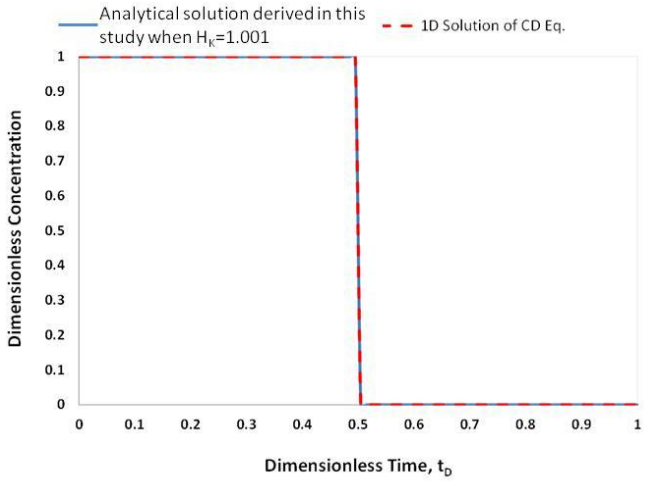

Figure A.2: A comparison between the concentrations obtained from Eq. (A.20) and the 1D solution of CD equation when H_K=1.001, X_D=0.5, and α_D =1E-10.

Appendix B: Tracer Slug Injection Equation Derivative

In this Appendix, the equations of the slug tracer injection are derived.

Adsorption is described as the adhesion of the atoms, ions, and molecular from a gas, liquid, or dissolved solid to a surface. In reservoir simulator, it uses the Langmuir adsorption isotherm equation below to calculate the adsorbed moles of component MM per unit pore volume. Absorption is the main reason to cause the delay of injected tracer.

$$ad = \frac{(tad1+tad2*xnacl)*ca}{(1+tad3*ca)} \tag{B.1}$$

Where tad1 is the first parameter in Langmuir adsorption isotherm equation. Tad2 is the second parameter in Langmuir adsorption isotherm equation, which associated with salt effect. Tad3 is the third parameter in Langmuir adsorption isotherm equation. Ca is the mole fraction of component in phase. Xnacl is the salinity of brine. When the concentration is high enough, maximum adsorption is reached. The equation can be rewritten as

$$ad_{max} = \frac{tad1+tad2*xnacl}{tad3} \tag{B.2}$$

Convection-dispersion equation defined as

$$\frac{dC}{dt} + u_x \frac{dC}{dx} - D_L \frac{d^2C}{dx^2} = 0 \tag{B.3}$$

Where u_x is the interstitial velocity in x direction, and D_L is the longitudinal dispersion coefficient.

Eq. (B.3) can be rewritten in terms of Darcy velocity instead of the interstitial velocity as

$$\frac{dC}{dt} + \frac{v_x}{\Phi} \frac{dC}{dx} - D_L \frac{d^2C}{dx^2} = 0 \tag{B.4}$$

Where v_x is the Darcy velocity. We can also rewrite this equation by including retardation of the solution, which is caused by adsorption of chemical species that stay on the surface of the porous medium.

$$\frac{dC}{dt} + \frac{u_x}{R_f}\frac{dC}{dx} - \frac{D_L}{R_f}\frac{d^2C}{dx^2} = 0 \tag{B.5}$$

R_f is the retardation factor, which is derived from material balance equation. R_f is defined as

$$R_f = 1 + D_i \tag{B.6}$$

Where

$$D_i = \frac{(1-\phi)C_{is}}{\phi C_i} = \frac{(1-s_w)C_{io}}{S_w C_{iw}} = \frac{1-S_w}{S_w}k_{di} \tag{B.7}$$

When R_f is equal to 1, there is no retardation. If R_f is larger than 1, the adsorption of the chemical species is delayed. It also means the one with adsorption will have lower travel speed than the one without adsorption.

We can rewrite equation (B.3) in dimensionless form.

$$\frac{dC_D}{dt_D} + \frac{dC}{dx_D} - \frac{1}{N_{Pe}}\frac{d^2C_D}{dx_D^2} = 0 \tag{B.8}$$

Where

$$C_D = \frac{C(x,t)-C_i}{C_j-C_i} \tag{B.9}$$

$$t_D = \frac{u_x t}{L} = \frac{qt}{A\phi L} = \frac{qt}{net\ sweep\ volume} \tag{B.10}$$

$$x_D = \frac{x}{L} \tag{B.11}$$

$$N_{Pe} = \frac{u_x L}{D_L} = \frac{qL}{A\phi D_L} \tag{B.12}$$

N_{Pe} is known as the Peclet number, a dimensionless number, which describes the transport phenomena in fluid flows. It is defined as the ratio of advection and dispersion.

Ogata and Banks (1961) solve Eq. (B.3) by using Laplace transformation equation. The solution is:

$$C(x,t) = \frac{C_j}{2}\left[erfc\left(x - \frac{u_x t}{2\sqrt{D_L t}}\right) + e^{\frac{u_x t}{D_L}} erfc\left(\frac{u_x t}{2\sqrt{D_L t}}\right)\right] \quad \text{(B.13)}$$

Where erfc is the complementary error function.

Rewrite (B.13) in dimensionless form as:

$$C_D(x_D, t_D) = \frac{1}{2}\left[erfc\left(\frac{x_D - t_D}{2\sqrt{t_D/N_{Pe}}}\right) + e^{x_D N_{Pe}} erfc\left(\frac{x_D - t_D}{2\sqrt{t_D/N_{Pe}}}\right)\right] \quad \text{(B.14)}$$

The first term of the right hand can often be neglected. (B.14) Becomes

$$C_D(x_D, t_D) = \frac{1}{2}\left[erfc\left(\frac{x_D - t_D}{2\sqrt{\frac{t_D}{N_{Pe}}}}\right)\right] \quad (3)$$

However, this equation has restrictive conditions: 1) homogeneous and isotropic porous medium, 2) the injected fluid has the same density as the displaced fluid, 3) the injected fluid has the same viscosity as the displaced fluid. (3) Can be written with the retardation factor as

$$C_D(x_D, t_D) = \frac{1}{2}\left[erfc\left(\frac{x_D - \frac{t_D}{R_f}}{2\sqrt{\frac{t_D}{N_{Pe} R_f}}}\right)\right] \quad \text{(B.15)}$$

The concentration of slug injection can be calculated by superposition.

$$C_i = \frac{C_{iI} + C_{iK}}{2} + \frac{(C_{iJ} - C_{iI})}{2}\text{erf}\left(\frac{x_D - t_D}{2\sqrt{\frac{t_D}{N_{Pe}}}}\right) + \frac{(C_{iJ} - C_{iK})}{2}\text{erf}\left(\frac{x_D - (t_D - t_{Ds})}{2\sqrt{\frac{t_D - t_{Ds}}{N_{Pe}}}}\right), t_D > t_{Ds} \quad \text{(B.16)}$$

For the inert tracer concentration at a layer with cumulative storage capacity of C can be expressed as:

$$C_i|_c = \frac{C_{iI} + C_{iK}}{2} + \frac{(C_{iJ} - C_{iI})}{2}\,\mathrm{erf}\left(\frac{x_D - \left.\frac{\partial F}{\partial C}\right|_c t_D}{2\sqrt{\alpha_D \left.\frac{\partial F}{\partial C}\right|_c t_D}}\right)$$

$$+ \frac{(C_{iJ} - C_{iK})}{2}\,\mathrm{erf}\left(\frac{x_D - \left.\frac{\partial F}{\partial C}\right|_c (t_D - t_{Ds})}{2\sqrt{\alpha_D \left.\frac{\partial F}{\partial C}\right|_c (t_D - t_{Ds})}}\right), t_D > t_{Ds}$$

(B.17)

For the active tracer concentration at a layer with cumulative storage capacity of C can be expressed as:

$$C_i|_c = \frac{C_{iI} + C_{iK}}{2} + \frac{(C_{iJ} - C_{iI})}{2}\,\mathrm{erf}\left(\frac{x_D - \left.\frac{\partial F}{\partial C}\right|_c t_D/R_f}{2\sqrt{\alpha_D \left.\frac{\partial F}{\partial C}\right|_c t_D/R_f}}\right)$$

$$+ \frac{(C_{iJ} - C_{iK})}{2}\,\mathrm{erf}\left(\frac{x_D - \left.\frac{\partial F}{\partial C}\right|_c (t_D - t_{Ds})/R_f}{2\sqrt{\alpha_D \left.\frac{\partial F}{\partial C}\right|_c (t_D - t_{Ds})/R_f}}\right), t_D > t_{Ds}$$

(B.18)

Objective function is defined as:

$$Objective = \sum_{i=1}^{N}[(c_{active,i} - c_{cal\_active,i})^2 + (c_{inert,i} - c_{cal\_inert,i})]^2 \quad \text{(B.19)}$$

Appendix C: Permeability Field

In this appendix, the procedure to generate heterogeneous permeability field is presented. Permeability affects flow and displacement more than other properties. Thus, heterogeneity measurement of permeability is very important. Heterogeneity of permeability is defined as formation with two or more non-communicating members, each possibly with different specific and relative permeability characteristics. Heterogeneity is a single statistic that describes the permeability variation.

To describe the permeability of reservoir heterogeneity, we are using Dykstra-Parsons Coefficient.

$$V_{DP} = \frac{k_{0.50} - k_{0.16}}{k_{0.50}}, \quad \text{(C.1)}$$

Where $k_{0.50}$ is the median permeability and $k_{0.16}$ is the permeability on standard deviation blow $k_{0.50}$ on a log-probability plot. For homogeneous reservoir, V_{DP} will be zero. For hypothetical infinitely heterogeneity, V_{DP} will be one. Equation C.1 can be simplified to

$$V_{DP} = 1 - \exp(-\sigma), \quad \text{(C.2)}$$

Where $\ln(k) \sim N(\mu, \sigma 2)$ and $\ln(k)$ satisfies normal distribution.

The Koval factor is related with VDP:

$$\log_{10}(H_k) = V_{DP}/(1 - V_{DP})^{0.2} \quad \text{(C.3)}$$

To generalize the heterogeneity reservoir, we used Stanford Geo-Statistical Modeling software (SGeMS). SGeMS implements many of the classical geo-statistics algorithms, and we apply sequential Gaussian simulation to generate the permeability field with certain range distance in both x and y directions. λ_x represents range distance

in the x-direction and λ_y represents range distance in the y-direction. Figures below show the cases with different value set of λx and λy.

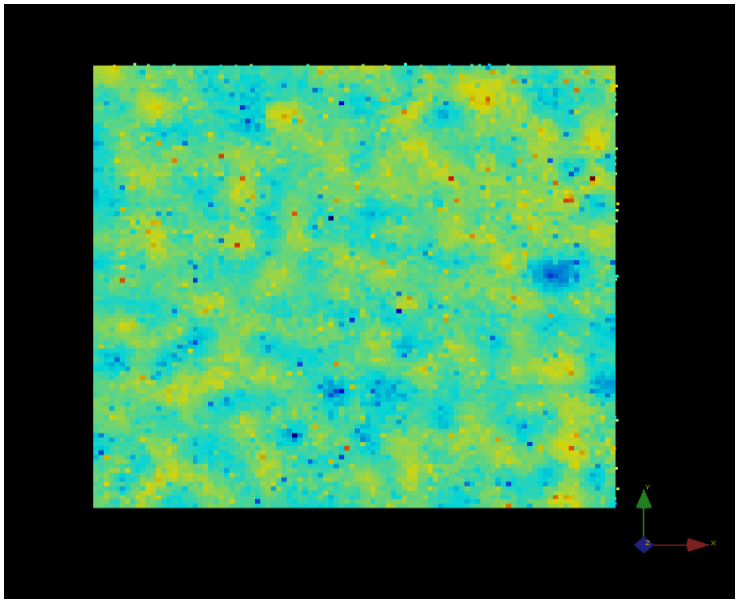

Figure C.1 shows the log value of permeability generated by modeling software for Case 1, V_{DP}=0.6, λ_x=0.01, and λ_y=0.01.

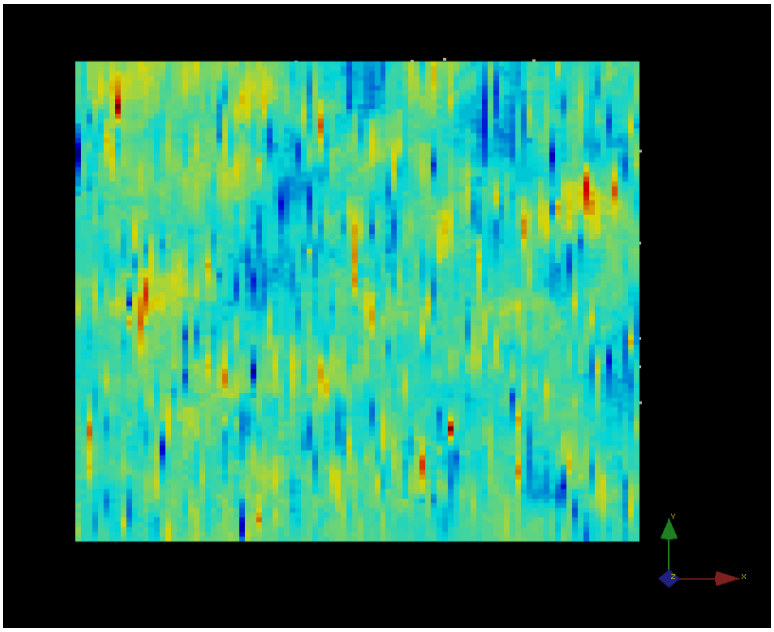

Figure C.2 shows the log value of permeability generated by modeling software in case 2: Case 2, VDP=0.6, λx=0.01, and λy=0.1

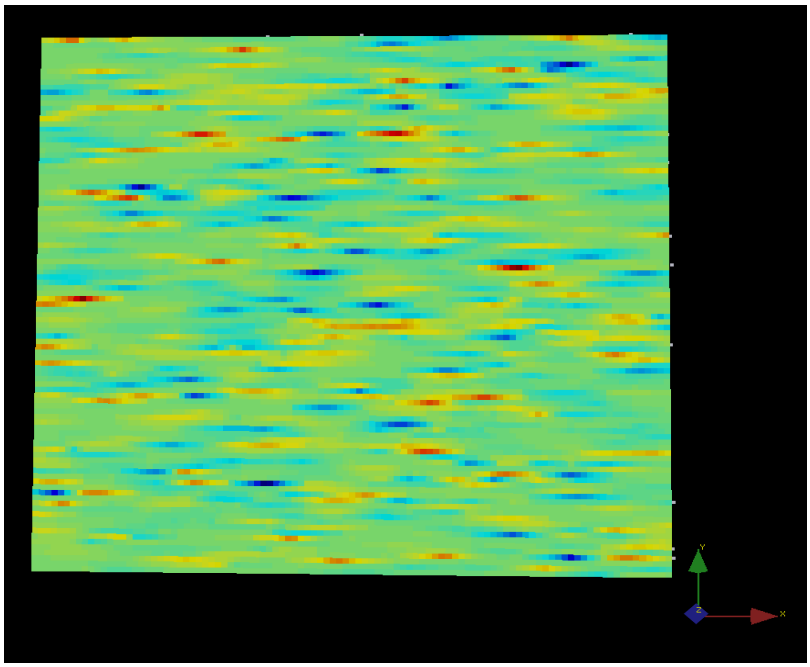

Figure C.3 shows the log value of permeability generated by modeling software in case 3: VDP=0.6, λx=0.1, and λy=0.01

Appendix D: MATLAB Code

```
% This is desinged for slug injection
clc;
clear all;
xd = 1.0;
hk = 0;
alpha = 0;
bigc = 0:.01:1;
%AAA=1;
AAA=textread('Tracer_Data.txt');
t = AAA(:,1);
t=t';
cactive = AAA(:,2); %EtFm, active
cactive=cactive';
cinert = AAA(:,3); %PrOH, inert
cinert=cinert';
count = 0;
b = 1;
Rf=1.15; %1.15
hkbest = 0;
alphabest = 0.1;
totalerrorold = 100;
A = 10;
ts = 0.1;
C_inject=1;
Number=length(t);
% for i=2:Number
%     if cinert(i)==0.5
%         t_swept=t(i);
%         t=t/t_swept;
%     end;
%     if cinert(i-1)<0.5 && cinert(i)>0.5
%         t_swept=t(i-1)+(0.5-cinert(i-1))*(t(i)-t(i-1))/(cinert(i)-
cinert(i-1));
%         t=t/t_swept;
%         COUNT=i;
%     end;
% end;
Match_before=Number;
% to calculate the swept volume
product=cinert.*t;
%t_swept_try=trapz(t(1:Number),product(1:Number))/trapz(t(1:Number),ci
nert(1:Number))-ts/2;
%t_swept_try=2.8818;
%t=t/t_swept_try;
%td_s=ts/t_swept_try;
td_s=ts;
number_to_integrate=length(bigc);
for alpha=0.3%0.01:0.01:0.4
    for hk=3%1:0.1:3
       for ii=1:Match_before
           for jj=1:number_to_integrate
            if t(ii)<=td_s
```

```
                dfdcactive(jj) = (hk)/((1+(hk-1)*bigc(jj))^2);
%Find the value for df/dc
                cdactive(jj,ii) = -C_inject*0.5*(1-erf((xd-
(dfdcactive(jj)*t(ii)/Rf))/(2*(alpha*dfdcactive(jj)*t(ii)/Rf)^0.5)));
%Calculate the cd vector. I think that using .* and ./ will give
vectors which is what I need
                dfdcinert = dfdcactive;%(hk)./(((1+(hk-1).*bigc).^2));
                cdinert(jj,ii) = -C_inject*0.5*(1-erf((xd-
(dfdcinert(jj)*t(ii)))/(2*(alpha*dfdcinert(jj)*t(ii))^0.5)));
            else
                dfdcactive(jj) = (hk)/((1+(hk-1)*bigc(jj))^2);
%Find the value for df/dc
                cdactive(jj,ii) = -C_inject*0.5*(erf((xd-
(dfdcactive(jj)*t(ii)/Rf))/(2*(alpha*dfdcactive(jj)*t(ii)/Rf)^0.5)))+C
_inject*0.5*(erf((xd-(dfdcactive(jj)*(t(ii)-
td_s)/Rf))/(2*(alpha*dfdcactive(jj)*(t(ii)-td_s)/Rf)^0.5)));
                dfdcinert = dfdcactive;%(hk)./(((1+(hk-1).*bigc).^2));
                cdinert(jj,ii) = -C_inject*0.5*(erf((xd-
(dfdcinert(jj)*t(ii)))/(2*(alpha*dfdcinert(jj)*t(ii))^0.5)))+C_inject*
0.5*(erf((xd-(dfdcinert(jj)*(t(ii)-
td_s)))/(2*(alpha*dfdcinert(jj)*(t(ii)-td_s))^0.5)));
            end;
           end;
           canalyticactive(1,ii) = trapz(bigc,cdactive(:,ii));
%This will find the integration
           canalyticinert(1,ii) = trapz(bigc,cdinert(:,ii));
       end;
       %error = ((abs(cactive-canalyticactive)).^2) + ((abs(cinert-
canalyticinert)).^2);
%Calculates the current error, hopefully will produce a vector for
each t
       %error = ((abs(cactive(1:Match_before)-
canalyticactive(1:Match_before))./2^0.5) +
((abs(cinert(1:Match_before)-canalyticinert(1:Match_before))./2^0.5);
       error = ((abs(cinert(1:Match_before)-
canalyticinert(1:Match_before))./2^0.5);    %only calculate inert
tracer error

       totalerror = sum(error);
%If I have a vector from previous step of all errors, this will sum
all those errors up


r_1=corrcoef(cactive(1:Match_before),canalyticactive(1:Match_before));

r_2=corrcoef(cinert(1:Match_before),canalyticinert(1:Match_before));
       %totalerror=r_1(1,2)^2+r_2(1,2)^2;

       count = count + 1;
%Just keeps a count for the following if statement to work
       %     count100=isequal(round(count/100000)*100000, count);
       %     if count100
       %             count=count
       %     end;
       if (totalerror<totalerrorold)
%this check to see it the total eror has decreased and
```

```
            hkbest = hk;
%if it has will store the current h and alpha values
            alphabest = alpha;
            totalerrorold = totalerror;
            c_active_result=canalyticactive;
            c_inert_result=canalyticinert;
        end;
    end;
end;
plot(t(1:Match_before),c_inert_result(1:Match_before),'*',t(1:Match_be
fore),cinert(1:Match_before));
%plot(t(1:Match_before),c_active_result(1:Match_before),'+',t(1:Match_
before),cactive(1:Match_before),t(1:Match_before),c_inert_result(1:Mat
ch_before),'*',t(1:Match_before),cinert(1:Match_before));
ylabel('Dimensionless Concentration');
xlabel('Dimensionless Time');
hkbest
alphabest
```

Appendix E: Simulation Code for Multi-Layer System

```
*interrupt *stop
*INUNIT *FIELD
TITLE1 'Interwell'
TITLE2 'RW-1D-2P-Flow-Partitioning'
TITLE3 'Single layer'
*wrst 5
WPRN SECTOR TIME
OUTPRN WELL ALL
WSRF SECTOR TIME
WSRF WELL TIME
OUTSRF GRID ALL
OUTSRF SPECIAL MOLEFRAC  'PRODUC' 'PrOH' OIL
OUTSRF SPECIAL MOLEFRAC  'PRODUC' 'PrOH' WATER
OUTSRF SPECIAL MOLEFRAC  'PRODUC' 'EtFm' WATER
OUTSRF SPECIAL MOLEFRAC  'PRODUC' 'EtAl' WATER
OUTSRF SPECIAL MOLEFRAC  'Well-4' 'EtAl' WATER
OUTSRF SPECIAL MOLEFRAC  'INJECT 1' 'PrOH' WATER
OUTSRF SPECIAL MOLEFRAC  'INJECT 1' 'EtFm' WATER
OUTSRF SPECIAL MOLEFRAC  'INJECT 2' 'PrOH' WATER
OUTSRF SPECIAL MOLEFRAC  'INJECT 2' 'EtFm' WATER
OUTSRF SPECIAL MASSFRAC  'PRODUC' 'PrOH' WATER
OUTSRF SPECIAL MASSFRAC  'PRODUC' 'PrOH' OIL
OUTSRF SPECIAL MASSFRAC  'PRODUC' 'EtFm' WATER
OUTSRF SPECIAL MASSFRAC  'PRODUC' 'EtAl' WATER
OUTSRF SPECIAL MASSFRAC  'Well-4' 'EtAl' WATER
OUTSRF SPECIAL MASSFRAC  'INJECT 1' 'PrOH' WATER
OUTSRF SPECIAL MASSFRAC  'INJECT 1' 'EtFm' WATER
OUTSRF SPECIAL MASSFRAC  'INJECT 2' 'PrOH' WATER
OUTSRF SPECIAL MASSFRAC  'INJECT 2' 'EtFm' WATER

** WPRN WELL TIME (not supported by stars)
**$  Distance units: ft
RESULTS XOFFSET         0.0000
RESULTS YOFFSET         0.0000

**$  (DEGREES)
RESULTS ROTATION          0.0000  **  (DEGREES)
RESULTS AXES-DIRECTIONS 1.0 -1.0 1.0

**$
**********************************************************************
*****
**$ Definition of fundamental cylindrical grid
```

```
**$
**********************************************************************
*****
GRID VARI 100 1 2
KDIR DOWN
DI IVAR
 100*2
DJ JVAR
 2
DK ALL
 100*6 100*4
DTOP
 100*6415
REFINE 10,1,1 INTO 1 2 1
REFINE 10,1,2 INTO 1 2 1

NULL CON           1
POR  CON         0.1
*PERMI *KVAR 100 100
PERMJ EQUALSI
PERMK *CON 0
PINCHOUTARRAY CON 1

END-GRID

ROCKTYPE 1
*MODEL  7  7  7  5 ** 7 total components, 7 fluid , 7 liquid , 5 aqueous
*COMPNAME    'Water'  'NaCl'     'PrOH'      'EtFm'     'EtAl'  'Dead_Oil' 'Soln_Gas'
**         --------   --------   -------  -------   -------    -------  --------   --------
*CMM         0.0000   58.4400    6.096     66.00     46.069    299.8980   24.3930 **
Component MW
*PCRIT         0.00     0.00      0.00      0.00      0.00     225.04     764.99  ** Component
critical pressure (kPa | psi | kPa).
*TCRIT         0.00     0.00      0.00      0.00      0.00     975.87    -32.16  ** Component
critical temperature (C | F | C)
*KV1       0.000E+0   0.0000      0.00      0.00      0.00     2.843E+6   2.375E+5
*KV2       0.000E+0   0.0000      0.00      0.00      0.00     0.000E+0   0.000E+0
*KV3       0.000E+0   0.0000      0.00      0.00      0.00     0.000E+0   0.000E+0
*KV4       0.000E+0   0.0000      0.00      0.00      0.00     -13557.5    -2453.1
*KV5       0.000E+0   0.0000      0.00      0.00      0.00     -459.67    -459.67
*MOLDEN   3.3619      0.0000      3.3619      0.00       0.00     1.969E-01  9.784E-01 **
Molar density at reference pressure and temperature
*CP       3.507E-09   0.0000      3.507E-09      0.00       0.00     3.507E-09  2.632E-05 **
Liquid compressibility (1/kPa | 1/psi) at constant temperature
*CT1      0.000E+00   0.0000      0.00      0.00       0.00     1.688E-04  1.110E-03 **
thermal expansion correlation (1/C | 1/F).
```

```
*AVISC    0.0500      3713.8   0.0500  0.1634264   0.102069  2.469E-01 3.916E-01    **
visc=avisc*exp(-bvisc/T)
*BVISC    1184.85     1659.8   1184.85    769.284    1235.952    1389.43    210.37
*SURFLASH  *KVALUE
** K_SURF is the k value between liquid and gas
*K_SURF 'EtAl' 0
*K_SURF 'EtFm' 0
*K_SURF 'PrOH' 0
*K_SURF 'Water' 0
*PRSR  4925.0 ** reference pressure,     corresponding to the density
*TEMR   219.0 ** reference temperature,  corresponding to the density
*PSURF   14.7 ** pressure at surface,    for reporting well rates, etc.
*TSURF   60.0 ** temperature at surface, for reporting well rates, etc.

*LIQLIQKV               ** Flag for liquid-liquid k-values, Kow=xi/wi >0 usually in the
range of 2.0 to 8.0
*KVTABLIM 14 9000 60 220 ** plow  phigh  Tlow  Thigh
*KVTABLE 'EtFm'          ** Multiply usual mass based k-value by
MWoil/MWwater=7
25.62 25.62
25.62 25.62

**       'WATER' 'NaCL'   'PrOH'  'EtFm'        'EtAl'  'oil' 'gas'
**STOREAC    0      0       0       1         0          0     0
**STOPROD    0      0       0       0         1    0     0

**FREQFAC  0 **units are 1/day 0.0136 for first test and 0.0089 for the second test,
reaction rate
**SOLID_DEN 'EtFm'    1E+5 0 0  ** Mass density is 0.1969*0.04

*ROCKFLUID
*RPT 1 *WATWET *STONE2
*SWT
0.0500  0.000E+00  1.000E+00  0
0.0755  2.100E-03  9.070E-01  0
0.1491  1.010E-02  7.260E-01  0
0.2574  3.250E-02  4.650E-01  0
0.3462  6.400E-02  2.740E-01  0
0.4208  1.060E-01  1.390E-01  0
0.5035  1.610E-01  4.940E-02  0
0.5791  2.550E-01  1.270E-02  0
0.5842  2.590E-01  1.080E-02  0
0.6057  2.990E-01  7.000E-03  0
0.6333  3.670E-01  3.900E-03  0
0.6496  4.170E-01  1.600E-03  0
0.6966  5.920E-01  8.500E-04  0
```

```
0.7201  6.930E-01  4.200E-04  0
0.7365  7.750E-01  2.300E-04  0
0.7538  8.690E-01  1.300E-04  0
0.7691  1.000E+00  5.506E-05  0
0.8774  1.000E+00  0.000E+00  0
1.0000  1.000E+00  0.000E+00  0
*SLT
0.050000  1.000  0  0
0.299998  0.507  0  0
0.349999  0.336  0.00049  0
0.396003  0.201  0.00126  0
0.454996  0.093  0.00372  0
0.510001  0.0644  0.00676  0
0.564001  0.0404  0.0138  0
0.592000  0.0285  0.0174  0
0.618001  0.0223  0.0234  0
0.646     0.0142  0.0355  0
0.672001  0.0105  0.0537  0
0.715     0.00645  0.0974  0
0.761003  0.00332  0.129  0
0.800998  0.00194  0.214  0
0.860996  0.00126  0.404  0
0.949998  0.000454  0.786  0
1         0              1  0

*** total dispersion this is wrong.
**DISPI_WAT 'EtAl' *CON 10
**DISPJ_WAT 'EtAl' *CON 0
**DISPK_WAT 'EtAl' *CON 0
**DISPI_OIL 'EtAl' *CON 10
**DISPJ_OIL 'EtAl' *CON 0
**DISPK_OIL 'EtAl' *CON 0

*KRTYPE con 1

*INITIAL
*VERTICAL *DEPTH_AVE
**$ Data for PVT Region 1
**$ ----------------------------------
*INITREGION 1
*REFPRES 4925.
REFDEPTH 6415.
*DWOC 6415.0
**$ Property: Water Saturation  Max: 0.05  Min: 0.05
SW CON   1
MFRAC_OIL 'Soln_Gas' CON           0
```

```
MFRAC_OIL 'Dead_Oil' CON          1
MFRAC_WAT 'Water' CON          1
MFRAC_WAT 'PrOH' CON          0
MFRAC_WAT 'NaCl' CON          0
MFRAC_WAT 'EtFm' CON          0
MFRAC_WAT 'EtAl' CON          0

*NUMERICAL
CONVERGE TOTRES 0.0001
*MAXSTEPS 999999999
*SDEGREE *GAUSS
*MAXPRES 1.450377E+05
*TFORM *ZT
*ISOTHERMAL
*AIM STAB

RUN

DATE 2011 01 01 ** year month day
DTWELL 0.001
** WELL 1 'PRODUC'
**
WELL  'PRODUC'
PRODUCER 'PRODUC'
OPERATE MIN BHP 100.0 CONT
OPERATE MAX BHF 1 CONT
**         rad  geofac wfrac skin
** liquid rate in bbl/day
**$ UBA            ff  Status  Connection
**         rad  geofac  wfrac  skin
GEOMETRY  K  0.2  0.5  1.0  0.0
PERF  GEO  'PRODUC'
** UBA       ff   Status  Connection
   100 1 1  1.0  OPEN    FLOW-TO  'SURFACE'  REFLAYER
   100 1 2  1.0  OPEN    FLOW-TO  1
**
**
**
** **
** WELL 2 'INJECT 1' VERT 1 1
**
**
**
WELL  'INJECT 1'  VERT  1  1
INJECTOR 'INJECT 1'
**       'WATER' 'NaCL'   'PrOH'  'EtFm'       'EtAl'  'oil' 'gas'
```

```
INCOMP WATER 0.9995     0.00     0.0       0.0       0.0005           0.0       0.0
OPERATE MAX BHP 99999.0 CONT
OPERATE MAX BHW 0.9 CONT
**          rad  geofac wfrac skin
**$ UBA           ff  Status  Connection
**          rad  geofac  wfrac  skin
GEOMETRY  K  0.2  0.5  1.0  0.0
PERF  GEO  'INJECT 1'
** UBA     ff   Status  Connection
   1 1 1  1.0  OPEN    FLOW-FROM  'SURFACE'
**
**
** WELL 3 'INJECT 2' VERT 1 1
**
**
**
WELL  'INJECT 2'  VERT  1  1
INJECTOR 'INJECT 2'
**       'WATER' 'NaCL'   'PrOH'  'EtFm'       'EtAl'  'oil' 'gas'
INCOMP WATER 0.9995     0.00     0.0       0.0       0.0005           0.0       0.0
OPERATE MAX BHP 99999.0 CONT
OPERATE MAX BHW 0.1 CONT
**          rad  geofac wfrac skin
**$ UBA           ff  Status  Connection
**          rad  geofac  wfrac  skin
GEOMETRY  K  0.2  0.5  1.0  0.0
PERF  GEO  'INJECT 2'
** UBA     ff   Status  Connection
   1 1 2  1.0  OPEN    FLOW-FROM  'SURFACE'
**
WELL  'Well-4'
PRODUCER 'Well-4'
OPERATE  MIN  BHP  100.0  CONT
OPERATE  MAX  BHF  0.1  CONT
**          rad  geofac  wfrac  skin
GEOMETRY  K  0.28  0.249  1.0  0.0
PERF  GEOA  'Well-4'
** UBA           ff   Status  Connection
   10 1 1 / 1 2 1  1.0  OPEN    FLOW-TO  'SURFACE'


WELL  'Well-5'
INJECTOR UNWEIGHT 'Well-5'
**       'WATER' 'NaCL'   'PrOH'  'EtFm'       'EtAl'  'oil' 'gas'
INCOMP  WATER  1.0    0.0             0.0     0.0    0.0  0.0  0.0
OPERATE  MAX  BHP  99999.0  CONT
```

```
OPERATE  MAX  BHW  0.1  CONT
**         rad  geofac  wfrac  skin
GEOMETRY  K  0.28  0.249  1.0  0.0
PERF  GEOA  'Well-5'
** UBA             ff   Status  Connection
   10 1 2 / 1 2 1  1.0  OPEN    FLOW-FROM  'SURFACE'

DTMAX   0.1
TIME  0.5
TIME  1
TIME  1.5
INJECTOR 'Well-5'
**       WATER'        NaCL'  'PrOH' EtFm'  EtAl'   'oil'     'gas'
INCOMP WATER     1.00     0         0         0         0.0      0         0
OPERATE MAX BHP 99999.0 CONT

OPERATE MAX BHW 0.1 CONT

TIME  2
TIME  2.5
INJECTOR 'INJECT 1'
**       'WATER' 'NaCL'   'PrOH'  'EtFm'      'EtAl'  'oil' 'gas'
INCOMP WATER      1        0.00    0.0       0.0       0         0.0       0.0
OPERATE MAX BHP 99999.0 CONT
OPERATE MAX BHW 0.9 CONT
INJECTOR 'INJECT 2'
**       'WATER' 'NaCL'   'PrOH'  'EtFm'      'EtAl'  'oil' 'gas'
INCOMP WATER      1        0.00    0.0       0.0       0         0.0       0.0
OPERATE MAX BHP 99999.0 CONT
OPERATE MAX BHW 0.1 CONT

TIME  3.5
INJECTOR 'Well-5'
**       WATER'        NaCL'  'PrOH' EtFm'  EtAl'   'oil'     'gas'
INCOMP WATER     0.99991          0         0         0         0.00009          0         0
OPERATE MAX BHP 99999.0 CONT

OPERATE MAX BHW 0.1 CONT
TIME  4.5
INJECTOR 'Well-5'
**       WATER'        NaCL'  'PrOH' EtFm'  EtAl'   'oil'     'gas'
INCOMP WATER     0.99976          0         0         0         0.00024          0         0
OPERATE MAX BHP 99999.0 CONT

OPERATE MAX BHW 0.1 CONT
TIME  5.68
```

```
INJECTOR 'Well-5'
**      WATER'      NaCL' 'PrOH' EtFm'  EtAl'  'oil'    'gas'
INCOMP WATER    0.9996764    0       0       0       0.000323634  0       0
OPERATE MAX BHP 99999.0 CONT

OPERATE MAX BHW 0.1 CONT
TIME  7
INJECTOR 'Well-5'
**      WATER'      NaCL' 'PrOH' EtFm'  EtAl'  'oil'    'gas'
INCOMP WATER    0.9997733    0       0       0       0.0002267    0       0
OPERATE MAX BHP 99999.0 CONT

OPERATE MAX BHW 0.1 CONT
TIME  9
INJECTOR 'Well-5'
**      WATER'      NaCL' 'PrOH' EtFm'  EtAl'  'oil'    'gas'
INCOMP WATER    0.999939     0       0       0       0.000061     0       0
OPERATE MAX BHP 99999.0 CONT

OPERATE MAX BHW 0.1 CONT
TIME  11
INJECTOR 'Well-5'
**      WATER'      NaCL' 'PrOH' EtFm'  EtAl'  'oil'    'gas'
INCOMP WATER    0.999991     0       0       0       0.000009     0       0
OPERATE MAX BHP 99999.0 CONT

OPERATE MAX BHW 0.1 CONT
TIME  13
INJECTOR 'Well-5'
**      WATER'      NaCL' 'PrOH' EtFm'  EtAl'  'oil'    'gas'
INCOMP WATER    1.0     0       0       0       0.0     0       0
OPERATE MAX BHP 99999.0 CONT

OPERATE MAX BHW 0.1 CONT

TIME  14
TIME  15
TIME  16
.
.
.
TIME  249

Stop
```

Appendix F: Nomenclature

a = exponent in exponential decline equation

A = area, L^2

b = coefficient in exponential decline equation

C = cumulative storage capacity

$c_{D\,i}$ = dimensionless concentration of component i

$C_{D_{produce}}$ = is total dimensionless tracer concentration observed from the producer

C_{D_1} = dimensionless concentration produced from the high permeable layer

C_{D_2} = dimensionless concentration produced from the low permeable layer

C_i = concentration of component i, M/L^3

C_{iI} = concentration of component i in original fluids, M/L^3

C_{iJ} = concentration of component i in slug fluids, M/L^3

C_{iK} = concentration of component i in chase fluids, M/L^3

D_L = the longitudinal dispersion coefficient, L^2/t

D_L =the longitudinal dispersion coefficient, dimensionless

F_1 = the dynamic fraction of injected volume that is producing at Layer 1, fraction

F_2 = the dynamic fraction of injected volume that is producing at Layer 2, fraction

F = Flow Capacity, fraction

f_j = fractional flow of phase j, fraction

$f_{crossflow}$= the amount of tracer flowing through the crossflow

h_1 = thickness of layer l, L

H_k = Koval factor

H_t = total thickness, L

$k_{0.50}$ = the median permeability

$k_{0.16}$ = the permeability on standard deviation blow $k_{0.50}$

L = length of the streamline, L

N_{pe} = Peclet number, dimensionless

N_{Pe}^{-1} = reciprocal of the Peclet number, dimensionless

q_{inj} = injection rate, L^3/t

R_L = effective aspect ratio

R_f = the retardation factor, dimensionless

S_j = saturation of phase j, fraction

S_{orm} = residual miscible oil saturation, fraction

S_{or} = residual oil saturation, fraction

$S_{o_{ave}}$ = average oil saturation before water breakthrough, fraction

t = time, t

t_D = dimensionless time (injected pore volume)

t_{D_1} = dimensionless time for pseudo layer 1

t_{D_2} = dimensionless time for pseudo layer 2

t_{D_s} = slug injection time, t

t_D = dimensionless time

t_{field} = actual field time, t

t_{adjust} = time after adjusted, t

u_x = the interstitial velocity in x direction, L/t

v_x = the Darcy velocity, L/t

V_{DP} = the Dykstra-Parson coefficient of variation

x_D = dimensionless distance

z = interim variable

ϕ = porosity, fraction

α_L = dispersivity in the longitudinal direction

α_D = dimensionless dispersivity equivalent to the reciprocal of the Peclet number

α_{HK} = input dispersivity required to match Eq. (A.20) with the simulation results

α_{Input} = simulation input dispersivity

α_T = dispersivity in the transverse direction

β = fraction of the injected fluid enters each layer, fraction

Δt_D = the maximum dimensionless time step in the simulation

λ_{xD} = dimensionless range distance in the x-direction

σ = Standard deviation